JLAB USER GROUP

Jefferson Lab PAC29
Proposal Cover Sheet
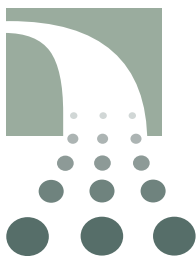
Experimental Hall: _____A_____

Days Requested for Approval: ____13____

❐ Proposal Title:

Measurement of the Neutron d_2 : Towards the Electric χ_E and Magnetic χ_M Color Polarizabilities.

Proposal Physics Goals
Indicate any experiments that have physics goals similar to those in your proposal.

A**pproved, Conditionally Approved, and/or Deferred Experiment(s) or proposals:**

E01–111, E03–107, E94–010, E97–103, E99–117, E01–012 and E01–006

Contact Person
Name: Brad Sawatzky
Institution: Temple University
Address: Jefferson Lab
Address: 12000 Jefferson Avenue
City, State, ZIP/Country: Newport News, VA, USA 23606
Phone/Fax: (757) 269–5947   (757) 584–5493
E-Mail: brads@jlab.org

Spokespersons:
1. S. Choi
2. X. Jiang
3. Z.–E. Meziani
4. B. Sawatzky
5.
6.

Jefferson Lab Use Only

Receipt Date:_____

By:_____

BEAM REQUIREMENTS LIST

JLab Proposal No.: _____   Date: _____12/05/2005_____

Hall: ___A___   Anticipated Run Date: _____   PAC Approved Days: _____

Spokesperson: S. Choi, X. Jiang, Z.–E. Meziani, B. Sawatzky   Hall Liaison: _____J.P. Chen_____
Phone: (757) 269–5947
E-mail: brads@jlab.org

List all combinations of anticipated targets and beam conditions required to execute the experiment. (This list will form the primary basis for the Radiation Safety Assessment Document (RSAD) calculations that must be performed for each experiment.)

Condition No.	Beam Energy (MeV)	Mean Beam Current (μA)	Polarization and Other Special Requirements (e.g., time structure)	Target Material (use multiple rows for complex targets — e.g., w/windows)	Material Thickness (mg/cm²)	Est. Beam-On Time for Cond. No. (hours)
1	5700.	15.	Polarization 75%	^{3}He	50	267
	1140.	15.		Glass window	44	
2	5700.	5.	Polarization 75%	^{3}He	50	8
	1140.	5.		Glass window	44	
3	1140.	30	Polarization 75%	Carbon multifoil	7*55	8

The beam energies, E_{Beam}, available are: $E_{Beam} = N \times E_{Linac}$ where N = 1, 2, 3, 4, or 5. E_{Linac} = 800 MeV, i.e., available E_{Beam} are 800, 1600, 2400, 3200, and 4000 MeV. Other energies should be arranged with the Hall Leader before listing.

Computing Requirements List

Proposal Title: Measurement of the Neutron d_2 : Towards the Electric χ_E and Magnetic χ_M Color Polarizabilities.

Spokesperson: S. Choi, X. Jiang, Z.–E. Meziani, B. Sawatzky   **Experimental Hall:** A

Raw Data Expected

Total: 3000 GB   **Per Year (long duration experiments only):** N/A

Simulation Compute Power (SPECint95 hours) Required: N/A

On–Line Disk Storage Required: 200 GB

Imported Data Amount from Outside Institutions: N/A

Exported Data Amount to Outside Institutions:w N/A

Expected Mechanism for Imported/Exported Data: N/A

Special Requirements
For example, special configuration of data acquisition systems) that may require resources and/or coordination with JLab's Computer Center. Please indicate, if possible, what fraction of these resources will be provided by collaborating institutions and how much is expected to be provided by JLab.

_____

_____

_____

_____

_____

HAZARD IDENTIFICATION CHECKLIST

JLab Proposal No.: _____   Date : _____12/05/2005_____

Check all items for which there is an anticipated need.

Cryogenics
_____ beamline magnets
_____ analysis magnets
_____ target
type: _____
flow rate: _____
capacity: _____

Electrical Equipment
_____ cryo/electrical devices
_____ capacitor banks
_____ high voltage
_____ exposed equipment

Radioactive/Hazardous Materials
List any radioactive or hazadorous/
toxic materials planned for use:
_____
_____
_____
_____

Pressure Vessels
__19 mm__ inside diameter
__13 atm__ operating pressure
__Glass__ window material
__~100 µm__ window thickness

Special Target Materials
__x__ * Helium (^{3}He)
___ Deuterium

Flammable Gas or Liquids
type: _____
flow rate: _____
capacity: _____

Drift Chambers
type: _____
flow rate: _____
capacity: _____

Other Target Materials
___ Beryllium (Be)
___ Lithium (Li)
___ Mercury (Hg)
___ Lead (Pb)
___ Tungsten (W)
___ Uranium (U)
__x__ Other (list below)

_____^{3}He, N$_2$, andRb_____
_____

Vacuum Vessels
_____ inside diameter
_____ operating pressure
_____ window material
_____ window thickness

Radioactive Sources
_____ permanent installation
_____ temporary use
type: _____
strength: _____

Large Mech. Structure/System
_____ lifting devices
_____ motion controllers
_____ scaffolding or
_____ elevated platforms

Lasers
type: __Laser diode system__
wattage: _____7x30 W_____
class: _____IV_____

Installation:
____x____ permanent
_____ temporary
Use:
_____ calibration
_____ alignment

Hazardous Materials
____ cyanide plating materials
____ scintillation oil (from)
____ PCBs
____ methane
____ TMAE
____ TEA
____ photographic developers
____ other (list below)

_____
_____

General

Experiment Class:

_____ Base Equipment
__x__ Temp. Mod. to Base Equip.
_____ Permanent Mod. to
       Base Equipment
_____ Major New Apparatus

Other: __Polarized He−3 target__
       __Cherenkov package added__
       __to BigBite__

LAB RESOURCES LIST

JLab Proposal No.: _____   Date _____12/05/2005_____

List below significant resources — both equipment and human — that you are requesting from Jefferson Lab in support of mounting and executing the proposed experiment. Do not include items that will be routinely supplied to all running experiments such as the base equipment for the hall and technical support for routine operation, installation, and maintenance.

Major Installations *(either your equip. or new equip. requested from JLab)*

_____BigBite Spectrometer (w/ Cherenkov package)_____

_____Polarized He–3 Target_____

_____

_____

_____

New Support Structures: _____

_____

_____

Data Acquisition/Reduction

Computing Resources: _____

_____

_____

New Software: _____

_____

_____

_____

Major Equipment

Magnets*:*   _____

_____

Power Supplies*:* _____

_____

Targets*:*   _____

_____

Detectors*:* BigBite Spectrometer (w/ Cherenkov package)

Polarized He–3 Target_____

Electronics*:* _____

_____

Computer Hardware*:* _____

_____

Other*:*   _____

_____

Other:

_____

_____

_____

Precision Measurement of the Neutron d_2: Towards the Electric χ_E and Magnetic χ_B Color Polarizabilities

X. Zheng
Argonne National Laboratory, Argonne, IL 60439, USA

P. Bertin
Université Blaise Pascal De Clermont-Ferrand, Aubiere 63177, France

J.-P. Chen, E. Chudakov, C. W. de Jager, R. Feuerbach, J. Gomez, J. -O. Hansen,
D.W. Higinbotham, J. LeRose, W. Melnitchouk, R. Michaels, S. Nanda, A. Saha,
B. Wojtsekhowski
Jefferson Lab, Newport News, VA 23606, USA

S. Frullani, F. Garibaldi, M. Iodice, G. Urciuoli, F. Cusanno
Istituto Nazionale di Fiscica Nucleare, Sezione Sanità, 00161 Roma, Italy

R. DeLeo, L. Lagamba
Istituto Nazionale di Fiscica Nucleare, Bari, Italy

A.T. Katramatou, G.G. Petratos
Kent State University, Kent, OH 44242

W. Korsch
University of Kentucky, Lexington, KY 40506, USA

W. Bertozzi, Z. Chai, S. Gilad, M. Rvachev, Y. Xiao
Massachusetts Institute of Technology, Cambridge, MA 02139, USA

L. Gamberg
Penn State Berks, Reading, PA, 19610 USA

F. Benmokhtar, R. Gilman, C. Glashausser, E. Kuchina,
X. Jiang (co-spokesperson), G. Kumbartzki, R. Ransome
Rutgers University, Piscataway, NJ 08855, USA

Seonho Choi(co-spokesperson)
University of Seoul, Seoul, South Korea

B. Sawatzky (co-spokesperson), F. Butaru, A. Lukhanin,
Z.-E. Meziani (co-spokesperson), P. Solvignon, H. Yao
Temple University, Philadelphia, PA 19122, USA

S. Binet, G. Cates, N. Liyanage, J. Singh, A. Tobias
University of Virginia, Charlottesville, VA 22901, USA

T. Averett, J. M. Finn, D. Armstrong, K. Griffioen, V. Sulkosky
College of William and Mary, Williamsburg, VA 23185, USA

and the

Hall A COLLABORATION

December 5, 2005

Contact: B. Sawatzky (brads@jlab.org)

Abstract

We propose to perform a measurement of the spin-dependent structure function g_2 by measuring the asymmetries $A_\perp$ and $A_\parallel$ of longitudinally polarized electrons scattering off a transversely and longitudinally polarized ^{3}He target respectively. This measurement will cover excitation energies exclusively in the deep inelastic valence quark region where x and Q^2 are large ($0.2 \leq x \leq 0.7$ and $2 \leq Q^2 \leq 6$ GeV^2). We will extract the higher twist piece of the spin structure function $\bar{g}_2$ and evaluate the quantity $d_2^n = \int_0^1 \bar{g}_2 \, dx = \int_0^1 x^2(2g_1 + 3g_2) \, dx$ related to the twist three matrix element.

The quantity d_2^n reflects the response of the *color* electric and magnetic fields to the polarization of the nucleon (alignement of its spin along one direction). It is important to note that d_2^n is dominated by the contributions from the large x region because it is a higher moment of structure functions. CEBAF at Jefferson Lab is an ideal place for such a measurement.

This measurement will provide a *benchmark* test of lattice QCD by reducing the statistical uncertainty in the present value of d_2^n by about a factor of four. Precision data in the large x region would allow us to make meaningful comparisons with several quark model predictions which include quark-gluon correlations and thus test our understanding of the nucleon spin structure beyond the parton model in the valence quark region.

Contents

1 Preface

An earlier version of this proposal (E01-111) was considered and defered by PAC 20. It was updated as proposal E03-107 and reconsidered by PAC 24 which deferred it with *regret* (PAC reports attached in the next 2 pages). The major concern of PAC 24 remained the "doubtful" interpretation of the proposed d_2 measurement as a twist-three matrix element due to the large contribution of the resonances when Q^2 is kept constant at 2 GeV^2. Furthermore due to the same resonance contributions, the extraction of the neutron d_2 from ^{3}He is further complicated. Both concerns were addressed in PAC 24 where we were successful in convincing the PAC that the nuclear corrections can be handled properly because d_2 is a moment of structure functions. However, PAC 24 remained concerned about the interpretation of a measurement still dominated by the resonance region and thus by twists higher than twist-three.

In response to the key concerns of both PACs, namely interpreting a measured d_2 made over a region dominated by the resonances contributions, we have modified our proposed measurement to be performed exclusively in the Deep Inelastic Region (DIS) and at a larger (but not constant) average Q^2. This in turn requires higher counting rates in order to achieve the necessary statistical accuracy for a meaningful measurement in a reasonable amount of beam time. Due to the small solid angle and momentum acceptance of the Hall A high resolution spectrometers, they are not a suitable option to carry the bulk of data taking in this case. Therefore, we plan to use the large acceptance BigBite spectrometer to achieve a statistical uncertainty comparable to the projected systematic uncertainty in approximately 11 days of production data. In the same time we also plan to use the HRS left arm to measure the cross sections over the appropriate kinematical range. We hope that the larger average Q^2 coupled with keeping the invariant mass $W \geq 2$ GeV, addresses the concerns of the previous PACs regarding the physics interpretation of the proposed measurement within the framework of the Operator Product Expansion.

In short, we have modified the proposal to perform a precision measurement of the g_2 neutron spin structure function in the large x deep inelastic ($0.2 \leq x \leq 0.65$ and $W \geq 2 GeV$) region and evaluate d_2^n at an average Q^2 of 3 GeV^2. We are requesting 13 days to perform this measurement which would dramatically improve the experimental determination of this quantity. This would then provide a benchmark test for the ever more sophisticated lattice QCD calculations. It also allow us to test our understanding of initial state interactions between quarks and gluons through quark models calculations.

Individual Proposal Report

Proposal: PR-01-111

Title: Measurement of the Neutron d^n_2 Matrix Element: a Linear Combination of the Electric χ_E and Magnetic χ_B Color Polarizabilities.

Spokespersons: X. Jiang and Z.-E. Meziani

Motivation: The motivation is to test model calculations (in particular, lattice models) of the d^n_2 matrix element, which in the framework of the Operator Product Expansion is sensitive to twist-three quark-gluon correlations, and to electric and magnetic color polarizabilities.

Measurement and Feasibility: The measurement uses longitudinally polarized electron scattering from polarized ^{3}He to measure the spin structure functions $g_1(x)$ and $g_2(x)$ at fixed Q^2=2 (GeV/c)^2. The spin asymmetry for inclusive electron scattering is measured in the standard Hall A spectrometers. The d^n_2 matrix element is evaluated by integrating $x^2(2g_1+3g_2)$ over the measured region, with extrapolations to x=0 and x=1 to cover the unmeasured regions. Models are used to correct for the difference between a polarized ^{3}He nucleus and a free polarized neutron. The experiment appears to be feasible, building on a foundation of several similar experiments in Hall A. The experiment could provide a factor-of-four smaller error than existing data for the neutron d^n_2 matrix element.

Issues: The principal issue is that the integral will be strongly affected by contributions in the resonance region, which may introduce significant higher-twist contributions, clouding the interpretation in terms of quark-gluon correlations. A secondary concern is the reliability of the extraction of the value of d^n_2 of the neutron from the data on ^{3}He. Since the nuclear effects are largest at high x, it is not obvious that these are negligible in an integral that is weighted by x^2.

Recommendation: Defer

Scientific Rating: N/A

Individual Proposal Report

Proposal: PR 03-107

Scientific Rating: N/A

Title: Measurement of the Neutron d_2:Towards the Electric χ_E and Magnetic χ_B Color Polarizabilities

Spokespersons: Z.-E. Meziani, S. Choi, and X. Jiang

Motivation: The aim of the experiment is a precise determination of moments of the neutron spin structure functions, namely the integral of g_2^n and the x^2-moment of a particular combination of g_1 and g_2, called d_2. In the framework of the Operator Product Expansion, the latter is sensitive to twist-3 quark-gluon correlations, and to electric and magnetic color polarizabilities. This quantity would be compared to lattice QCD predictions and to other model calculations.

Measurement and Feasibility: The measurement uses scattering of longitudinally polarized electrons from a polarized ^{3}He target, to measure longitudinal and transverse asymmetries, together with the unpolarized cross section, from which the spin structure functions $g_1(x)$ and $g_2(x)$ are extracted at fixed $Q^2 = 2$ (GeV/c)^2. The experiment is optimized to minimize the uncertainty on d_2, obtained by integrating $x^2(2g_1 + 3g_2)$ over the measured region (x from 0.24 to 0.8). Extrapolations to x=0 and x=1 are applied to cover the unmeasured regions. A correction to account for the difference between a polarized ^{3}He and a free polarized neutron is applied. The experiment uses existing equipment and proven techniques. It is judged feasible. It would complement the low Q^2 results obtained by E-94-010 and the (significantly less precise) SLAC determination of d_2^n at 5 (GeV/c)^2. Lattice QCD calculations performed at $Q^2 = 2$ (GeV/c)^2 should be available in the near future, enhancing the interest in the measurement.

Issues: The principal issue is that the measured integral is dominated by contributions in the resonance region, thus making the interpretation in terms of color polarizabilities doubtful. However, investigating whether the twist expansion breaks down in this region is of interest, and connected to the question of quark-hadron duality. Nuclear corrections seem to be under control for the moment being addressed, d_2^n.

The PAC would have liked to see this experiment performed, but due to limitations in the available beam time, the proposal cannot be accepted at this time.

Recommendation: Defer with Regret.

2 Introduction and Motivation

In inclusive polarized lepton-nucleon deep-inelastic scattering, one can access two spin-dependent structure functions of the nucleon, g_1 and g_2. In the last twenty five years, measurements of g_1 have been used to test Quantum Chromodynamics (QCD) through the Björken sum rule and investigate the spin content of the nucleon in term of its constituents. While g_1 can be understood in terms of the Feynman parton model which describes the scattering in terms of *incoherent* parton scattering, g_2 cannot. Rather, one has to consider parton correlations initially present in the target nucleon, and the associated process is given a *coherent* parton scattering in the sense that more than one parton takes part in the interaction. Indeed, using the operator product expansion (OPE) [1, 2], it is possible to interpret the g_2 spin structure function beyond the simple quark-parton model as a higher twist structure function. As such, it is exceedingly interesting because it provides a unique opportunity to study the quark-gluon correlations in the nucleon which cannot otherwise be accessed.

In a recent review Fillipone and Ji [3] explained that most higher-twist processes cannot be cleanly separated from the leading twist because of the so-called infrared renormalon problem first recognized by t'Hooft. This ambiguity arises from separating quarks and gluons pre-existing in the hadron wave function from those produced in radiative processes. Such a separation turns out to be always scheme dependent. However, the g_2 structure function is an *exception* because it contributes at the leading order to the spin asymmetry of longitudinally-polarized lepton scattering on transversely-polarized nucleons. Thus, g_2 **is among the cleanest higher-twist observables**.

Why does the g_2 structure function contain information about the quark and gluon correlations in the nucleon? From the optical theorem, g_2 is the imaginary part of the spin-dependent Compton amplitude for the process $\gamma^*(+1) + N(1/2) \to \gamma^*(0) + N(-1/2)$,
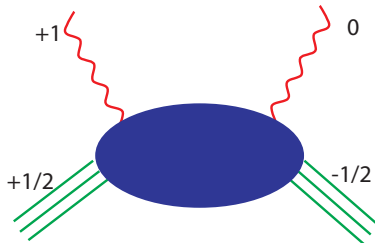
Figure 1: Compton amplitude of $\gamma^*(+1) + N(1/2) \to \gamma^*(0) + N(-1/2)$.

where γ^* and N denote the virtual photon and the nucleon, respectively, and the numbers in the brackets are the helicities. Thus this Compton scattering involves the t-channel helicity exchange $+1$. When factorized in terms of parton sub-processes, the intermediate partons must carry this helicity exchange. Because chirality is conserved in vector coupling, massless quarks in perturbative processes cannot produce a helicity flip. QCD allows this helicity exchange to occur in two ways (see Fig. 2): first, single quark scattering in which the quark carries one unit of orbital angular momentum through its transverse momentum wave function; second, quark scattering with an additional transversely-polarized gluon from the nucleon target. The two mechanisms are combined in such a way to yield a gauge-invariant result. Consequently, g_2 provides a direct probe of the quark-gluon correlations in the nucleon wave function.

Figure 2: Twist-two and twist-three contributions to virtual Compton scattering

2.1 The twist-three reduced matrix element

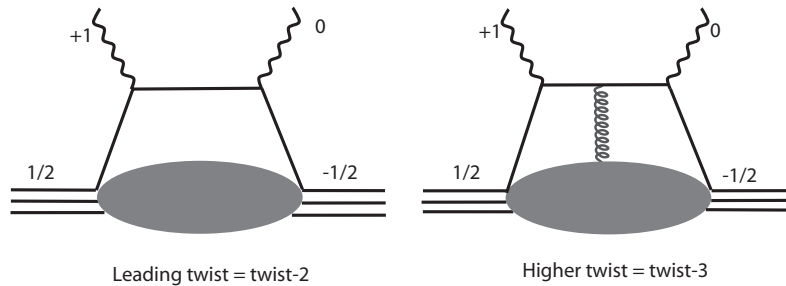The piece of interesting physics we want to focus on in this proposal is contained in the second moment in x of a linear combination of g_1 and g_2, namely

$$d_2(Q^2) = \int_0^1 x^2 [2g_1(x, Q^2) + 3g_2(x, Q^2)]dx \tag{1}$$

$$= 3\int_0^1 x^2 \left[g_2(x, Q^2) - g_2^{WW}(x, Q^2) \right] dx \tag{2}$$

$$= 3\int_0^1 x^2 \left[\bar{g}_2(x, Q^2) \right] dx$$

where g_2^{WW}, known as the Wandzura-Wilczek [4] term, depends only on g_1

$$g_2^{WW}(x, Q^2) = -g_1(x, Q^2) + \int_x^1 \frac{g_1(y, Q^2)}{y} dy. \tag{3}$$

and

$$\bar{g}_2(x, Q^2) = -\int_x^1 \frac{dy}{y} \frac{d}{dy} \left[\frac{m}{M} h_T(y, Q^2) + \xi(y, Q^2) \right] \tag{4}$$

is expressed in terms of the transverse polarization density $h_T(x, Q^2)$ function (Transversity) suppressed by the quark mass m over the nucleon mass M and the twist-3 term ξ which arises from quark-gluon correlations.

It is interesting to note that the quantity d_2 also appears in the first moment of g_1 when at large Q^2 ($Q^2 \gg \Lambda_{QCD}^2$) it is expressed in terms of a twist expansion [8, 7]:

$$\Gamma_1(Q^2) = \int_0^1 g_1(Q^2, x)dx = \frac{1}{2}a_0 + \frac{M^2}{9Q^2}\left(a_2 + 4d_2 + 4f_2 \right) + O\left(\frac{M^4}{Q^4} \right), \tag{5}$$

where a_0 is the leading twist, dominant contribution. It is determined, apart from QCD radiative corrections [9], by the triplet g_A and octet a_8 axial charges and the net quark spin contribution to the total nucleon spin. These axial charges are extracted from measurements of the neutron and hyperons weak decay measurements [10]. Here a_2 is a second moment of the g_1 structure function and arises from the target mass correction [7]. The quantities d_2 and f_2 are the twist-3 and the twist-4 reduced matrix elements. These matrix elements contain non-trivial quark-gluon interactions beyond the parton model. A first extraction of f_2 has been carried by Ji and Melnitchouk in [11] using the world data but with poor statistical precision below $Q^2 = 1$ GeV^2. Other investigations

of higher twist contributions in the case of spin-dependent structure functions were performed and reported in Ref. [12, 13]. Recent extractions of f_2 have also been carried out combining the existing high Q^2 world data with new low Q^2 data from Jefferson Lab [14, 15]. The new data allowed us to gauge the size of higher twist contribution (beyond twist-4), thus checking the convergence of the expansion, and provding for an improved precision in the extraction of f_2.

In QCD, d_2 and f_2 can be expressed as linear combinations of the induced color electric and magnetic polarizabilities χ_E and χ_B [3, 16] when a nucleon is polarized. This twist expansion may be valid down to $Q^2 \approx 1$ GeV^2 if higher order terms are small.

At large Q^2 where an OPE expansion becomes valid, the quantity d_2 reduces to a twist-3 matrix element which is related to a certain quark-gluon correlation.

$$d_2 S^{[\mu} P^{\{\nu\}} P^{\lambda\}} = \frac{1}{8} \sum_q \langle P, S | \bar{\psi}_q \ g \bar{F}^{\{\mu\nu} \gamma^{\lambda\}} \psi_q | P, S \rangle \ , \tag{6}$$

where g is the QCD coupling constant, $\bar{F}^{\mu\nu} = (1/2)\epsilon^{\mu\nu\alpha\beta} F_{\alpha\beta}$, $F_{\alpha\beta}$ are the gluon field operators, and the parentheses $\{\cdots\}$ and $[\cdots]$ denote symmetrization and antisymmetrization of indices, respectively. The structure of the above operator suggests that it measures a quark *and* a gluon amplitude in the initial nucleon wavefunction [1, 2].

The twist-4 contribution is defined by the matrix element

$$f_2 \ M^2 S^\mu \ = \ \frac{1}{2} \sum_q e_q^2 \ \langle P, S | g \ \bar{\psi}_q \ \widetilde{F}^{\mu\nu} \gamma_\nu \ \psi_q | P, S \rangle \ , \tag{7}$$

where $\widetilde{F}^{\mu\nu}$ is the dual gluon field strength tensor. f_2 can also be defined (generalized) in terms of the structure functions:

$$f_2(Q^2) = \frac{1}{2} \int_0^1 dx \ x^2 \Big(7g_1(x, Q^2) + 12g_2(x, Q^2) - 9g_3(x, Q^2) \Big), \tag{8}$$

where g_3 is the 3rd spin structure function, which has not yet been measured but could be accessed by an asymmetry measurement of unpolarized lepton scattering off a longitudinally polarized target. With only g_1 and g_2 data available, f_2 can also be extracted through Eqn. 5 if the twist-6 or higher terms are not significant.

The physical significance of $d_2(Q^2)$ has been articulated by Ji and we quote,

"we ask when a nucleon is polarized in its rest frame, how does the gluon field inside of the nucleon respond? Intuitively, because of the parity conservation, the color magnetic field $\vec{B}$ can be induced along the nucleon polarization and the color electric field $\vec{E}$ in the plane perpendicular to the polarization."

After introducing the color-singlet operators $O_B = \psi^\dagger g \vec{B} \psi$ and $O_E = \psi^\dagger \vec{\alpha} \times g \vec{E} \psi$, we can define the gluon-field polarizabilities χ_B and χ_E in the rest frame of the nucleon[5, 6]

$$\langle PS | O_{B,E} | PS \rangle = \chi_{B,E} 2M^2 \vec{S} \ . \tag{9}$$

Then d_2 can be written as

$$d_2 = (\chi_E + 2\chi_B))/8 \ . \tag{10}$$

Thus d_2 is a measure of the response of the color electric and magnetic fields to the polarization of the nucleon. The reduced matrix element f_2 can be expressed also as a different linear combination of the same color polarizabilities

$$f_2 = (\chi_E - \chi_B)/3 \ . \tag{11}$$

Ultimately the color electric and magnetic polarizabilities will be obtained from $d_2(Q^2)$ and $f_2(Q^2)$ when high precision data on both g_1 and g_2 become available. In this proposal we are aiming at providing precision data for d_2^n at large Q^2.

2.2 Burkhardt-Cottingham Sum rule

The g_2 structure function itself obeys the Burkhardt-Cottingham (BC) sum rule [18]

$$\Gamma_2(Q^2) = \int_0^1 g_2(x, Q^2) \, dx = 0 \ , \tag{12}$$

which was derived from the dispersion relation and the asymptotic behavior of the corresponding spin-flip Compton amplitude. This sum rule is true at all Q^2 and does not follow from the OPE. It is rather a super-convergence relation based on Regge asymptotics as articulated in the review paper by Jaffe [19]. Many scenarios which could invalidate this sum rule have been discussed in the literature [2, 20, 21]. However, this sum rule was confirmed in perturbative QCD at order α_s with a $g_2(x, Q^2)$ structure function for a quark target [22]. Surprisingly a first precision measurement of g_2 by the E155 collaboration [17] at $Q^2 = 5$ GeV^2 but within the experimentally limited range of x has revealed a violation of this sum rule on the proton at the level of three standard deviations. In contrast, the neutron sum rule is poorly measured but consistent with zero within one standard deviation. New high precision neutron g_2 data [23, 24] shown in Fig. 6 at Q^2 below 1 GeV suggest that the BC sum rule is verified within errors. While a full test of the BC sum rule cannot be performed within the limited x range of this proposal, this measurement will provide useful data to further explore the large x contributions to the sum rule in the neutron/^{3}He.

3 Experimental status of $d_2^{p,n}(Q^2)$ and $\Gamma_2^n(Q^2)$ measurements

The early measurements of the g_2 spin structure function performed by the SMC [25] and E142 [26, 27] collaborations in the 90's were meant to reduce the systematic errors when extracting g_1 due to g_2's contribution to the measured parallel asymmetries. As the statistical precision of g_1 improved, a better measurement of g_2 was required to minimize the error on g_1. Therefore, in SLAC E143 [28], E154 [29] and E155 [30] more data on g_2 were collected and d_2 was evaluated and published by these collaborations. But since the statistical errors of these experiments were still large and as the interest in the physics of g_2 rose, a dedicated experiment known as SLAC E155x [31] was approved to measure g_2 at relatively large Q^2 to investigate the higher twist effects in the proton and deuteron. This led to an evaluation of d_2 with much improved statistical precision compared to what existed previously for both the proton and the deuteron [31]. At lower Q^2 another dedicated experiment known as JLab E97-103 [34] was performed at Jefferson Lab to look for higher twists effects by exploring the Q^2 evolution of g_2^n using a polarized ^{3}He target from $Q^2 = 1.4$ GeV^2 down to $Q^2 = 0.6$ GeV^2 at $x = 0.2$. The statistical precision was improved by almost an order of magnitude. Two other Jlab experiments, E99-117 [32] and E94-010 [23, 24], had the opportunity to measure the g_2 structure function in a non-dedicated mode while focusing on a measurement of the g_1^n structure function. The first one provided three data points in the valence quark DIS region $(x, Q^2) = (0.33, 2.71)$, $(0.47, 3.52)$ and $(0.6, 4.83)$ while the second one was carried out in the resonance region at Q^2 below 1 GeV^2.

Fig. 3 shows d_2 from SLAC E155X for the proton in the upper panel and the SLAC E155x and JLab E99-117 combined neutron result compared to several calculations. The proton result is generally consistent with the chiral quark model [40, 41] and some bag models [42, 7, 11] while one to two standard deviations away from the QCD sum rule calculations [44, 45, 46]. More importantly,

the comparison with the recent lattice QCD calculation of the QCDSF collaboration [47] shows consistency with the experimental datum of the proton. However, it clearly indicates the need for an improvement on the experimental precision for the neutron datum. In fact Jefferson Lab E99-117 measurements of g_2^n at large x combined with SLAC E155X have improved on the total error by almost a factor of two. At the same time the latest QCDSF lattice calculation reported here has improved also by a factor of two compared to their previous results published in 2001 [48]. Of course it is difficult to guess the total error on the lattice calculation but at this time the neutron d_2 result is two standard deviations away from the experimental value including the lattice and chiral extrapolation errors. The experimental error bar is still dominated by the statistical uncertainty.

The Lattice Hadron Physics Collaboration (LHPC) based at Jefferson Lab has plans to extract this matrix element for the proton and the neutron [49] and provides a different check on the QCDSF collaboration lattice calculations.
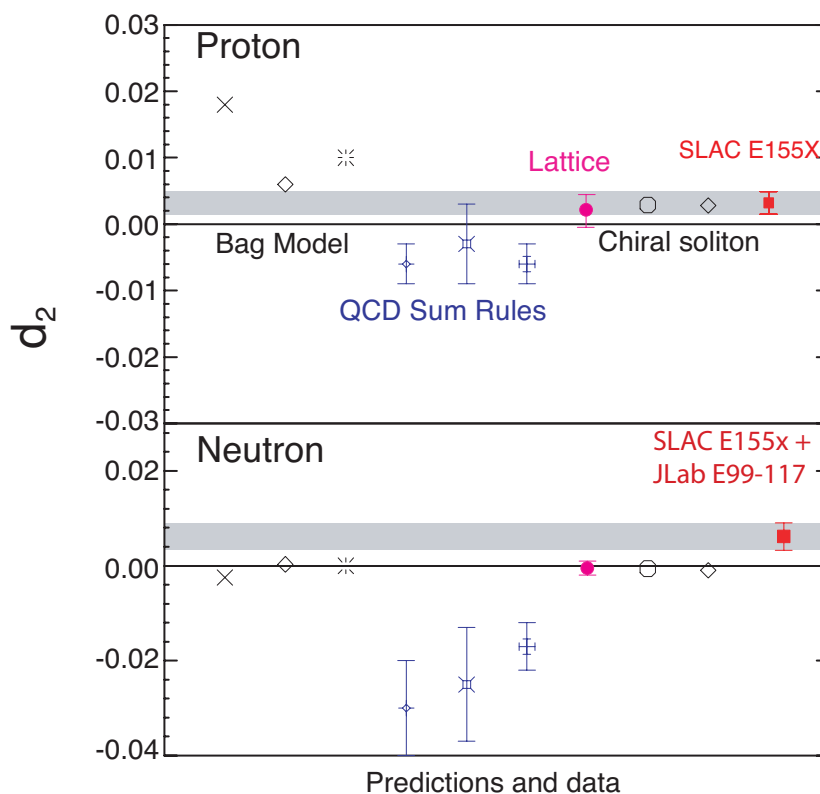
Figure 3: d_2 SLAC E155X results of the proton and SLAC E155x combined with Jlab E99-117 results of the neutron results compared to several theoretical calculations including lattice QCD (see text). Upper panel is for the proton and lower panel is for the neutron.

It is woth noting that except for the QCD sum rule calculation all nucleon bag models or chiral soliton models predict values consistent with the lattice QCD result. The experimental result is thus 2σ away from zero all available calculations. In these models g_2^n is negative at large x therefore it is conceivable that the poor precision (Fig. 5) of the data in this region is affecting the overall sign of the result. It is important to note that from the point of view of a simple quark model, the d_2 matrix element of the neutron should be much smaller than that of the proton because of SU(6)

spin-flavor symmetry. Thus, with the present precision of the combined SLAC E155x and JLab E99-117 neutron data it is difficult to draw any conclusions on the sign and size of the neutron higher twist (twist-three) contribution. However because d_2 is a second moment in x of the linear combination $(2g_1 + 3g_2)$ the neutron data set can be improved significantly at Jefferson Lab with a dedicated measurement like the one proposed here. Due to the x^2 weighting, the contribution of the small x region is supressed and thus using the existing world data to cover the region $x < 0.23$ should be sufficient to complete the integral. In fact the average Q^2 value of the world low x data is close to the value $Q^2 = 3$ GeV^2 of this proposal.

During JLab experiment E94-010 [23], which was aimed at measuring the Gerasimov-Drell-Hearn extended sum, data on g_2 were taken using a polarized ^{3}He target across the resonance in the range $0.1 < Q^2 < 0.9$ GeV^2. New results on two moments of the neutron spin structure functions, Γ_2^n and d_2^n, are now available from this experiment. These low Q^2 results are shown in Fig. 4 along with the SLAC E155x and JLab E99-117 combined results. The results published in [24] give a glimpse of the Q^2 evolution of the quantity $\bar{d}_2^n$ which does not include the elastic contribution (at $x = 1$) to the integral. However this contribution is negligible above $Q^2 = 3 GeV^2$ but dominate the quantity d_2 below $Q^2 = 1$ GeV^2. Note that no comparable data exist for the proton.
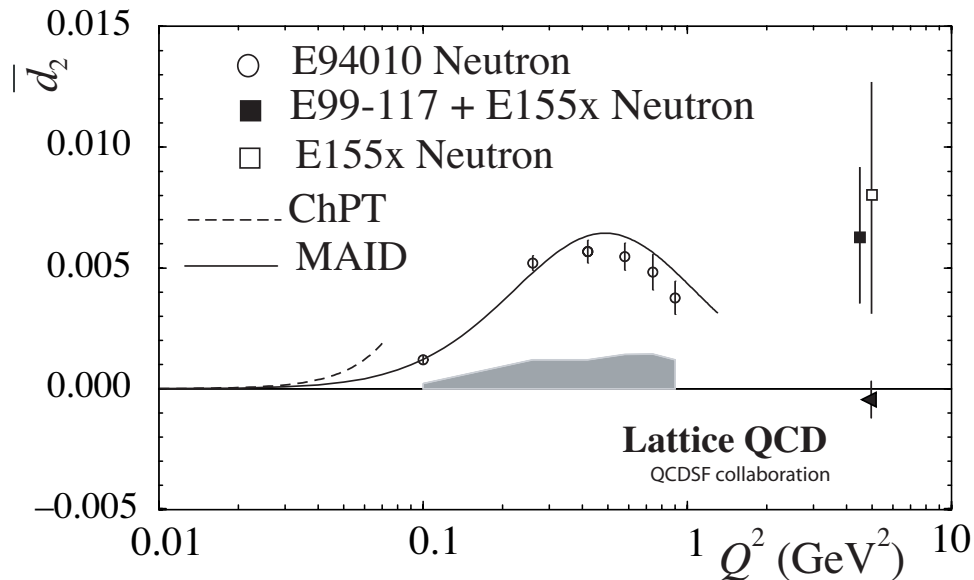
Figure 4: $\bar{d}_2(Q^2)$ results of JLab E94-010 without the nucleon elastic contribution are presented. The grey band represents their corresponding systematic uncertainty. The SLAC E155 [31] neutron result is also shown here (open square). The solid line is the MAID calculation[51] while the dashed line is a HBχPT calculation[52] valid only at very low Q^2. The lattice prediction [47] at $Q^2 = 5$ GeV^2 for the neutron d_2 reduced matrix element is negative but consistent with zero. We note that all models shown in Fig. 3 predict a negative value or zero at large Q^2 where the elastic contribution is negligible. At moderate Q^2 the data show a positive $\bar{d}_2^n$, and indicate a slow decrease with Q^2. The combined SLAC+JLab datum shows a positive d_2^n value but with still a large error bar.

In the investigation of higher twists contributions an important step has already been taken with JLab experiment E97-103 [34], which has provided precision data of g_2^n in the deep inelastic region

and determined its Q^2 evolution in the range $0.56 < Q^2 < 1.4$ GeV^2 for a fixed value of $x \approx 0.2$. The unprecedented statistical accuracy achieved in JLab E97-103 was critical to probe the size of higher twists contributions by comparing directly the measured g_2^n to the leading twist contribution (the twist-two contribution known as $g_2^{n(WW)}$ [36]). The experiment has been completed and the results published [34] showing a small but finite size of higher twists as Q^2 decreases below 1 GeV^2. Nevertheless, this experiment has little impact on the evaluation of the d_2 quantity because of the low x value it was performed at, although it is important for direct comparison between the measured g_2 and the leading twist piece of g_2.

Two other recently completed experiments, JLab experiment E01-012 [37] which used a polarized ^{3}He target, and JLab experiment E01-006 [38] which uses polarized NH$_3$ and ND$_3$ targets, will add to the wealth of neutron spin structure functions data (g_1^n and g_2^n) in the resonance region. However, the first measurement emphasises the investigation of g_1 while the second provides data at $Q^2 = 1.3$ GeV^2 for g_2^p with high precision but limited precision for g_2^n.
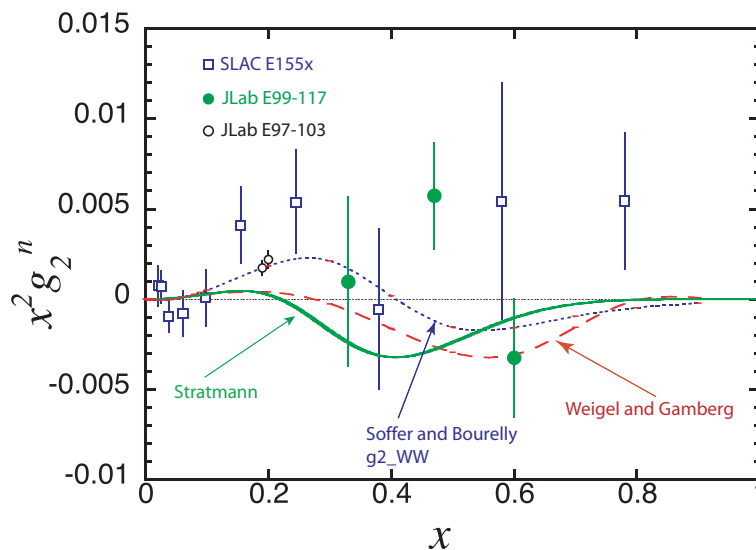
Figure 5: Present world $x^2 g_2^n$ data for $Q^2 \geq 1$ GeV^2 along with some model calculations and g_2^{WW}. SLAC E155X neutron results are derived from measurements using polarized NH$_3$ and ND$_3$ targets as described in Ref.[35, 17]. The JLab experiments used a polarized ^{3}He target in Hall A. We note the consistency between the data. The solid curve is a quark model calculation by Stratmann [42], the dashed line is a chiral soliton calculation by Weigel and Gamberg [40]. The dotted line represent the evaluation of g_2^{WW} using g_1 from the statistical model of the nucleon by Bourelly and Soffer [50].

We summarize the situation of the quality of the neutron g_2 spin structure data in Fig. 5 where we report the world data with Q^2 greater than 1 GeV^2 and show a comparison with some model calculations as well as the Wandzura-Wilzeck g_2^{WW} contribution to g_2. The neutron result of g_2 extracted from the proton and deuteron measurements of E155X are shown in Fig. 5. The statistical accuracy already achieved in JLab E97-103 is shown for their highest Q^2 kinematics point, namely

$Q^2 = 1.4$ GeV^2 and $x = 0.2$. We should point out that this proposed experiment is optimized to minimize the error on the determination of d_2^n not g_2^n. Obviously, time limitations would not allow us to provide for the ultimate statistical precision at each x value for the best possible stringent comparison with models of $g_2^n(x, Q^2)$.

Finally, turning to the BC sum rule, the experimental situation is summarized in Fig. 6 where we show Γ_2^n measured in E94-010 (solid circles) and, including the elastic contribution (open circles) evaluated using a dipole form factor for G_M^n and the Galster fit for G_E^n. The positive light grey band corresponds to the total experimental systematic errors while the dark negative band represents an estimated DIS contribution using g_2^{WW}. The solid line is the resonance contributions evaluated using MAID and the negative light-grey band is the neutron elastic contribution added to the measured data to determine Γ_2^n. The results are quite encouraging since the data show that the BC sum rule is verified within uncertainties over the Q^2 range measured. Our result is at odds with the reported violation of this sum rule on the proton at high Q^2 (where the elastic contribution is negligible) [17]. It is, however, consistent with the neutron result of SLAC E155 (open square) which unfortunately has a rather large error bar. In light of our results, a high statistical precision measurement in the range 1 GeV$^2 \leq Q^2 \leq 5$ GeV^2 would be very useful for both the proton and neutron even if the x range is limited.
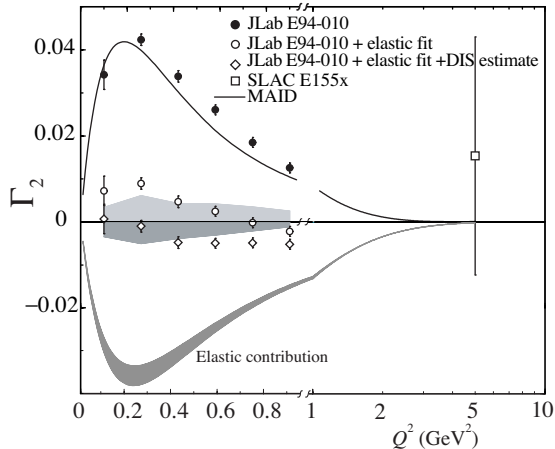
Figure 6: Results of Γ_2^n (open diamonds) along with the average of the world data from DIS. The theoretical prediction for this quantity is zero (see text).

In the next section we shall describe how we plan to improve on the statistical precision of the g_2 neutron data at large x which will result in a reduction of the satistical error bar of d_2^n by a factor of almost four as well as provide a reasonable add-on to the BC sum evaluations at $< Q^2 > = 3$ GeV^2.

4   Proposed Experiment

We propose to measure the unpolarized cross section $\sigma_0^{^3He}$, the parallel asymmetry $A_{\parallel}^{^3He}$ and the perpendicular asymmetry $A_{\perp}^{^3He}$ and extract the g_2 structure function in the large x region with good precision. We will use the longitudinally polarized ($P_b = 0.75$) CEBAF electron beam and a 40-cm-long high pressure polarized ^{3}He target. The measurement will be performed at one incident

Figure 7: Proposed kinematic range for the measurement at a constant energy and angle. The bands represents the horizontal angular acceptance of the Bigbite spectrometer.

electron beam energy $E_i = 5.7$ GeV (or higher) and one scattering angle, $\theta = 45.0°$.

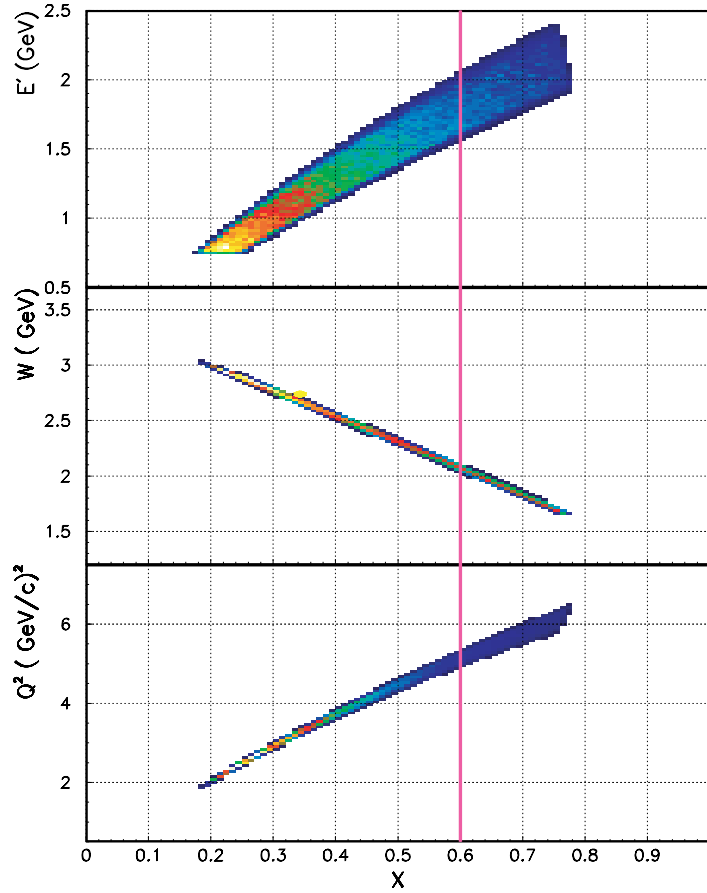The Bigbite spectrometer will be used to acquire the asymmetry data (perpendicular and parallel) while the left arm HRS spectrometer will be used to measure the absolute cross section. Both spectrometers will bet set at a scattering angle of $\theta = 45.0°$ on each side of the incident beam line. One magnetic field setting of the Bigbite spectrometer will cover more than the useful kinematic range $0.20 \leq x \leq 0.65$ and $2.0 \leq Q^2 \leq 5$ GeV^2 of this proposal. The left HRS momentum will be stepped across the same kinematic range to measure the absolute cross section as a function of x. The target polarization orientation will be set transverse or longitudinal to the beam with a value of $P_t = 0.40$ while the beam helicity will be reversed at a rate of 30 Hz. A beam current of 15 μA combined with a target density of 2.5×10^{20} atoms/cm^3 provides a luminosity of about 1 $\times 10^{36}$ cm^{-2}s^{-1} on the effective target length at 45°.

Using the Bigbite spectrometer at a full current setting with a field of B= 1.2 Tesla we will have a continuous kinematic coverage as shown in Fig. 7. The left HRS spectrometer momentum will be stepped through central values listed in table 2 to match the same kinematic domain.

4.1 The Polarized Beam

In this proposal we shall assume that the achievable beam polarization at CEBAF is 75% with a current of $15\mu A$ although 80% electron beam polarization has been delivered on a regular basis in Hall A. The polarization of the beam will be measured with the Hall A Moller and Compton polarimeters.

4.2 The Polarized ^{3}He Target

The polarized target is the standard ^{3}He polarized target in Hall A [53]. It is based on the principle of spin exchange between optically pumped alkali-metal vapor and noble-gas nuclei [55, 56, 57] and has been used in JLab experiments E94-010, E95-001 [54], E97-103 and E99-117 in Hall A. In those experiments we regularly achieved 35-40% target polarization in-beam.

A central feature of the target will be sealed glass target cells, which under operating conditions, contain a ^{3}He pressure of about 10 atmospheres. As indicated in Fig. 8, the cells will have two chambers, an upper chamber in which the spin exchange takes place, and a lower chamber, through which the electron beam will pass. In order to maintain the appropriate number density of the alkali-metal Rubidium the upper chamber will be kept at a temperature of 170–200°C using an oven constructed of high temperature plastic Torlon. The density of the target will be about 2.5×10^{20} atoms/cm^3. The lower cell length will be 30 cm such that the end glass windows will be shielded from the spectrometer acceptance. The effective target length the spectrometer acceptance sees is about 20 cm/$\sin 45°$

The main components of the target are shown in Fig. 8. The main "coils" shown are large Helmholtz coils used to apply a static magnetic field of about 25 Gauss. Also shown are the components for the NMR and EPR polarimetry. The NMR components of the target include a set of RF drive coils, and a separate set of pickup coils. Not shown in the figure are the NMR electronics, which include an RF amplifier, a lock-in amplifier, some bridge circuitry, and the capability to sweep the static magnetic field. The EPR components include an EPR excitation coil and a photodiode for detection of the EPR line. The oven shown in Fig. 8 is heated with forced hot air. The optics system include a system of 4 diode lasers for longitudinal pumping and 4 for transverse pumping. A polarizing beam splitter, lens system and a quarter wave plate are required to condition each laser beam line and provide circular polarization.

4.2.1 Target Cells

The length of the cells is chosen to be 40 cm which places the target windows outside the length acceptance of the BigBite spectrometer at 45°. The end windows themselves will be about 100 μm thick.

4.2.2 The Optics System

As mentioned above, approximately 90 W of "usable" light at 795 nm will be required. By "usable", we mean circularly polarized light that can be readily absorbed by the Rb. It should be noted that the absorption line of Rb has a full width of several hundred GHz at the high pressures of ^{3}He at which we will operate. Furthermore, since we will operate with very high Rb number densities that are optically quite thick, even light that is not well within their absorption line width can still be absorbed.

The laser system consists of commercially available 30 Watt fiber-coupled diode laser systems (from COHERENT INC.). Four such lasers are used to pump along the transverse direction and
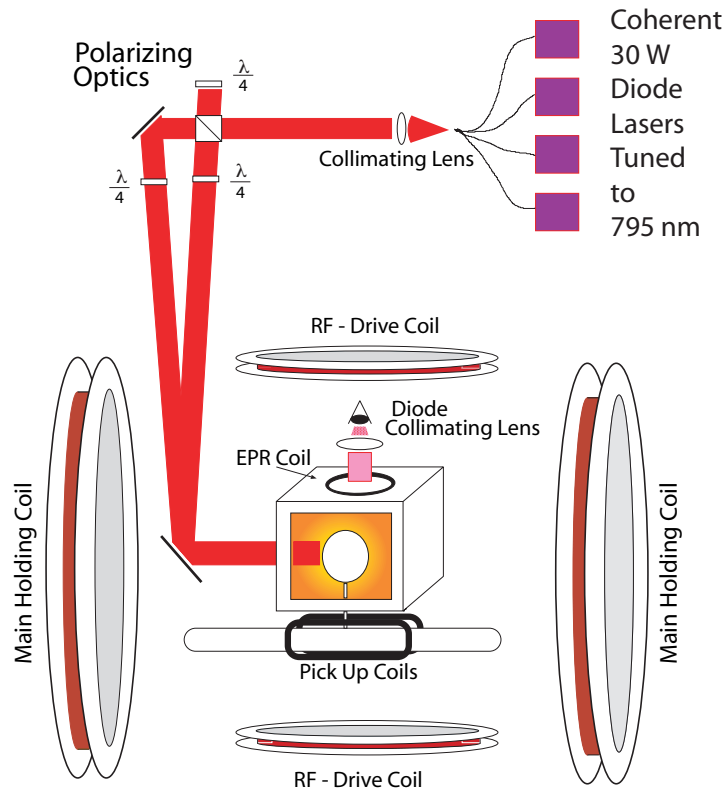
Figure 8: JLab Hall A polarized ^{3}He target setup.

three along the longitudinal direction. The efficiency of these lasers has been tested in many occasions and found to be totally adequate for this experiment's needs.

4.2.3 Polarimetry

Polarimetry is accomplished by two means. During the experiment, polarization is monitored using the NMR technique of adiabatic fast passage (AFP)[62]. The signals are calibrated by comparing the ^{3}He NMR signals with those of water. The calibration is then independently verified by studying the frequency shifts that the polarized ^{3}He nuclei cause on the electron paramagnetic resonance (EPR) lines of Rb atoms [61]. Both methods were used in E94-010 and we found as expected that the NMR measurements with water calibration are consistent with the EPR results.

4.3 The Spectrometers setup

We plan to use the Bigbite spectrometer in Hall A to take the bulk of the data, and one HRS spectrometer, the left arm, to perform cross section measurements and calibrations. Both will be located at 45° symmetrically with respect to the incident beam line.

4.3.1 the BigBite spectrometer

The BigBite spectrometer will be positioned at a distance of 1.5 m from the target and its dipole magnet set at full current providing a central field of $B = 1.2$ T The BigBite detector package (see

Fig.9) will consist of

- Two sets Multiwire Drift Chambers (MWDC) for tracking information

- A Gas Cherenkov counter between the two MWDCs for pion rejection.

- A set of scintillators for triggering on charged particles.

- A double layer lead glass calorimeter for additional pion rejection.

The detector package configuration for BigBite similar to that of experiments E02-013 and E03-004 except that we plan to remove the third MWDC (placed in the middle) and install a thresold gas Cherenkov counter. Since the proposed experiment is inclusive the addition of the Cherenkov counter for pion and proton rejection is critical.

Each set of MWDC consists of three wire planes for U-U', V-V', and X-X' with sense wire separation of 2.0 cm. GEANT Monte Carlo simulations [63] show a momentum resolution of about 2% and angular resolution about 3.0 mrad. The vertex reconstruction along the beam will be better than 2 cm, enough to allow for removing the target glass windows in the offline analysis. The DIS spectrum at 5.7 GeV and 45° is smooth enough that the designed momentum resolution will be more than adequate for the 10% momentum bins used in this proposal.

The electron identification in our case is provided by the Cherenkov counter in combination with the electromagnetic calorimeter. The latter is composed by of two sub-packages. The first a preshower detector made out of blocks of TF-5 lead glass spanning an active area of 210×74 cm^2 with 10 cm depth (3 r.l.) along the particle direction. This is followed by a shower detector composed with total absorption blocks of TF-2 lead glass covering an area of 221×85 cm^2 with 34 cm depth which should contain showers with energies up to 10 GeV. The resolution of the calorimeter is about $8\%/\sqrt{(E)}$ leading to an expected pion rejection of 100:1.

The Cherenkov counter we plan to build for this experiment will be located in the gap between the first and third wire chamber (replacing the currently installed middle wire chamber) has the following dimensions: 200x60x60 cm^3. These dimensions allow the existing BigBite frame to be used with no change in solid angle coverage. Eight mirrors configured in a tiled 4x2 arrangement will focus the Cherenkov light on 2 columns of 4 photomultipliers (PMT) mounted on each side of the box. We plan to use 3" quartz-windows PMTs from Photonis. Our preferred choice of Cherenkov radiator is C_4F_{10} gas (pion threshold: 2521 MeV/c) currently used in CLAS, however, Freon 12 would also be an option with some loss in the number of photo-electrons.

Assuming a 40 cm track length in C_4F_{10}, a 'medium detailed' calculation predicts a mean PMT response of 28 measured photo-electrons per electron with a quartz-window PMT (vs. 16-18 with a more conventional PMT like the Burle 8854) This estimate includes the PMT quantum efficiency, PMT window transparency, and is multiplied by a factor of 0.81 to accommodate a 10% loss from both the mirror and reflection off the PMT front surface (the latter may be conservative).

The high number of registered photons allow a high online threshold (4-5 p.e.'s) to be applied which essentially removes all of the 1-2 p.e. background while capturing $> 99\%$ of the electron tracks (with a healthy margin of error).

We expect a pion rejection ratio of about 1000 and when coupled with cuts on the shower/pre-shower we expect to achieve a total pion rejection of 10^5. This should be more than adequate for this experiment. The pion asymmetry will also be measured in the same experiment.

The total angular acceptance provided by the BigBite spectrometer in this configuration is about 64 msr with a vertical angular acceptance of ± 240 mrad and horizontal angular acceptance of ± 67 mrad.
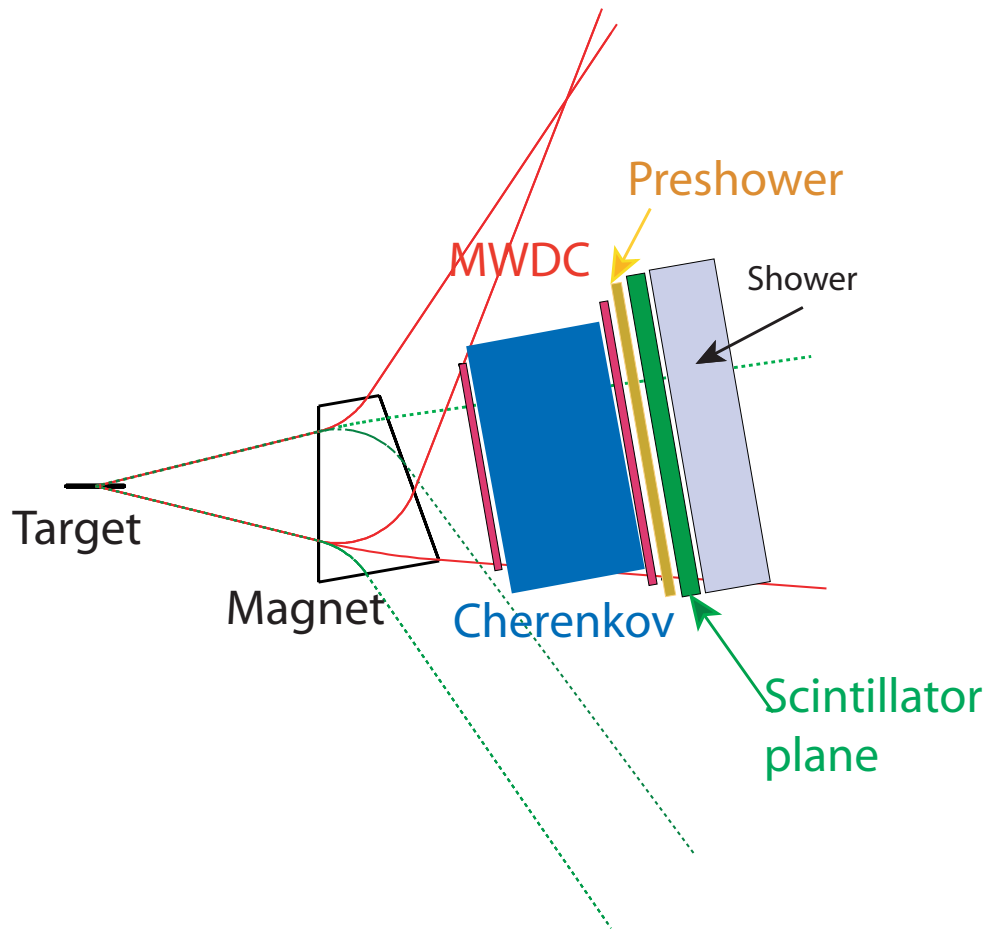
Figure 9: Bigbite spectrometer detector setup with full current. The trajectories missing the detector are charged particles with momentum less than 200 MeV/c. Also shown are trajectories of charged particles with momentum equal to 1.8 GeV/c

4.3.2 Left High Resolution Spectrometer

The Hall A left High Resolution Spectrometer (HRS) will be positioned at 45° to measure absolute cross sections in the same x range as the the BigBite spectrometer. We will use the left HRS with its standard detector package for electrons which consists of :

- Two vertical Drift Chambers (VDCs) for the measurement of momentum and production angle.

- Threshold Gas Cherenkov counter for pion rejection.

- A set of scintillators for triggering on charged particles.

- A double layer lead glass calorimeter for additional pion rejection.

As the E99-117 analysis shows, the pion rejection factor with the Cherenkov counter and the lead glass calorimeter are better than 1×10^5 with an electron detection efficiency of 98%. This is sufficient for our worst case scenario.
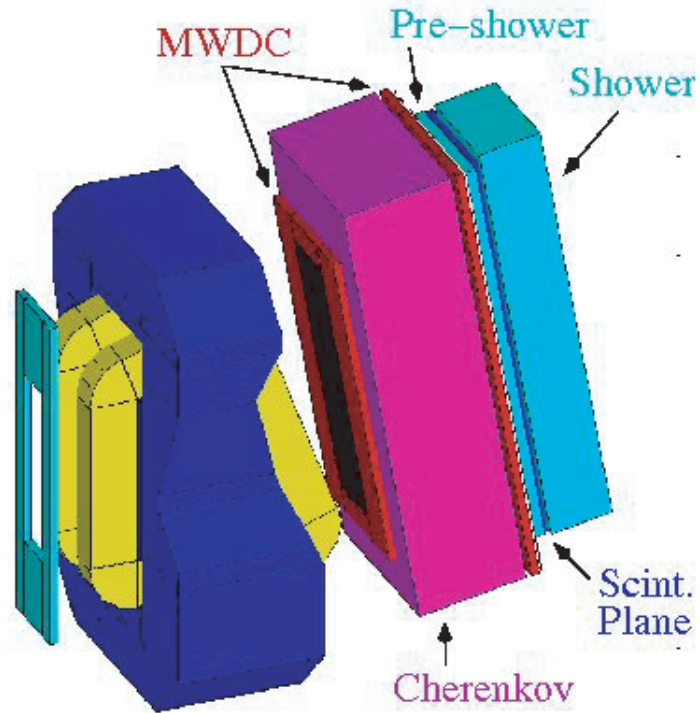
Figure 10: Diagram of the BigBite spectrometer with its detector package.

Specific advantages make the HRS spectrometer a well matched tool for the proposed measurement.

- Good electron events in the spectrometer are in principle due only to electron scattering off ^{3}He nuclei since the target cell glass windows are outside the spectrometer acceptance. However, excellent target reconstruction by the HRS spectrometers allows for better background rejection.

- An excellent resolution of the spectrometers permits the measurement of elastic scattering off ^{3}He needed for an absolute calibration of the detector in order to measure absolute cross sections.

4.4   Positron contamination

The dilution factor due to eletrons from symmetric (e$^+$,e$^-$) pairs contamination will be measured using the left HRS spectrometer set at the same angle $45°$ but with a reversed polarity from its electron detection mode. Measurement of the positron production cross section during JLab E99-117 shows that it is less than 3% of the total cross section at $x = 0.33$ and scattering angle of $35°$. It was also found that the asymmetry was negligible compared to the statistical uncertainty of the measurement which was similar to this experiment. In any case we plan to measure the positron cross sections with the left HRS and spectrometer.
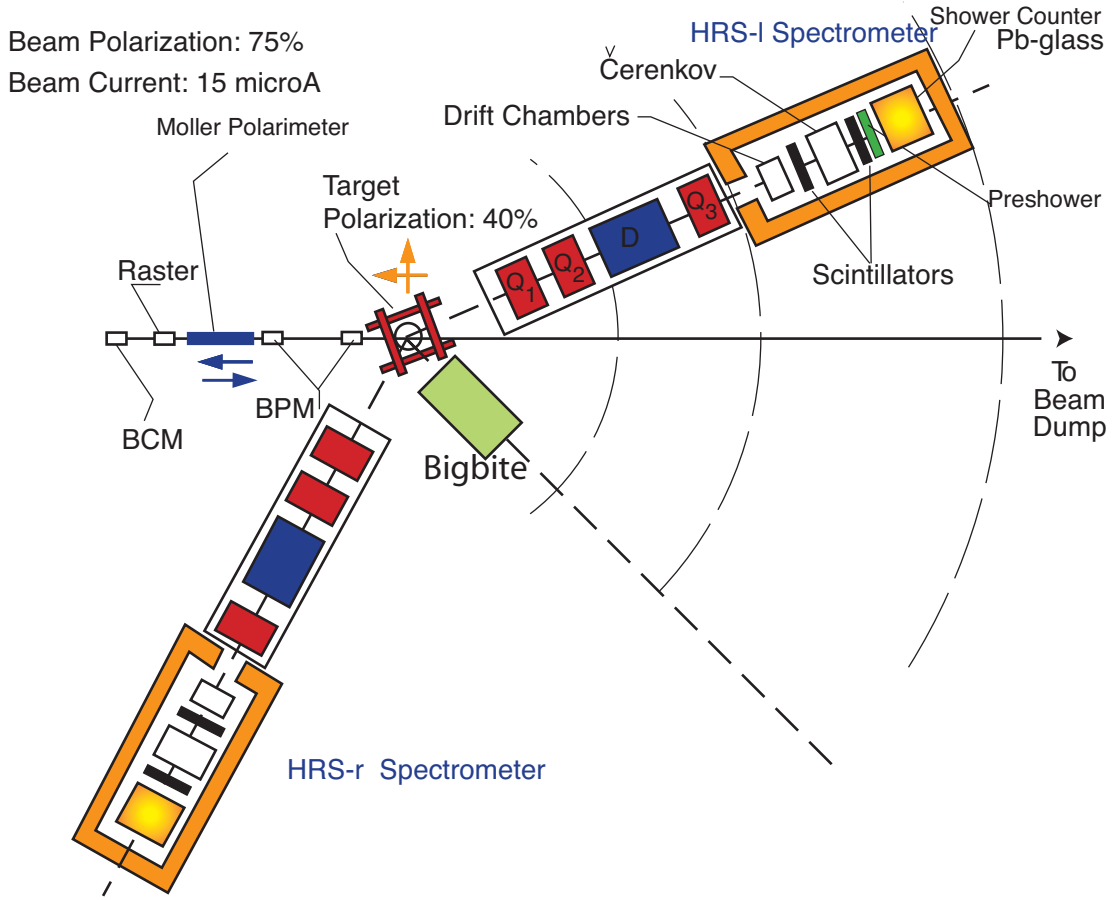
Figure 11: JLab Hall A floor setup using the Bigbite, the left HRS spectrometer and the polarized 3He target.

5 Optimization of the d_2^n measurement

The goal of this experiment is to obtain d_2 from a measurement of the unpolarized cross section σ_0 and the parallel $A_\parallel$ and perpendicular $A_\perp$ asymmetries on ^{3}He. Equivalently d_2 is obtained from the measurement of the linear combination of the spin structure functions $g_1(x, Q^2)$ and $g_2(x, Q^2)$ and forming the second moment of this combination:

$$d_2(Q^2) = \int_0^1 x^2 [2g_1(x, Q^2) + 3g_2(x, Q^2)]\ dx = \int_0^1 \tilde{d}_2(x, Q^2)\ dx \tag{13}$$

The spin structure functions can be expressed in terms of asymmetries and unpolarized cross sections as follow;

$$g_1 = \frac{MQ^2}{4\alpha^2} \frac{y}{(1-y)(2-y)} 2\sigma_0 \left[A_\parallel + \tan\frac{\theta}{2} A_\perp \right] \tag{14}$$

$$g_2 = \frac{MQ^2}{4\alpha^2} \frac{y^2}{2(1-y)(2-y)} 2\sigma_0 \left[-A_\parallel + \frac{1 + (1-y)\cos\theta}{(1-y)\sin\theta} A_\perp \right] \tag{15}$$

where σ_0 is the unpolarized cross section, Q^2 is the four momentum transfer, α the electromagnetic coupling constant, θ the scattering angle and $y = (E - E')/E$ the fraction of energy transferred to the target. $A_\parallel$ and $A_\perp$ are the parallel and perpendicular asymmetries,

$$A_\parallel = \frac{\sigma^{\downarrow\Uparrow} - \sigma^{\uparrow\Uparrow}}{2\sigma_0}, \qquad A_\perp = \frac{\sigma^{\downarrow\Rightarrow} - \sigma^{\uparrow\Rightarrow}}{2\sigma_0} \tag{16}$$

From (12), (13) and (14) we can express the integrand of d_2 directly in terms of measured asymmetries and unpolarized cross section as follows:

$$\begin{aligned} \tilde{d}_2(x, Q^2) &= x^2[2g_1(x, Q^2) + 3g_2(x, Q^2)] \tag{17} \\ &= \frac{MQ^2}{4\alpha^2} \frac{x^2 y^2}{(1-y)(2-y)} \sigma_0 \left[\left(3\frac{1 + (1-y)\cos\theta}{(1-y)\sin\theta} + \frac{4}{y}\tan\frac{\theta}{2}\right) A_\perp + \left(\frac{4}{y} - 3\right) A_\parallel \right] \tag{18} \end{aligned}$$

The above expression of the integrand is used for the following purposes:

- Determination of the time sharing between the transverse and the longitudinal measurement to minimize the statistical error on d_2 not on g_2 as in previous experiments.

- Determination of the effect of the target polarization orientation misalignment on the systematic error of d_2

- Determination of the systematic error on d_2 due to the systematic errors of the cross section and asymmetries measurements.

The measurement consists of collecting data at one incident energy, $E_i = 5.7$ GeV, and one scattering scattering angle, $\theta = 45°$, on both the Bigbite spectrometer and the left HRS spectrometer. In the case of the left HRS spectrometer nine momentum settings allow to cover the range $0.23 \leq x \leq 0.65$ for a cross section measurement of electron scattering. The positron rate will be measured starting from the lowest x bins until it becomes negligible as x becomes larger.

The measured raw ^{3}He counting parallel asymmetry $\Delta_\parallel$ and perpendicular asymmetry $\Delta_\perp$ are converted to the experimental asymmetries $A_\parallel^{^3He}$, and $A_\perp^{^3He}$ respectively, using the relation

$$A_\perp^{^3He} = \frac{\Delta_\perp}{P_b P_t \cos\phi} \qquad\qquad A_\parallel^{^3He} = \frac{\Delta_\parallel}{P_b P_t} \tag{19}$$

$$\Delta_\perp = \frac{(N^{\uparrow\Rightarrow} - N^{\uparrow\Rightarrow})}{(N^{\uparrow\Rightarrow} + N^{\uparrow\Rightarrow})} \qquad\qquad \Delta_\parallel = \frac{(N^{\downarrow\Uparrow} - N^{\uparrow\Uparrow})}{(N^{\downarrow\Uparrow} + N^{\uparrow\Uparrow})} \tag{20}$$

where $N^{\uparrow\Downarrow}$ ($N^{\uparrow\Uparrow}$) and $N^{\uparrow\Rightarrow}$ ($N^{\uparrow\Rightarrow}$) represent the rate of scattered electrons for each bin in x and Q^2 when the electron beam helicity and target spin are parallel or perpendicular. ϕ is the angle between the scattering plane and the plane formed by the incoming beam and the perpendicular target polarization. $P_b = 0.75$ and $P_t = 0.40$ are the beam and target polarization respectively. The target length (40 cm) is chosen such that no extra dilution of the asymmetry occurs from unpolarized scattering off the glass windows. However, empty target measurements will be performed to insure that no spurious unpolarized background originating in the target area reduces the measured physics asymmetries. The kinematics and electron rates are presented in Table 2. We used the Whitlow 1990 [64] parametrization of unpolarized structure functions from measurements of deep inelastic scattering on the proton and the deuteron. We added incoherently the appropriate structure functions to generate the ^{3}He cross sections. The rates were determined assuming a solid angle

evaluated from the bins shown in Fig. 7 and a luminosity of about 1×10^{36} cm^{-2}s^{-1}. The times for the transverse and longitudinal measurements were determined by optimizing the time sharing for the best precision on the integrand $\tilde{d}_2$. If we set

$$\alpha = \frac{MQ^2}{4\alpha^2} \frac{x^2 y^2}{(1-y)(2-y)} \sigma_0 \left(3 \frac{1+(1-y)\cos\theta}{(1-y)\sin\theta} + \frac{4}{y}\tan\frac{\theta}{2} \right) \tag{21}$$

$$\beta = \frac{MQ^2}{4\alpha^2} \frac{x^2 y^2}{(1-y)(2-y)} \sigma_0 \left(\frac{4}{y} - 3 \right) \tag{22}$$

The optimum ratio between the parallel and perpendicular counts is

$$N_\parallel = \frac{\beta}{\alpha} N_\perp \tag{23}$$

The total number of counts $N_\perp$ is given by

$$N_\perp = \frac{\alpha(\alpha+\beta)}{P_b^2 P_t^2 f^2 (\Delta \tilde{d}_2)^2} \tag{24}$$

$f = W_1^n / W_1^{^3He}$ is the fraction of scattering originating from the neutron compared to ^{3}He. We required an absolute statistical uncertainty on the integrand $\Delta \tilde{d}_2^n = 3 \times 10^{-3}$. This in turn leads to an absolute statistical precision on d_2^n of $\Delta d_2^n \approx 5.4 \times 10^{-4}$. The total error expected expected to be about $\Delta d_2^n \approx 7.5 \times 10^{-4}$, a 4-fold improvement over the world $\Delta d_2^n = 2.8 \times 10^{-3}$ of SLAC E155X combined with JLab E99-117.

The charged pion background was estimated using the EPC program [65] which was normalized against measurements carried at JLab in a similar kinematic range. The results of the estimate show that π/e^- ratio ranges from a negligible value in the highest x bin to a value of about 500 in the lowest x bin. Given the combined pion rejection performance of the Cherenkov and lead glass calorimeter, we should be able to keep this correction at a negligible level. Furthermore, we shall also measure the pion asymmetry using the left HRS spectrometer in the lowest two or three x bins.

The radiative corrections (RC) will be performed in two stages. First, the internal corrections will be evaluated following the procedure developed by Bardin and Shumeiko[66] for the unpolarized case and extended to the spin dependent lepto-production cross sections by Akushevish and Shumeiko[67, 68]. Second, using these internally corrected cross sections, the external corrections (for thick targets) are applied by extending the procedure developed for the unpolarized cross sections by Tsai[69, 70] with modifications appropriate for this experiment.

To evaluate the experimental systematic uncertainty of d_2^n we used relative uncertainties in the cross sections and asymmetries achieved in JLab E94-010, E97-103 and E99-117. Table 5 summarizes these uncertainties. One item of concern was the effect of the target relative spin misalignment between the transverse and longitudinal direction measurements. Fig. 12 shows this effect at each value of x on the integrand of d_2. A relative error of 0.5° in the relative direction of the transverse versus perpendicular results in a relative error $\Delta d_2/d_2 = 0.15\%$. Using the Weigel et al. [40] model of g_2 and g_1 we estimated $\Delta d_2/d_2$ to be of the order of 10 % and thus an absolute systematic uncertainty of about 10^{-3}. We believe we can achieve a relative error of 0.2° in the target spin alignment.

With our improved projected statistical precision the total uncertainty in d_2^n is is almost equally shared between the statistical and the systematic accuracy of the measurement.

An elastic scattering asymmetry measurement is planned at low energy ($E_i = 1.2$ GeV, $\theta = 20°$) using the HRS left spectrometer in order to calibrate our spin dependent absolute cross sections.

Table 1: List of the systematic error contributions to d_2^n

| Item description	Subitem description	Relative uncertainty
Target polarization		4 %
Beam polarization		3 %
Asymmetry (raw)		
	• Target spin direction $(0.5°)$	$\approx 1.5 \times 10^{-3}$
	• Beam charge asymmetry	200 ppm
Cross section (raw)		
	• PID efficiency	≈ 1 %
	• Background Rejection efficiency	≈ 1 %
	• Beam charge	< 1 %
	• Beam position	< 1 %
	• Acceptance cut	2-3 %
	• Target density	2-3 %
	• Nitrogen dilution	2-3 %
	• Dead time	<1 %
	• Finite Acceptance cut	<1%
Radiative corrections		≤ 10 %
From ^{3}He to Neutron correction		5 %
Total effect		≤ 10 %
Estimate of contributions	$\int_{0.003}^{0.23} \tilde{d}_2^n \ dx$	4.8×10^{-4}
from unmeasured regions	$\int_{0.70}^{0.999} \tilde{d}_2^n \ dx$	5.0×10^{-5}
Projected absolute statistical uncertainty		$\Delta d_2 \approx 5.4 \times 10^{-4}$
Projected absolute systematic uncertainty assuming $d_2 = 5 \times 10^{-3}$		$\Delta d_2 \approx 5 \times 10^{-4}$
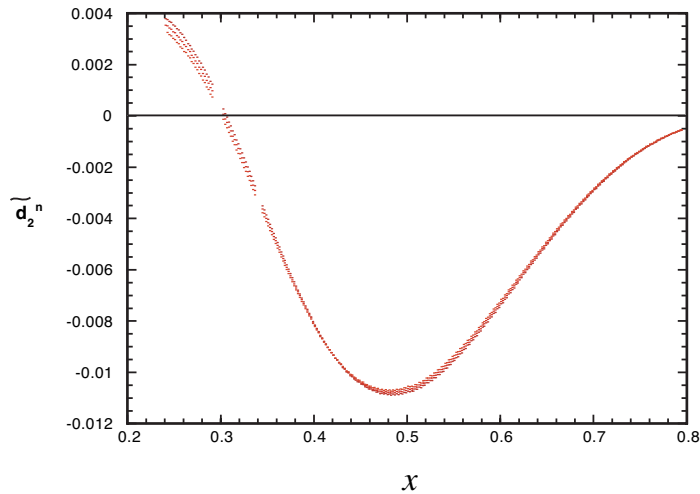
Figure 12: Effect of target relative spin misalignment by $0.5°$ between the transverse and longitudinal measurements

This quantity can be evaluated using the measured electric and magnetic form factors of ^{3}He. This measurement would actually determine the polarization of the ^{3}He nuclei along the electron beam path. This kinematics is matched to the previously taken elastic measurements in E99-117. False asymmetries will be checked to be consistent with zero by comparing data with target spins in opposite directions.

Also contributing to the dilution of the asymmetry is the pair-electron contamination. This correction is x dependent, and is relevant only in the low x region. This contamination was estimated to be no more than 6% in the worst case and will be measured in this experiment by reversing the spectrometer polarity on the left arm spectrometer.

Bigbite and the left HRS spectrometer will be used in a symmetric configuration at $45°$ when taking the data. While Bigbite will be used to take the bulk of asymmetry data for a total of 267 hours of beam on target the left HRS spectrometer will be used to measure the absolute cross sections at different x values, the pion contamination and the positron production cross section by reversing its polarity. Tables 2 shows the momentum settings of the left spectrometer and relevant kinematic parameters with the rates for each x bin of the BigBite spectrometer. We will use Bigbite and HRS-l for 270 hours with beam on target at 5.7 GeV incident beam energy. Measurements of the target polarization will be taken once each shift.

6   Spin Structure Functions: From ^{3}He to the Neutron

Because the deuteron polarization is shared roughly equally between the proton and neutron, extraction of neutron spin structure functions requires a precise knowledge of the proton spin structure, in addition to the nuclear effects [71]. This problem is compounded by the fact that the spin-dependent structure functions of the proton are typically much larger than those of the neutron, making extraction of the latter especially sensitive to small uncertainties in the proton structure functions. In ^{3}He, however, since the neutron carries almost 90% of the nuclear spin

Table 2: Parameters per bin in (Q^2,x) plane for the proposed experiment. Note that it is a single spectrometer setting for BigBite but different central momentum settings for the HRS_L.

E_i (GeV)	bin central p (GeV)	x	Δx	Q^2 (GeV^2)	W (GeV)	Rate (Hz)		
5.700	1.603	.696	.969E-01	5.35	1.79	0.90		
5.700	1.450	.607	.814E-01	4.84	2.00	1.5		
5.700	1.312	.532	.691E-01	4.38	2.18	2.1		
5.700	1.187	.468	.591E-01	3.96	2.32	2.7		
5.700	1.074	.413	.509E-01	3.59	2.44	3.1		Single
5.700	0.971	.324	.440E-01	3.24	2.55	3.5		Spectrometer
5.700	0.878	.365	.383E-01	2.93	2.65	3.8		Setting
5.700	0.794	.288	.335E-01	2.65	2.73	3.9		
5.700	0.718	.256	.293E-01	2.40	2.80	4.1		
5.700	0.650	.229	.259E-01	2.17	2.86	4.1		
							Time$_\perp$ hours	Time$_\parallel$ hours
Total							257	10

making polarized ^{3}He an ideal source of polarized neutrons.

The three-nucleon system has been studied for many years, and modern three-body wave functions have been tested against a large array of observables which put rather strong constraints on the nuclear models [72]. In particular, over the past decade considerable experience has been acquired in the application of three-body wave functions to deep-inelastic scattering [73, 74, 75].

The conventional approach employed in calculating nuclear structure functions in the region $0.3 < x < 0.8$ is the impulse approximation, in which the virtual photon scatters incoherently from individual nucleons in the nucleus [76]. Corrections due to multiple scattering, NN correlations or multi-quark effects are usually confined to either the small-x $(x < 0.2)$, or very large-x $(x > 0.9)$ regions. In the impulse approximation the g_1 structure function of ^{3}He, in the Bjorken limit $(Q^2, \nu \to \infty)$, is obtained by folding the nucleon structure function with the nucleon momentum distribution Δf_N $(N = p, n)$ in ^{3}He:

$$g_1^{^3\text{He}}(x) \;=\; \int_x^3 \frac{dy}{y} \; \{2\Delta f_p(y)\; g_1^p(x/y) \;+ \Delta f_n(y)\; g_1^n(x/y)\}, \qquad (25)$$

where y is the fraction of the ^{3}He momentum carried by the nucleon, and the dependence on the scale, Q^2, has been suppressed. The nucleon momentum distributions $\Delta f_N(y)$ are calculated from the three-body nuclear wave function, which are obtained by either solving the Faddeev equation [77] or using variational methods [74], and are normalized such that:

$$\int_0^3 dy \; \Delta f_N(y) \;=\; \rho_N , \qquad (26)$$

where ρ_N is the polarization of the nucleon in ^{3}He. While the full three-body wave function involves summing over many channels, in practice the three lowest states, namely the S, S' and D, account for over 99% of the normalization. Typically, one finds $\rho_n \approx 87\%$ and $\rho_p \approx -2\%$ [72, 73, 74, 75, 77].

The smearing in Eq.(25) incorporates the effects of Fermi motion and nuclear binding. Correctly accounting for these effects is important when attempting to extract information on nucleon structure functions from nuclear data at $x > 0.6$, as well as for determining higher moments of structure functions, in which the large-x region is more strongly weighted.

The nuclear corrections to the g_2^n structure function can be evaluated analogously to those for g_1^n. One can estimate the order of magnitude of the effects by considering firstly the twist-2 part of g_2^n, which is determined from g_1^n through the Wandzura-Wilczek relation [36, 80]:

$$g_2^{^3\text{He}}(x)\Big|_{\text{tw}-2} = -g_1^{^3\text{He}}(x) + \int_x^3 \frac{dy}{y}\, g_1^{^3\text{He}}(x/y)\ , \tag{27}$$

where $g_1^{^3\text{He}}$ is given by Eq.(25). The main effect numerically at moderate to large x is due to the difference between the neutron and ^{3}He polarizations, as the effects due to smearing peaks at the level of a few percent at $x \sim 0.6$. Similarly, the difference in the second moments of $g_2^{^3\text{He}}$ between the convolution results using different ^{3}He wave functions is a few percent [68,69]. Moreover, since the main objective of the experiment is to extract the second moment of $3g_2^n + 2g_1^n$, namely $\int dx\, x^2(3g_2^n(x)+2g_1^n(x))$, the sensitivity of the correction to x variations of the integrand is reduced compared to a direct extraction of the g_2 or g_1 structure functions themselves.

While the nuclear model dependence of the nuclear correction appears to be relatively weak for the twist-2 approximation in the Bjorken limit, an important question for the kinematics relevant to this experiment is how are these effects likely to be modified at finite Q^2? To address this question one needs to obtain generalizations of Eqs. (25) and (27) which are valid at any Q^2, and which can incorporate the twist-3 component of g_2. In fact, at finite Q^2 one finds contributions from g_1^N to $g_2^{^3\text{He}}$, and from g_2^N to $g_1^{^3\text{He}}$. The latter vanish in the Bjorken limit, but the former are finite, although they depend on the Fermi momentum of the bound nucleons. These corrections can be calculated by working directly in terms of the (unintegrated) spectral function $S(\vec{p}, E)$, where p is the bound nucleon momentum and E is the separation energy, rather than in terms of the momentum distribution functions $\Delta f_N(y)$. Following Schulze & Sauer [75], it is convenient to parameterize the ^{3}He spectral function according to:

$$S(\vec{p}, E) = \frac{1}{2}\left(f_0 + f_1 \vec{\sigma}_N \cdot \vec{\sigma}_A + f_2\left[\vec{\sigma}_N \cdot \hat{p}\, \vec{\sigma}_A \cdot \hat{p} - \frac{1}{3}\vec{\sigma}_N \cdot \vec{\sigma}_A\right]\right)\ , \tag{28}$$

where $\vec{\sigma}_N$ and $\vec{\sigma}_A$ are the spin operators of the nucleon and ^{3}He, respectively, and the functions $f_{0,1,2}$ are scalar functions of $|\vec{p}|$ and E. The function f_0 contributes to unpolarized scattering only, while f_1 and f_2 determine the spin-dependent structure functions. In terms of these functions, at finite Q^2 one has a set of coupled equations for $g_1^{^3\text{He}}$ and $g_2^{^3\text{He}}$ [82]:

$$xg_1^{^3\text{He}}(x, Q^2) + (1 - \gamma^2)xg_2^{^3\text{He}}(x, Q^2)$$
$$= \sum_{N=p,n}\int d^3p\, dE\, (1 - \frac{\epsilon}{M})\left\{\left[\left(1 + \frac{\gamma p_z}{M} + \frac{p_z^2}{M^2}\right)f_1 + \left(-\frac{1}{3} + \hat{p}_z^2 + \frac{2\gamma p_z}{3M} + \frac{2p_z^2}{3M^2}\right)f_2\right]zg_1^N(z, Q^2)\right.$$
$$\left. + (1 - \gamma^2)(1 + \frac{\epsilon}{M}\left[f_1 + \left(\frac{p_z^2}{\vec{p}^2} - \frac{1}{3}\right)f_2\right]\frac{z^2}{x}g_2^N(z, Q^2)\right\}\ , \tag{29}$$

$$xg_1^{^3\text{He}}(x, Q^2) + xg_2^{^3\text{He}}(x, Q^2)$$
$$= \sum_{N=p,n}\int d^3p\, dE\, (1 - \frac{\epsilon}{M})\left\{\left[\left(1 + \frac{p_x^2}{M^2}\right)f_1 + \left(\vec{p}_x^2 - \frac{1}{3} + \frac{2p_x^2}{3M^2}\right)f_2\right]zg_1^N(z, Q^2)\right.$$
$$\left. + \left[\left(1 + \frac{p_x^2}{M^2}(1 - z/x)\right)f_1 + \left(\vec{p}_x^2 - \frac{1}{3} + \frac{2p_x^2}{3M^2}(1 - z/x) - \frac{\gamma p_z \hat{p}_x^2}{M}\frac{z}{x}\right)f_2\right]zg_2^N(z, Q^2)\right\}\ , \tag{30}$$

with $\gamma = \sqrt{1+4M^2x^2/Q^2}$ a kinematical factor parameterizing the finite Q^2 correction, $\epsilon \equiv \vec{p}^{\,2}/4M - E$, and $z = x/(1+(\epsilon+\gamma p_z)/M)$. Equations (29) and (30) can then be solved to obtain $g_1^{3\text{He}}$ and $g_2^{3\text{He}}$ explicitly. For $Q^2 \to \infty$ Eqs. (29) and (30) reduce to simple one-dimensional convolution expressions, as in Eq. (25). At finite Q^2, however, the smearing function effectively becomes x and Q^2 dependent, so that the amount of smearing in general will depent on the shape of the nucleon structure functions.

The nuclear correction of most interest for this experiment is that to the g_2 structure function. One can test the sensitivity to the kinematical Q^2 dependence, as distinct from the Q^2 dependence in the nucleon structure function itself, by taking the same input neutron structure function for all values of Q^2 at which $xg_2^{3\text{He}}$ is evaluated. One finds [82] that the effect of the kinematical Q^2 dependence turns out to be rather small at $Q^2 \sim 1$–4 GeV^2, and only becomes noticable for low $Q^2 \sim 0.2$ GeV^2. Furthermore, at these values of Q^2 the g_1^n contribution to $g_2^{3\text{He}}$ is negligible compared with the lowest order neutron polarization correction. This confirms earlier analyses of the nuclear corrections by the Rome-Perugia group [83].

There was also an investigation in Ref. [81] into the role of the $\Delta(1232)$ in deep-inelastic scattering on polarized ^{3}He and its effects on the g_1 neutron spin structure function extraction. The authors estimated that when taking the effect of the Δ into account the values of the first moment of g_1^n increases by 6 - 8 %.

In summary, all of the nuclear structure function analyses that have been performed suggest that both the neutron g_1^n and g_2^n deep-inelastic structure functions can be extracted from ^{3}He data with minimal uncertainties associated with nuclear corrections. Estimating all the corrections and their uncertainties we come to the conclusion that in this experiment the statistical error on the final result is still the dominant error.

7 Summary and Beam Request

In summary, we propose to carry out a precision determination of d_2^n. We will determine asymmetries in the region $(0.23 \le x \le 0.65)$ (see Fig 13 and Fig. 14) from a measurement using a high pressure polarized ^{3}He target ($P_t = 40\%$) and the highest available energy (5.7 GeV) of the polarized beam ($P_b = 75\%$). This measurement requires 257 hours of beam on target for the measurement of the transverse asymmetry and 10 hours for the measurement of the longitudinal asymmetry, along with 48 hours for the beam energy change, elastic scattering calibration, nitrogen dilution, and beam and target polarization measurements. We therefore request a total of 312 hours (13 days) of beam time to achieve a total uncertainty on d_2^n of $\Delta d_2^n \approx 7.4 \times 10^{-4}$ at $Q^2 \approx 3.0$ GeV^2.
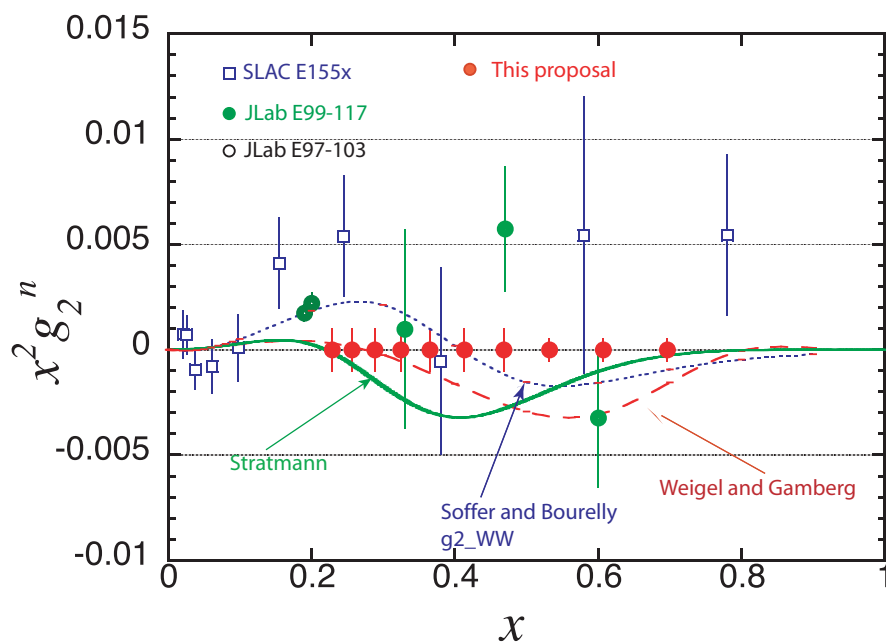
Figure 13: Same as Fig.5. The solid circles along the x axis show the anticipated statistical accurary of this proposed measurement.
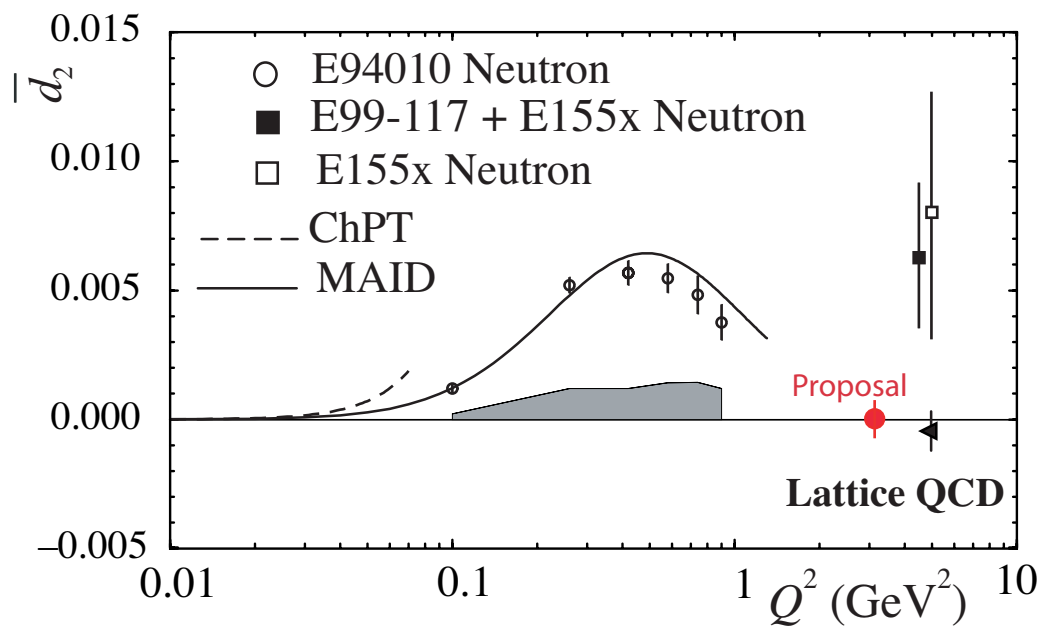

Figure 14: Top panel:d_2^n projected results at $<Q^2> = 3$ GeV^2 from this proposal compared to JLab E94-010, SLAC E155X and SLACE155X combined with JLab E99-117.

References

[1] E. Shuryak and A. Vainshtein, Nuc. Phys. B **201** (1982) 141.

[2] R. L. Jaffe and X. Ji, Phys. Rev. D **43** (1991) 724.

[3] B. W. Filippone and X. Ji, Adv. in Nucl. Phys. **26**, 1 (2001).

[4] S. Wandzura and F. Wilczek, Phys. Lett. B **72**, 195 (1977).

[5] E. Stein, P. Gornicki, L. Mankiewicz and A. Schäfer, Phys. Lett. B 353, 107 (1995).

[6] X. Ji, arXiv:hep-ph/9510362.

[7] X. Ji and P. Unrau, Phys. Lett. B **333** (1994) 228.

[8] X. Ji Nucl. Phys. **B402** (1993) 217.

[9] S. A. Larin, T. van Ritbergen and J.A. Vermaseren, Phys. Lett. **404**, 153 (1997); S. A. Larin, Phys. Lett. B **334**, 192 (1994).

[10] F. E. Close and R. G. Roberts, Phys. Lett. B **336**, 257 (1994).

[11] X. Ji and W. Melnitchouk, Phys. Rev. D **56**, 1 (1997).

[12] J. Edelmann, G. Piller, W. Weise, N. Kaiser, Nucl. Phys. A **665** (2000) 125.

[13] S. Simula, M. Osipenko, G. Ricco and M. Tauiti, hep/0205118 and references therein.

[14] M. Osipenko *et al.*, Phys. Lett. B **609**, 259 (2005) [arXiv:hep-ph/0404195].

[15] Z. E. Meziani *et al.*, Phys. Lett. B **613**, 148 (2005) [arXiv:hep-ph/0404066].

[16] X. Ji, in Proceeding of the Workshop on Deep Inelastic scattering and QCD, Editors: JF. Laporte et Y. Sirois Paris, France, 24-28 April, 1995 (ISBN 2-7302-0341-4).

[17] P. L. Anthony *et al.* [E155 Collaboration], Phys. Lett. B **458**, 529 (1999) [arXiv:hep-ex/9901006].

[18] H. Burkhardt and W. N. Cottingham, Ann. Phys. **56** (1970) 453.

[19] R. Jaffe, Comments Nucl. Part. Phys. 19 (1990) 239.

[20] I. P. Ivanov *et al.*, Phys. Rep. **320**, 175 (1999).

[21] M. Anselmino, A. Efremov and E. Leader, Phys. Rep. **261**, 1 (1995).

[22] G. Altarelli, B. Lampe, P. Nason and G. Ridolfi, Phys. Lett. B **334**, 187 (1994).

[23] M. Amarian *et al.*, Phys. Rev. Lett. **89**, 242301 (2002).

[24] M. Amarian *et al.*, Phys. Rev. Lett. **92**, 022301 (2004).

[25] D. Adams *et al.*, Phys. Lett. **B336** (1994) 125.

[26] P. L. Anthony *et al.*, Phys. Rev. Lett. **71** (1993) 959.

[27] P. L. Anthony *et al.*, Phys. Rev. D **54** (1996) 6620.

[28] K. Abe *et al.*, Phys. Rev. Lett. **76** (1996) 587.

[29] K. Abe *et al.*, Phys. Lett. B **404** (1997) 377.

[30] P. L. Anthony *et al.*, Phys. Lett. B**458** (1999) 529.

[31] P. L. Anthony *et al.* [E155x Collaboration], Phys. Lett. B **553**, 18 (2003) [arXiv:hep-ex/0204028].

[32] X. Zheng *et al.* [Jefferson Lab Hall A Collaboration], Phys. Rev. C **70**, 065207 (2004) [arXiv:nucl-ex/0405006].

[33] X. Ji and W. Melnitchouk, Private communication

[34] K. Kramer *et al.*, Phys. Rev. Lett. **95**, 142002 (2005) [arXiv:nucl-ex/0506005].

[35] K. Abe *et al.*, Phys. Rev. D **58** (1998) 112003-1.

[36] S. Wandzura and F. Wilczek, Phys. Lett. B **72** (1977) 195.

[37] JLab E01-012 experiment, Spokespeople N. Liyanage, J. P. Chen and Seonho Choi.

[38] JLab E01-006 experiment, Spokesperson O. Rondon and M. Jones

[39] JLab SANE experiment, Spokespersons: O. Rondon, Z.-E. Meziani and Seonho Choi.

[40] H. Weigel, L. Gamberg, H. Reinhart, Phys. Rev. D**55** (1997) 6910.

[41] M. Wakamatsu, Phys. Lett B **487** (2000) 118.

[42] M. Stratmann, Z. Phys. C **60** (1993) 763.

[43] X. Song, Phys. Rev. D **54** (1996) 1955.

[44] E. Stein, Phys. Lett. B **343** (1995) 369.

[45] B. Ehrnsperger, A Schäfer, Phys. Rev. D **52** (1995) 2709.

[46] I. Balitsky, V. Barun, A. Kolesnichenko, Phys. Lett. B **242** (1990) 245; B **318** (1995) 648 (E).

[47] M. Gockeler *et al.*, Phys. Rev. D **72**, 054507 (2005) [arXiv:hep-lat/0506017].

[48] M. Gockeler *et al.*, Phys. Rev. D **63**, 074506 (2001), [hep-lat/0011091].

[49] R. G. Edwards *et al.* [LHPC Collaboration], Private communication

[50] C. R. V. Bourrely, J. Soffer and F. Buccella, Eur. Phys. J. C **41**, 327 (2005) [arXiv:hep-ph/0502180].

[51] D. Drechsel, S. Kamalov and L. Tiator, Phys. Rev. D **63**, 114010 (2001).

[52] C. W. Kao, T. Spitzenberg and M. Vanderhaeghen, Phys. Rev. D **67**, 016001 (2003).

[53] J. Alcorn *et al.*, Nucl. Instrum. Meth. A **522**, 294 (2004).

[54] W. Xu *et al.*, Phys. Rev. Lett. **85**, 2900 (2000) [arXiv:nucl-ex/0008003].

[55] M.A. Bouchiat, T.R. Carver and C.M. Varnum, Phys. Rev. Lett. **5** (1960) 373.

[56] N.D. Bhaskar, W. Happer, and T. McClelland, Phys. Rev. Lett. **49** (1982) 25.

[57] W. Happer, E. Miron, S. Schaefer, D. Schreiber, W.A. van Wijngaarden, and X. Zeng, Phys. Rev. A **29** (1984) 3092.

[58] T.E. Chupp, M.E. Wagshul, K.P. Coulter, A.B. McDonald, and W. Happer, Phys. Rev. C **36** (1987) 2244.

[59] K.P. Coulter, A.B. McDonald, W. Happer, T. E. Chupp, and M.E. Wagshul, Nuc. Inst. Meth. in Phys. Res. **A 270** (1988) 90.

[60] N.R. Newbury, A.S. Barton, P. Bogorad, G. D. Cates, M. Gatzke, H. Mabuchi, and B. Saam, Phys. Rev. A **48** (1993) 558.

[61] K.P. Coulter, A.B. McDonald, G.D. Cates, W. Happer, T.E. Chupp, Nuc. Inst. Meth. in Phys. Res. A**276** (1989) 29 .

[62] A. Abragam, Principles of Nuclear Magnetism (Oxford University Press, New York, 1961).

[63] G. Cates, B. Reitz and B. Wojtsekhowski, Jefferson Lab experiment E02-013:" Measurement of the Neutron Electric Form Factor G_E^n at High Q^2" (2002).

[64] L. Whitlow, SLAC-report-357 (1990).

[65] J. W. Lightbody Jr. and J.S. O'Connell, Computers in Physics **2** (1988) 57.

[66] D. Yu. Bardin and N. M. Shumeiko, Nucl. Phys. B **127** (1977) 1251.

[67] T.V. Kuchto and N. M. Shumeiko, Nucl. Phys. B **219** (1983) 412.

[68] I. V. Akushevich and N. M. Shumeiko, J. Phys. **G**: Nucl. Part. Phys. **20** (1994) 513.

[69] L. W. Mo and Y. S. Tsai, Rev. Mod. Phys. **41** (1969) 205.

[70] Y. S. Tsai, SLAC-PUB-848 (1971).

[71] W. Melnitchouk, G. Piller and A.W. Thomas, Phys. Lett. B **346** (1995) 165; S. A Kulagin, W. Melnitchouk, G. Piller and W. Weise Phys. Rev. C **52** (1995) 932.

[72] J.L. Friar et al., Phys. Rev. C **42** (1990) 2310.

[73] R.M. Woloshyn, Nucl. Phys. A **496** (1989) 749.

[74] C. Ciofi degli Atti, E. Pace and G. Salme, Phys. Rev. C **46** (1992) R1591; C. Ciofi degli Atti, S. Scopetta, E. Pace, G. Salme, Phys. Rev. C **48** (1993) 968;

[75] R.W. Schulze and P.U. Sauer, Phys. Rev. C **48** (1993) 38.

[76] D.F. Geesaman, K. Saito and A.W. Thomas, Ann. Rev. Nucl. Part. Sci. **45** (1995) 337.

[77] I.R. Afnan, F. Bissey and A.W. Thomas, Phys. Rev. C**64** (2001) 024004.

[78] E. Leader, A.V. Sidorov and D.B. Stamenov, Int. J. Mod. Phys. A **13** (1998) 5573; Phys. Rev. D **58** (1998) 114028.

[79] I.R. Afnan, F. Bissey, J. Gomez, A.T. Katramatou, W. Melnitchouk, G.G. Petratos and A.W. Thomas, Phys. Lett. B **493** (2000) 36.

[80] F. Bissey, W. Melnitchouk, A. W. Thomas, in preparation.

[81] C. Boros, V. Guzey, M. Strikman, A.W. Thomas, Phys. Rev. **D64** (2001) 014025 and hep-ph/0008064.

[82] S.A. Kulagin and W. Melnitchouk, in preparation.

[83] S. Scopetta, private communication.

Jefferson Lab PAC24
Proposal Cover Sheet

Experimental Hall: _____A_____

Days Requested for Approval: ___28___

❐ Proposal Title:

Measurement of the Neutron d$_2$: Towards the Electric χ_E and Magnetic χ_B Color Polarizabilities

Proposal Physics Goals
Indicate any experiments that have physics goals similar to those in your proposal.

Approved, Conditionally Approved, and/or Deferred Experiment(s) or proposals:

E94-010, E97-103, E99-117, E01-012 and E01-006

Contact Person
Name: Zein-Eddine Meziani
Institution: Temple University
Address: Department of Physics, Barton Hall A323
Address: 1900 North 13th Street
City, State, ZIP/Country: Philadelphia, PA, 19122/USA
Phone: (215) 204-5971   Fax: (215) 204-2569
E-Mail: meziani@temple.edu

BEAM REQUIREMENTS LIST

JLab Proposal No.: _____ Date: ___04/28/2003

Hall: ___A___ Anticipated Run Date: _____ PAC Approved Days: _____

Spokesperson: __S. Choi, X. Jiang, Z.-E. Mezianini__ Hall Liaison: _____J. P. Chen_____
Phone: _____(215) 204 5971_____
E-mail: ___meziani@temple.edu_____

List all combinations of anticipated targets and beam conditions required to execute the experiment.
(This list will form the primary basis for the Radiation Safety Assesment Document (RSAD) calculations that
must be performed for each experiment.)

Condition No.	Beam Energy (MeV)	Mean Beam Current (μA)	Polarization and Other Special Requirements (e.g., time structure)	Target Material (use multiple rows for complex targets — e.g., w/windows)	Material Thickness (mg/cm²)	Est. Beam-On Time for Cond. No. (hours)
1	6000.	15.	Polarization 80%	^{3}He	50	106
	6000.	15.		Glass window	44	
2	5700.	15.	Polarization 80%	^{3}He	50	512
	5700.	15.		Glass window	44	

The beam energies, E_{Beam}, available are: $E_{Beam} = N \times E_{Linac}$ where N = 1, 2, 3, 4, or 5. E_{Linac} = 800 MeV, i.e.,
available E_{Beam} are 800, 1600, 2400, 3200, and 4000 MeV. Other energies should be arranged with the
Hall Leader before listing.

HAZARD IDENTIFICATION CHECKLIST

JLab Proposal No.: _____ Date: _____04/28/2003_____

Check all items for which there is an anticipated need.

Cryogenics
_____ beamline magnets
_____ analysis magnets
_____ target
type: _____
flow rate: _____
capacity: _____

Electrical Equipment
_____ cryo/electrical devices
_____ capacitor banks
_____ high voltage
_____ exposed equipment

Radioactive/Hazardous Materials
List any radioactive or hazadorous/toxic materials planned for use:
_____
_____
_____
_____

Pressure Vessels
_19 mm_ inside diameter
13 atm operating pressure
Glass window material
_~100 μm_ window thickness

Flammable Gas or Liquids
type: _____
flow rate: _____
capacity: _____

Drift Chambers
type: _____
flow rate: _____
capacity: _____

Other Target Materials
___ Beryllium (Be)
___ Lithium (Li)
___ Mercury (Hg)
___ Lead (Pb)
___ Tungsten (W)
___ Uranium (U)
_X_ Other (list below)
___^{3}He, N$_2$ and Rb___
_____

Vacuum Vessels
_____ inside diameter
_____ operating pressure
_____ window material
_____ window thickness

Radioactive Sources
_____ permanent installation
_____ temporary use
type: _____
strength: _____

Large Mech. Structure/System
_____ lifting devices
_____ motion controllers
_____ scaffolding or
_____ elevated platforms

Lasers
type: _Laser diode system_
wattage: _7x30 W_
class: _IV_

Installation:
_X_ permanent *
_____ temporary
* for this experiment
Use:
_____ calibration
_____ alignment

Hazardous Materials
____ cyanide plating materials
____ scintillation oil (from)
____ PCBs
____ methane
____ TMAE
____ TEA
____ photographic developers
____ other (list below)
_____
_____

General:

Experiment Class:

_X_ Base Equipment
_____ Temp. Mod. to Base Equip.
_____ Permanent Mod. to Base Equipment
_____ Major New Apparatus

Other: _Polarized ^{3}He target_
with Laser Hut

Computing Requirements List

Proposal Title: __Measurement of the Neutron d2 Matrix Element: Towards__

__the Electric   and Magnetic   Color Polarizabilities__

Spokesperson: __S. Choi, X. Jiang, Z.-E. Meziani__   Experimental Hall: __A__

Raw Data Expected

Total: __3000 GB__   Per Year (long duration experiments only):_____

Simulation Compute Power (SPECint95 hours) Required: __N/A__

On-Line Disk Storage Required: __200 GB__

Imported Data Amount from Outside Institutions: __N/A__

Exported Data Amount to Outside Institutions:w __N/A__

Expected Mechanism for Imported/Exported Data: __N/A__

Special Requirements

For example, special configuration of data acquisition systems) that may require resources and/or coordination with JLab's Computer Center. Please indicate, if possible, what fraction of these resources will be provided by collaborating institutions and how much is expected to be provided by JLab.

_____

_____

_____

_____

_____

Measurement of the Neutron d_2: Towards the Electric χ_E and Magnetic χ_B Color Polarizabilities

X. Zheng
Argonne National Laboratory, Argonne, IL 60439, USA

P. Bertin
Université Blaise Pascal De Clermont-Ferrand, Aubiere 63177, France

J.-P. Chen, E. Chudakov, C. W. de Jager, R. Feuerbach, J. Gomez, J. -O. Hansen,
D.W. Higinbotham, J. LeRose, W. Melnitchouk, R. Michaels, S. Nanda, A. Saha, B. Reitz,
B. Wojtsekhowski
Jefferson Lab, Newport News, VA 23606, USA

S. Frullani, F. Garibaldi, M. Iodice, G. Urciuoli, F. Cusanno
Istituto Nazionale di Fiscica Nucleare, Sezione Sanità, 00161 Roma, Italy

R. DeLeo, L. Lagamba
Istituto Nazionale di Fiscica Nucleare, Bari, Italy

A.T. Katramatou, G.G. Petratos
Kent State University, Kent, OH 44242

W. Korsch
University of Kentucky, Lexington, KY 40506, USA

W. Bertozzi, Z. Chai, S. Gilad, M. Rvachev, Y. Xiao
Massachusetts Institute of Technology, Cambridge, MA 02139, USA

L. Gamberg
Penn State Berks, Reading, PA, 19610 USA

F. Benmokhtar, R. Gilman, C. Glashausser, K. McCormick,
X. Jiang (co-spokesperson), G. Kumbartzki, R. Ransome
Rutgers University, Piscataway, NJ 08855, USA

Seonho Choi(co-spokesperson), F. Butaru, A. Lukhanin,
Z.-E. Meziani (co-spokesperson), K. Slifer, P. Solvignon, H. Yao
Temple University, Philadelphia, PA 19122, USA

S. Binet, G. Cates, A. Deur, N. Liyanage, J. Singh, A. Tobias
University of Virginia, Charlottesville, VA 22901, USA

T. Averett, J. M. Finn, D. Armstrong, K. Griffioen, K. Kramer, V. Sulkosky, J. Roche
College of William and Mary, Williamsburg, VA 23185, USA

and the

Hall A COLLABORATION

April 28, 2003

Contact: Z.-E. Meziani (meziani@temple.edu)

Abstract

We propose to make a measurement of the spin-dependent scattering cross section for a longitudinally polarized electron beam off a transversely and longitudinally polarized ^{3}He target. This measurement will cover excitation energies across the resonance and deep inelastic regions at constant 4-momentum transfer $Q^2 = 2$ (GeV/c)^2. We will extract the quantity $d_2^n = \int_0^1 x^2(2g_1 + 3g_2)\ dx$ and $\Gamma_2^n = \int_0^1 g_2\ dx$. This measurement will significantly improve the precision of the neutron d_2 world data and test the predictions of several models including the lattice QCD calculation of this quantity. Furthermore, the Burkhardt-Cottingham sum rule will be tested at $Q^2 = 2$ (GeV/c)^2. The quantity d_2^n reflects the response of the color electric and magnetic fields to the polarization of the nucleon. Because d_2^n is a higher moment of structure functions it is dominated by the contributions from the large x region. CEBAF at Jefferson Lab is ideal to perform such a measurement.

1   <u>Introduction and Motivation</u>

In inclusive polarized lepton-nucleon deep-inelastic scattering, one can access two spin-dependent structure functions of the nucleon, g_1 and g_2. While g_1 can be understood in terms of the Feynman parton model which describes the scattering in terms of *incoherent* parton scattering, g_2 cannot. Rather, one has to consider parton correlations initially present in the participating nucleon, and the associated process is given a *coherent* parton scattering in the sense that more than one parton takes part in the scattering. Indeed, using the operator product expansion (OPE) [1, 2], it is possible to interpret the g_2 spin structure function beyond the simple quark-parton model as a higher twist structure function. . As such, it is exceedingly interesting because it provides a unique opportunity to study the quark-gluon correlations in the nucleon which cannot otherwise be accessed.

In a recent review Ji [3] explained that higher-twist processes cannot be cleanly separated from the leading twist because of the so-called infrared renormalon problem first recognized by t' Hooft. This ambiguity arises from separating quarks and gluons pre-existing in the hadron wave function from those produced in radiative processes. Such a separation turns out to be always scheme dependent. Nevertheless, the g_2 structure function is an **exception** because it contributes at the leading order to the spin asymmetry of longitudinally-polarized lepton scattering on transversely-polarized nucleons. Thus, g_2 is among the *cleanest* higher-twist observables.

Why does the g_2 structure function contain information about the quark and gluon correlations in the nucleon? According to the optical theorem, g_2 is the imaginary part of the spin-dependent Compton amplitude for the process $\gamma^*(+1) + N(1/2) \to \gamma^*(0) + N(-1/2)$,

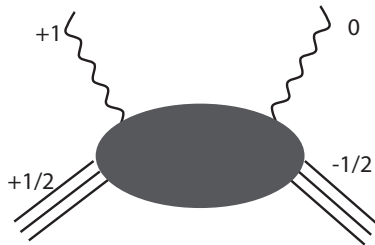Figure 1: Compton amplitude of $\gamma^*(+1) + N(1/2) \to \gamma^*(0) + N(-1/2)$.

where γ^* and N denote the virtual photon and the nucleon, respectively, and the numbers in the brackets are the helicities. Thus this Compton scattering involves the t-channel helicity exchange $+1$. When it is factorized in terms of parton sub-processes, the intermediate partons must carry this helicity exchange. Because of the chirality conservation in vector coupling, massless quarks in perturbative processes cannot produce a helicity flip. Nevertheless, in QCD this helicity exchange may occur in the following two ways (see Fig. 2): first, single quark scattering in which the quark carries one unit of orbital angular momentum through its transverse momentum wave function; second, quark scattering with an additional transversely-polarized gluon from the nucleon target. The two mechanisms are combined in such a way to yield a gauge-invariant result. Consequently, g_2 provides a direct probe of the quark-gluon correlations in the nucleon wave function.

1.1   The twist-three reduced matrix element

The piece of interesting physics we want to focus on in this proposal is contained in the second moment in x of a linear combination of g_1 and g_2, namely

$$d_2(Q^2) \;\; = \;\; \int_0^1 x^2[2g_1(x, Q^2) + 3g_2(x, Q^2)]dx \tag{1}$$
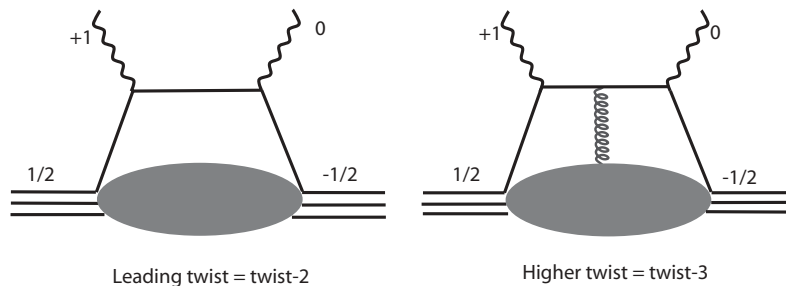
Figure 2: Twist-two and twist-three contributions to virtual Compton scattering

$$= 3 \int_0^1 x^2 \left[g_2(x, Q^2) - g_2^{WW}(x, Q^2) \right] dx$$

where g_2^{WW}, known as the Wandzura-Wilczek [13] term, depends only on g_1

$$g_2^{WW}(x, Q^2) = -g_1(x, Q^2) + \int_x^1 \frac{g_1(y, Q^2)}{y} dy. \tag{2}$$

It is interesting to see that the quantity d_2 also appears in the first moment of g_1 when at large Q^2 ($Q^2 \gg \Lambda_{QCD}^2$) it is expressed in terms of a twist expansion [10, 11]:

$$\Gamma_1(Q^2) = \int_0^1 g_1(Q^2, x) dx = \frac{1}{2} a_0 + \frac{M^2}{9Q^2} \left(a_2 + 4d_2 + 4f_2 \right) + O\left(\frac{M^4}{Q^4} \right), \tag{3}$$

where a_0 is the leading twist, dominant contribution. It is determined, apart from QCD radiative corrections [12], by the triplet g_A and octet a_8 axial charges and the net quark spin contribution to the total nucleon spin. These axial charges are extracted from measurements of the neutron and hyperons weak decay measurements [14]. Here a_2 is a second moment of the g_1 structure function and arises from the target mass correction [11]. The quantities d_2 and f_2 are the twist-three and the twist-four reduced matrix elements. These matrix elements contain non-trivial quark gluon interactions beyond the parton model. A first attempt at extracting f_2 has been carried by Ji and Melnitchouk in [17] using the world data but with poor statistics below $Q^2 = 1$ GeV^2. Other investigations of higher twist contributions for spin-dependent structure functions were performed and reported in Ref. [18, 19]. In QCD, d_2 and f_2 can be expressed as linear combinations of the induced color electric and magnetic polarizabilities χ_E and χ_B [3, 16] when a nucleon is polarized. The above twist expansion may be valid down to $Q^2 \approx 1$ GeV^2 if higher order terms are small.

At large Q^2 where an OPE expansion becomes valid, the quantity d_2 reduces to a twist-3 matrix element which is related to a certain quark-gluon correlation.

$$\langle PS| \frac{1}{4} \bar{\psi} g \tilde{F}^{\sigma(\mu} \gamma^{\nu)} \psi |PS \rangle = 2d_2 S^{[\sigma} P^{(\mu]} P^{\nu)} , \tag{4}$$

where $\tilde{F}^{\mu\nu} = (1/2)\epsilon^{\mu\nu\alpha\beta} F_{\alpha\beta}$, and $(\cdots)$ and $[\cdots]$ denote symmetrization and antisymmetrization of indices, respectively. The structure of the above operator suggests that it measures a quark *and* a gluon amplitude in the initial nucleon wavefunction [1, 2].

The physical significance of $d_2(Q^2)$ has been articulated by Ji and we quote, "*we ask when a nucleon is polarized in its rest frame, how does the gluon field inside of the nucleon respond?*

Intuitively, because of the parity conservation, the color magnetic field $\vec{B}$ can be induced along the nucleon polarization and the color electric field $\vec{E}$ in the plane perpendicular to the polarization". After introducing the color-singlet operators $O_B = \psi^\dagger g\vec{B}\psi$ and $O_E = \psi^\dagger \vec{\alpha} \times g\vec{E}\psi$, we can define the gluon-field polarizabilities χ_B and χ_E in the rest frame of the nucleon,

$$\langle PS|O_{B,E}|PS\rangle = \chi_{B,E} 2M^2 \vec{S} . \tag{5}$$

Then d_2 can be written as

$$d_2 = (\chi_E + 2\chi_B))/8 . \tag{6}$$

Thus d_2 is a measure of the response of the color electric and magnetic fields to the polarization of the nucleon. The reduced matrix element f_2 can be expressed also as a different linear combination of the same color polarizabilities

$$f_2 = (\chi_E - \chi_B)/3 . \tag{7}$$

Ultimately from $d_2(Q^2)$ and $f_2(Q^2)$ the color electric and magnetic polarizabilities will be obtained when high precision data on both g_1 and g_2 of both quantities become available. In this proposal we are aiming at providing precision data for d_2^n at large Q^2.

1.2 Burkhardt-Cottingham Sum rule

The g_2 structure function itself obeys the Burkhardt-Cottingham (BC) sum rule [21]

$$\Gamma_2(Q^2) = \int_0^1 g_2(x,Q^2)\,dx = 0 , \tag{8}$$

which was derived from the dispersion relation and the asymptotic behavior of the corresponding Compton amplitude. This sum rule is true at all Q^2 and does not follow from the OPE. It is rather a super-convergence relation based on Regge asymptotics as articulated in the review paper by Jaffe [22]. Many scenarios which could invalidate this sum rule have been discussed in the literature [23, 24, 2]. However, this sum rule was confirmed in perturbative QCD at order α_s with a $g_2(x,Q^2)$ structure function for a quark target [26]. Surprisingly a first precision measurement of g_2 by the E155 collaboration [20] at $Q^2 = 5$ GeV^2 but within a limited range of x has revealed a violation of this sum rule on the proton at the level of three standard deviations. In contrast, the neutron sum rule is poorly measured but consistent with zero at the one standard deviation. New high precision data on the neutron g_2 [25] at Q^2 below 1 GeV suggest that the BC sum rule is verified within errors.

2 Experimental status of $d_2^{n,p}(Q^2)$ and $\Gamma_2(Q^2)$ measurements

The early measurements of the g_2 spin structure function performed by the SMC [4] and E142 [5, 6] collaborations in the 90's were meant to reduce the systematic errors when extracting g_1 due to g_2's contribution in the measured parallel asymmetries. As the statistical precision of g_1 improved a better measurement of g_2 was required to minimize the error on g_1. E143 [7], E154 [8] and E155 [9] collaborations evaluated d_2 and published their results. However, until recently a few dedicated experiments, were performed to measure g_2 and extract ultimately d_2 with much improved statistical precision on the proton and the deuteron [20, 32] and ^{3}He [25, 28].

Fig. 3 shows d_2 of SLAC E155X [20] combined with the world data compared to several calculations. The proton result is generally consistent with the chiral quark model [33, 34] and some

bag models [35, 11, 17] while one to two standard deviations away from the QCD sum rule calculations [37, 38, 39]. The comparison with the lattice QCD calculation [15] is promising but the error bar on this calculation is still large. The Lattice Hadron Physics Collaboration based at Jefferson Lab has plans to calculate this matrix element for the proton and the neutron [27] and improve on the precision of the present lattice calculations.
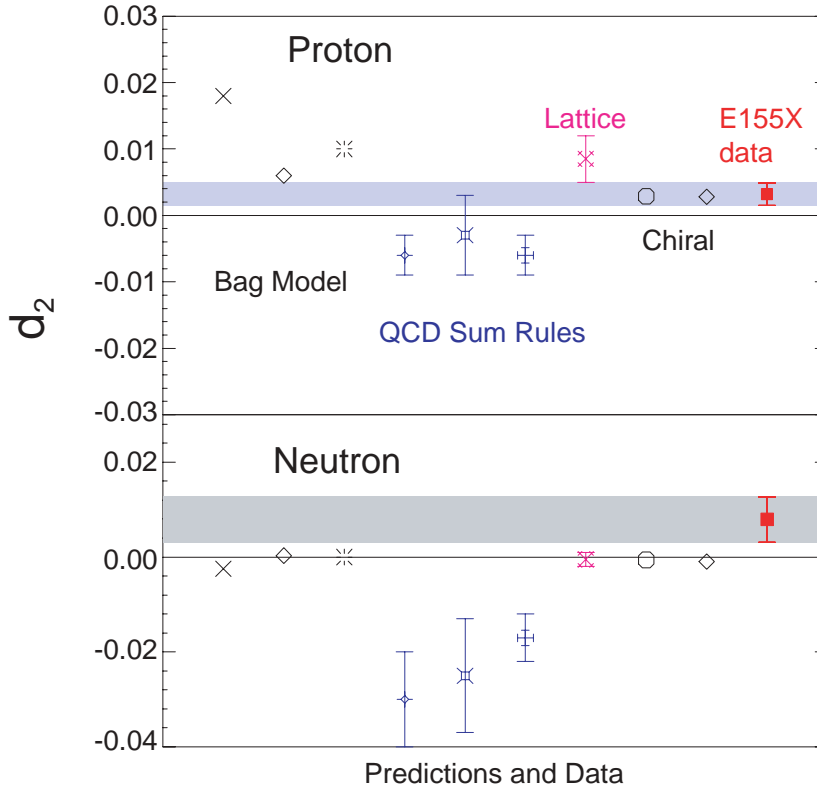

Figure 3: E155X results of the nucleon d_2 compared to several theoretical calculations (see text). Upper panel is for the proton and lower panel for the neutron.

For the neutron the situation is less clear since most models predict values consistent with a negative value or zero while the experimental result is positive and 2σ away from zero. In these models g_2^n is negative at large x therefore it is conceivable that the poor precision (Fig. 6) of the data in this region is affecting the overall sign of the result. It is important to note that from the point of view of a simple quark model, the d_2 matrix element of the neutron should be much smaller than that of the proton because of $SU(6)$ spin-flavor symmetry. Therefore with the present precision of E155x neutron data it is difficult to draw any conclusions on the sign and size of the neutron higher twist (twist-three) contribution. Because d_2 is a second moment in x of the linear combination $(2g_1 + 3g_2)$ the neutron data set can be improved significantly at Jefferson Lab. Due to the x^2 weighting, the contribution of the small x region is supressed and thus using the the existing world data and future data in the region $x < 0.24$ should be sufficient to complete the integral. In fact the average Q^2 value of the world low x data is close to the value $Q^2 = 2$ GeV^2 of this proposal.

During JLab experiment E94-010 [25] which was aimed at measuring the Gerasimov-Drell-Hearn

extended sum, data on g_2 were taken using a polarized ^{3}He target across the resonance and deep inelatic region in the range $0.1 < Q^2 < 0.9$ GeV^2. New results on two moments of the neutron spin structure functions namely Γ_2^n and d_2^n are now available from this experiment. These results are shown in Fig. 4.
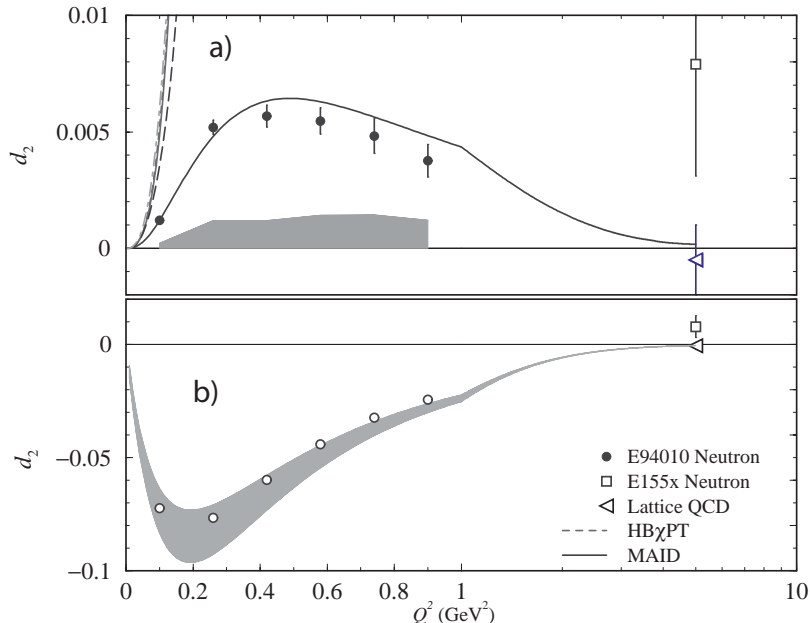

Figure 4: The quantity $d_2(Q^2)$ is shown at several values of Q^2. The results of JLab E94-010 without the nucleon elastic contribution are the solid circles (top panel). The grey band represents their corresponding systematic uncertainty. The SLAC E155 [20] neutron result shown if Fig. 3 is also shown here (open square). The solid line is the MAID calculation[40] while the dashed line is a HBχPT calculation[41] valid only at very low Q^2. The lattice prediction [15] at $Q^2 = 5$ GeV^2 for the neutron d_2 reduced matrix element is negative but close to zero. We note that all models shown in Fig. 3 predict a negative value or zero at large Q^2 where the elastic contribution is negligible. At moderate Q^2 the data show a positive d_2^n, and indicate a slow decrease with Q^2. The SLAC data also show a positive d_2^n value but with a rather large error bar. However, when the nucleon elastic contribution is added (bottom panel) the d_2^n quantity (open circles) is always negative and seems to approach the lattice result as Q^2 increases. The grey negative band represents the inelastic contribution from MAID added to a range of elastic contributions. Note the change of vertical scale.

In the investigation of higher twist contributions an important first step has already been taken with JLab experiment E97-103 [28], which will provide precision data of g_2^n in the deep inelastic region at low x ($0.17 < x < 0.21$) and will investigate its Q^2 evolution in the range $0.56 < Q^2 < 1.4$ (GeV^2) for a fixed value of $x \approx 0.2$. The unprecedented statistical accuracy expected in E97-103 allow us to probe the size of higher twists contributions by comparing directly the measured g_2^n to the leading twist contribution (twist-two contribution known as $g_2^{n(WW)}$ [30]). The experiment has been completed and the analysis is in its final stage. The preliminary results hint at a small but finite higher-twists contribution.

Two other approved experiments, JLab experiment E01-012 [31] which uses a polarized ^{3}He

target, and JLab experiment E01-006 [32] which uses polarized NH_3 and ND_3 targets, will add to the wealth of neutron spin structure functions data (g_1^n and g_2^n) in the resonance region. However, the first one emphasises the investigation of g_1 while the second provides data at $Q^2 = 1.3$ GeV^2 for g_2^p with high precision but limited precision for g_2^n.

The neutron result of g_2 extracted from the proton and deuteron measurements of E155X are shown in Fig. 6 along with what is expected from this proposal. The statistical accuracy already achieved in JLab E97-103 is shown for their highest Q^2 kinematics point, namely $Q^2 = 1.4$ GeV^2 and $x = 0.2$. We should point out that this proposed experiment is optimized to minimize the error on the determination of d_2^n not g_2^n. Obviously, time limitations would not allow us to provide for the statisticl precision at each x value for a direct comparison with models of g_2^n.

Finally, turning to the BC sum rule, the experimental situation is summarized in Fig. 5 where we show Γ_2^n measured in E94-010 (solid circles) and, including the elastic contribution (open circles) evaluated using a dipole form factor for G_M^n and the Galster fit for G_E^n. The positive light grey band corresponds to the total experimental systematic errors while the dark negative band in represents an estimated DIS contribution using g_2^{WW}. The solid line is the resonances contribution evaluated using MAID and the negative light-grey band is the neutron elastic contribution added to the measured data to determine Γ_2^n. The results are quite encouraging since the data show that the BC sum rule is verified within uncertainties over the Q^2 range measured. Our result is at odds with the reported violation of this sum rule on the proton at high Q^2 (where the elastic contribution is negligible) [20]. It is, however, consistent with the neutron result of SLAC E155 (open square) which unfortunately has a rather large error bar. In light of our results, a high statistical precision measurement in the range 1 GeV$^2 \leq Q^2 \leq 5$ GeV^2 would be of paramount importance for both the proton and neutron even if the x range is limited.
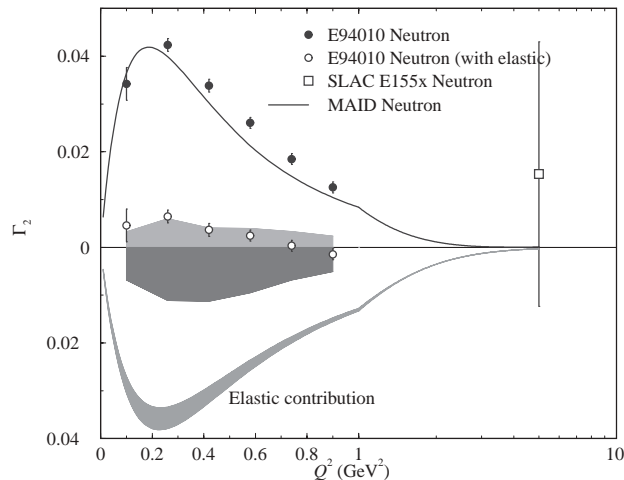
Figure 5: Results of Γ_2^n along with the average of the world data from DIS. The theoretical prediction for this quantity is zero (see text).

On the experimental side this situation can be improved using a target complementary to polarized deuterium (namely polarized ^{3}He) in order to extract the neutron information. JLab is in a unique position to provide high polarized luminosity to measure the large x region with good statistical precision. Unlike in previous experiments, world data fits of $R = \sigma_L/\sigma_T$, F_2 and g_1 will not be used to evaluate g_2, rather we shall measure absolute polarized cross sections for both

directions of the target spin, parallel and perpendicular and extract g_2 directly. Furthermore, in order to evaluate d_2 in those experiments, it is common practice to evolve the measured g_2 data from the measured Q^2 to a common Q^2 value, however, this evolution is not well understood for the twist-tree part of g_2. In contrast, our data will be measured at a constant Q^2.

We shall describe in this proposal how CEBAF is in a unique position to improve the neutron measurement of d_2^n by a factor of four and provide as well a reasonable test of the BC sum rule at $Q^2 = 2$ GeV^2.
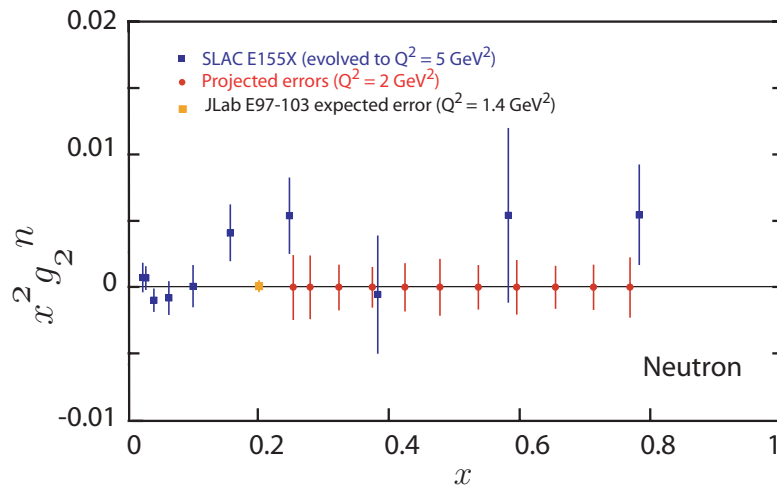

Figure 6: World average domiated by SLAC E155X results of the $x^2 g_2^n$ extracted by subtracting the proton from the deuteron following the prescription described in Ref.[29, 20]. Also shown are the statistical error achievable in this proposal on $x^2 g_2$ with a measurement rather optimized for determining d_2 with the best statistical precision.

3 Proposed Experiment

We propose to measure the unpolarized cross section σ_0^{3He}, the parallel asymmetry $A_\parallel^{3He}$ and perpendicular asymmetry $A_\perp^{3He}$ at a constant Q^2. We will use the longitudinally polarized ($P_b = 0.8$) CEBAF electron beam and a 40-cm-long high pressure polarized ^{3}He target. The measurement will be performed at two incident electron beam energies $E_i = 5.7$ GeV and 6.0 GeV using both HRS spectrometers at four scattering angles $\theta = 17.5°$, $20.0°$, $22.5°$ and $25.0°$. Five momentum settings for each spectrometer will cover the range $0.24 \leq x \leq 0.8$ at $Q^2 = 2.0$ GeV^2. The target polarization orientation will be set longitudinal or transverse to the beam with a value of $P_t = 0.40$ while the beam helicity will be reversed at a rate of 30 Hz. A beam current of 15 μA combined with a target density of 2.5×10^{20} atoms/cm^3 provides a luminosity ranging between 5.9×10^{35} cm^{-2}s^{-1} and 8.3×10^{35} cm^{-2}s^{-1} depending on the effective target length at various angles.

3.1 Kinematics

The kinematic settings were chosen to allow a measurement at constant Q^2 over as wide an excitation energy range as possible. Fig. 7 shows in the (Q^2, x) plane the experimental excitation
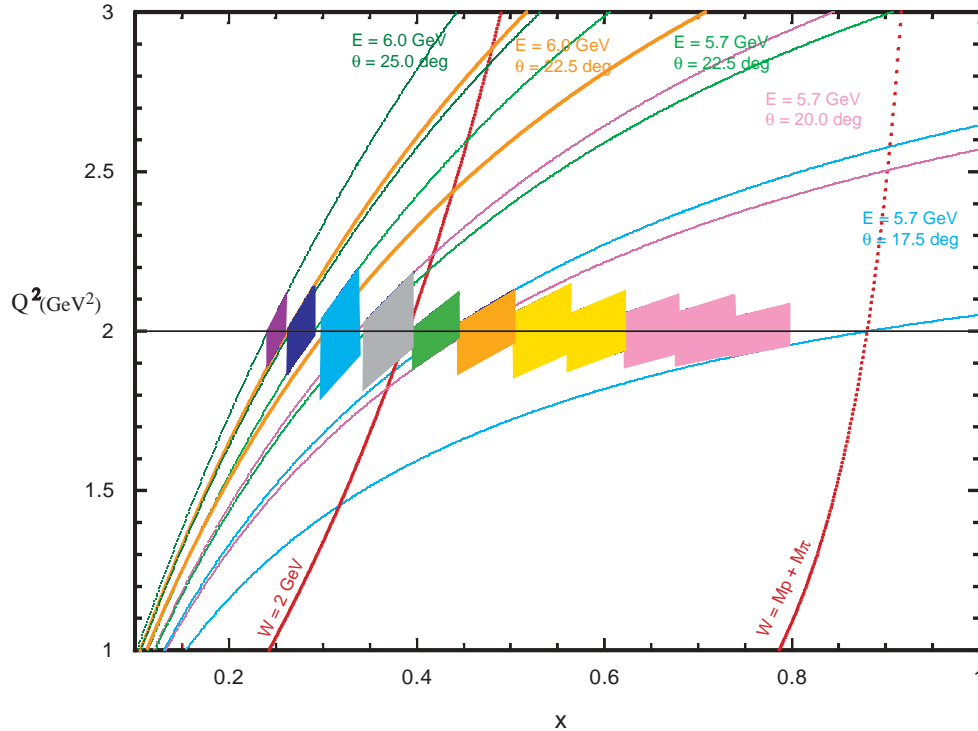
Figure 7: Proposed kinematic range for the measurement at a constant average Q^2 of 2 GeV^2. Each diamond represents the size of an (x,Q^2) bin chosen for this measurement. Each pair of common colored lines is plotted to indicate the possible range of (x,Q^2) due to the angular acceptance of the spectrometer for a fixed incident energy and scattering angle. The electron beam incident energy and the scattering angle and momentum of each spectrometer is chosen to keep the measured data at constant Q^2.

range we plan to cover from the pion threshold to the deep inelastic region including the nucleon resonance region. In order to keep Q^2 constant for each measured x bin, the scattering angle must range from 17.5° to 25°. Then by taking into account the angular acceptance of the HRS spectrometers ($\Delta\theta \approx \pm 25$ mrad) we find a continuous coverage of the x range at constant Q^2 (diamonds of different sizes shown on Fig. 7)

The main contribution to d_2 arises from the large x region because of the weighting of g_1 and g_2 by x^2 in the integration over x. The measurement of this region with high precision is important. In tables 3, 4 and 5 we have listed the kinematical conditions for each spectrometer needed to cover the proposed x region.

3.2   The Polarized Beam

In this proposal we shall assume, that the achievable beam polarization at CEBAF is 80% with a current of 15μA. While about 70% electron beam polarization has been delivered on a regular basis to E94-010 and E95-001 we are optimistic that by the time this experiment runs and with the experience gained using the strained GaAs cathodes, 80% beam polarization will be achieved. The polarization of the beam will be measured with the Hall A Moller and Compton polarimeters.

3.3   The Polarized ^{3}He Target

The polarized target will be based on the principle of spin exchange between optically pumped alkali-metal vapor and noble-gas nuclei [42, 43, 44]. It is the same as that used in JLab experiments E94-010, E95-001, E97-103 and E99-117 in Hall A.

A central feature of the target will be sealed glass target cells, which under operating conditions, will contain a ^{3}He pressure of about 10 atmospheres. As indicated in Fig. 8, the cells will have two chambers, an upper chamber in which the spin exchange takes place, and a lower chamber, through which the electron beam will pass. In order to maintain the appropriate number density of the alkali-metal Rubidium the upper chamber will be kept at a temperature of 170–200$°$ using an oven constructed of high temperature plastic Torlon. The density of the target will be about 2.5×10^{20} atoms/cm^3. The lower cell length will be 40 cm such that the end glass windows are not seen by the spectrometer acceptance when it is set at a scattering angle of 17.5$°$ and larger. The effective target thickness will range from 6.0×10^{21} atoms/cm^2 to 8.3×10^{21} atoms/cm^2, since the spectrometer acceptance sees a length of 7 cm/$\sin \theta_e$

The main components of the target are shown in Fig. 8. The main "coils" shown are large Helmholtz coils used to apply a static magnetic field of about 25 Gauss. Also shown are the components for the NMR and EPR polarimetry. The NMR components of the target include a set of RF drive coils, and a separate set of pickup coils. Not shown in the figure are the NMR electronics, which include an RF amplifier, a lock-in amplifier, some bridge circuitry, and the capability to sweep the static magnetic field. The EPR components include an EPR excitation coil and a photodiode for detection of the EPR line. The oven shown in Fig. 8 is heated with forced hot air. The optics system include a system of 4 diode lasers for longitudinal pumping and 4 for transverse pumping. A polarizing beam splitter, lens system and a quarter wave plate are required to condition each laser beam line and provide circular polarization.

3.3.1   Operating Principles

The time evolution of the ^{3}He polarization can be calculated from a simple analysis of spin-exchange and ^{3}He nuclear relaxation rates[45]. Assuming the ^{3}He polarization $P_{^3\text{He}} = 0$ at $t = 0$,

$$P_{^3\text{He}}(t) = P_{\text{Rb}} \left(\frac{\gamma_{\text{SE}}}{\gamma_{\text{SE}} + \Gamma_{\text{R}}} \right) \left(1 - e^{-(\gamma_{\text{SE}} + \Gamma_{\text{R}}) \, t} \right) \tag{9}$$

where γ_{SE} is the spin-exchange rate per ^{3}He atom between the Rb and ^{3}He, Γ_{R} is the relaxation rate of the ^{3}He nuclear polarization through all channels other than spin exchange with Rb, and P_{Rb} is the average polarization of the Rb atoms. Likewise, if the optical pumping is turned off at $t = 0$ with $P_{^3\text{He}} = P_0$, the ^{3}He nuclear polarization will decay according to

$$P_{^3\text{He}}(t) = P_0 \, e^{-(\gamma_{\text{SE}} + \Gamma_{\text{R}}) \, t}. \tag{10}$$

The spin exchange rate γ_{SE} is defined by

$$\gamma_{\text{SE}} \equiv \langle \sigma_{\text{SE}} \, v \rangle \, [\text{Rb}]_{\text{A}} \tag{11}$$

where, $\langle \sigma_{\text{SE}} \, v \rangle = 1.2 \times 10^{-19}$ cm^3/sec is the velocity-averaged spin-exchange cross section for Rb–^{3}He collisions[45, 46, 47] and $[\text{Rb}]_{\text{A}}$ is the average Rb number density seen by a ^{3}He atom. The target operates with $1/\gamma_{\text{SE}} = 8$ hours. From equation (9) it is clear that the best possible ^{3}He polarization is obtained by maximizing γ_{SE} and minimizing Γ_{R}. But from equation (11) we can see that maximizing γ_{SE} means increasing the alkali-metal number density, which in turn means more
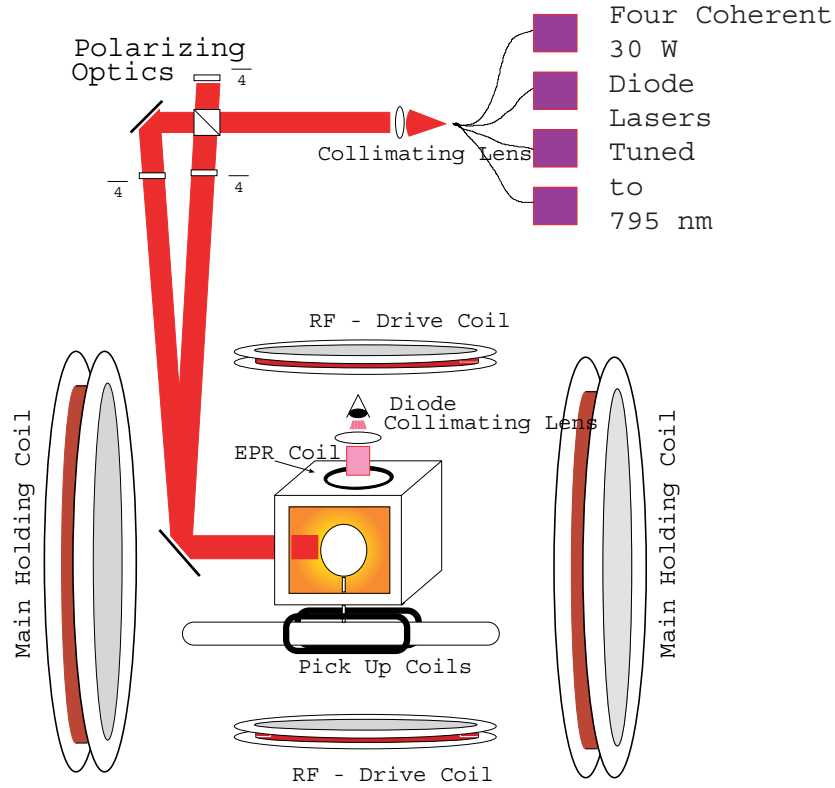
Figure 8: JLab Hall A polarized ^{3}He target setup.

laser power. The number of photons needed per second must compensate for the spin relaxation of Rb spins. In order to achieve $1/\gamma_{\text{SE}} = 8$ hours, about 50 Watts of usable laser light at a wavelength of 795 nm will be required.

The rate at which polarization is lost is characterized by Γ and has four principle contributions. An average electron beam current of about 15 μA will result in a depolarization rate of $\Gamma_{beam} = 1/30$ hours [48]. The cells produced in previous experiments typically have an intrinsic rate of $\Gamma_{cell} = 1/50$ hours. This has two contributions, relaxation that occurs during collisions of ^{3}He atoms due to dipole-dipole interactions, and relaxation that is largely due to the interaction of the ^{3}He atoms with the walls. Finally, relaxation due to magnetic field inhomogeneities was held to about $\Gamma_{\nabla B} = 1/100$ hours. Collectively, under operating conditions, we would thus expect

$$\Gamma_R = \Gamma_{beam} + \Gamma_{cell} + \Gamma_{\nabla B} = 1/30 \,\text{hours} + 1/50 \,\text{hours} + 1/100 \,\text{hours} = 1/16 \,\text{hours}.$$

Thus, according to equation (9), the target polarization cannot be expected to exceed

$$P_{max} = \frac{\gamma_{\text{SE}}}{\gamma_{\text{SE}} + \Gamma_{\text{R}}} = 0.66$$

Realistically, a Rb polarization of 100% in the pumping chamber will not be achieved, which will reduce the polarization to about 40%.

During E94-010 and E95-001 we achieved a polarization of about 30-35% when a beam current of 15μA was used. The beam depolarization was slightly larger than expected and this was the

first time that such a large beam current was used for an extended period time. An R&D effort is underway by JLab and the polarized ^{3}He target collaboration to improve the achievable polarization under the beam conditions proposed in this experiment.

3.3.2 Target Cells

The length of the cell has been chosen to be 40 cm so that the end windows are not within the acceptance of the Hall A spectrometers at angles equal to 17.5° and larger. The end windows themselves will be about 100 μm thick.

3.3.3 The Optics System

As mentioned above, approximately 50 W of "usable" light at 795 nm will be required. By "usable", we mean circularly polarized light that can be readily absorbed by the Rb. It should be noted that the absorption line of Rb has a full width of several hundred GHz at the high pressures of ^{3}He at which we will operate. Furthermore, since we will operate with very high Rb number densities that are optically quite thick, even light that is not well within their absorption line width can still be absorbed.

The laser system is similar to that used in E94-010. It consists of commercially available 30 Watt fiber-coupled diode laser systems (from COHERENT INC.). Four such lasers are used to pump along the transverse direction and three along the longitudinal direction. The efficiency of these lasers has been tested during experiment E94-010 and E95-001 and found to be totally adequate for this experiment's needs.

3.3.4 Polarimetry

Polarimetry is accomplished by two means. During the experiment, polarization is monitored using the NMR technique of adiabatic fast passage (AFP)[49]. The signals are calibrated by comparing the ^{3}He NMR signals with those of water. The calibration is then independently verified by studying the frequency shifts that the polarized ^{3}He nuclei cause on the electron paramagnetic resonance (EPR) lines of Rb atoms [48]. Both methods were used in E94-010 and we found as expected that the NMR measurements with water calibration are consistent with the EPR results.

3.4 The Spectrometers Setup

We plan to use both HRS spectrometers in Hall A. We will use the right spectrometer with its standard detector package for electrons and the left spectrometer with an added double layer lead glass calorimeter which was first used in E94-010. Each spectrometer will then consist of;

- Two vertical Drift Chambers (VDCs) for the measurement of momentum and production angle.

- Gas Čerenkov counter for pion rejection.

- A set of scintillators for triggering on charged particles.

- A double layer lead glass calorimeter for additional pion rejection.

As the E94-010 analysis shows, the pion rejection factor with the Čerenkov counter and the lead glass calorimeter are better than 2×10^{-4} which is sufficient for our worst case.

Because the maximum momentum attainable by each spectrometer is different (4.30 GeV for the HRS-l and 3.17 GeV for the HRS-r) we have assigned HRS-l to perform the measurements for electron momenta greater than 3 GeV and HRS-r for those measurements with momenta equal or less than 3 GeV. We optimized the time sharing between the two spectrometers (see Table 4 and 5). Although we need to make few spectrometer angle changes to keep our measurement at constant Q^2. Specific advantages make these spectrometers a well matched tool for the proposed measurement.

- Good electron events in the spectrometer are in principle due only to electron scattering off ^{3}He nuclei since the target cell glass windows are outside the spectrometer acceptance. However, excellent target reconstruction by the HRS spectrometers allows for better background rejection.

- An excellent resolution of the spectrometers permits the measurement of elastic scattering off ^{3}He needed for an absolute calibration of the detector in order to measure absolute cross sections.
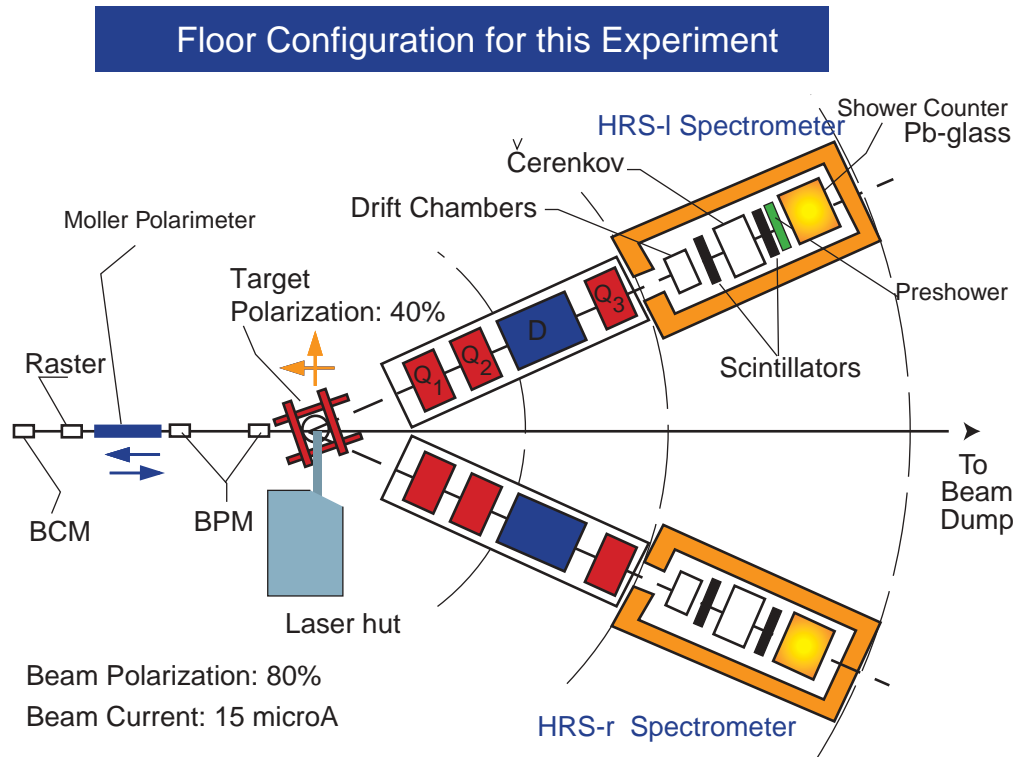

Figure 9: JLab Hall A floor setup using the HRS spectrometers and the polarized 3He target. Note that their maximum central momentum reach is not the same. It is 4.3 GeV for the left HRS and 3.17 GeV for right HRS

4   Evaluation of d_2^n

The goal of this experiment is to obtain the d_2 from a direct measurement of the unpolarized cross section σ_0 and the parallel $A_\parallel$ and perpendicular $A_\perp$ asymmetries on ^{3}He. Equivalently d_2 is obtained from the measurement of the linear combination of the spin structure functions $g_1(x, Q^2)$ and $g_2(x, Q^2)$ and forming the second moment of this combination namely,

$$d_2(Q^2) = \int_0^1 x^2 [2g_1(x, Q^2) + 3g_2(x, Q^2)] \; dx = \int_0^1 \tilde{d}_2(x, Q^2) \; dx \tag{12}$$

The spin structure functions can be expressed in terms of asymmetries and unpolarized cross sections as follow;

$$g_1 \;\; = \;\; \frac{MQ^2}{4\alpha^2} \frac{y}{(1-y)(2-y)} 2\sigma_0 \left[A_\parallel + \tan\frac{\theta}{2} A_\perp \right] \tag{13}$$

$$g_2 \;\; = \;\; \frac{MQ^2}{4\alpha^2} \frac{y^2}{2(1-y)(2-y)} 2\sigma_0 \left[-A_\parallel + \frac{1 + (1-y)\cos\theta}{(1-y)\sin\theta} A_\perp \right] \tag{14}$$

where σ_0 is the unpolarized cross section, Q^2 is the four momentum transfer, α the electromagnetic coupling constant, θ the scattering angle and $y = (E - E')/E$ the fraction of energy transferred to the target. $A_\parallel$ and $A_\perp$ are the parallel and perpendicular asymmetries,

$$A_\parallel = \frac{\sigma^{\downarrow\Uparrow} - \sigma^{\uparrow\Uparrow}}{2\sigma_0}, \qquad\qquad A_\perp = \frac{\sigma^{\downarrow\Rightarrow} - \sigma^{\uparrow\Rightarrow}}{2\sigma_0} \tag{15}$$

From (12), (13) and (14) we can express the integrand of d_2 directly in terms of measured asymmetries and unpolarized cross section as follows:

$$\tilde{d}_2(x, Q^2) \;\; = \;\; x^2 [2g_1(x, Q^2) + 3g_2(x, Q^2)] \tag{16}$$

$$= \;\; \frac{MQ^2}{4\alpha^2} \frac{x^2 y^2}{(1-y)(2-y)} \sigma_0 \left[\left(3\frac{1 + (1-y)\cos\theta}{(1-y)\sin\theta} + \frac{4}{y}\tan\frac{\theta}{2} \right) A_\perp + \left(\frac{4}{y} - 3 \right) A_\parallel \right] \tag{17}$$

The above expression of the integrand is used for the following purposes:

- Determination of the time sharing between the transverse and the longitudinal measurement to minimize the statistical error on d_2 not on g_2 as in previous experiments.

- Determination of the effect of the target polarization orientation misalignment on the systematic error of d_2

- Determination of the systematic error on d_2 due to the systematic errors of the cross section and asymmetries measurements.

The measurement consists of collecting data at two incident energies ($E_i = 5.7$ GeV and 6.0 GeV) and four scattering scattering angles ($\theta = 17.5°, 20.0°, 22.5°$ and $25.0°$) and for eight spectrometer momentum settings to cover the range $0.25 \leq x \leq 0.8$. The measured raw ^{3}He counting parallel asymmetry $\Delta_\parallel$ and perpendicular asymmetry $\Delta_\perp$ are converted to the experimental asymmetries $A_\parallel^{^3He}$, and $A_\perp^{^3He}$ respectively, using the relation

$$A_\perp^{^3He} \;\; = \;\; \frac{\Delta_\perp}{P_b P_t \cos\phi} \qquad\qquad A_\parallel^{^3He} \;\; = \;\; \frac{\Delta_\parallel}{P_b P_t} \tag{18}$$

$$\Delta_\perp \;\; = \;\; \frac{(N^{\uparrow\Rightarrow} - N^{\uparrow\Rightarrow})}{(N^{\uparrow\Rightarrow} + N^{\uparrow\Rightarrow})} \qquad\qquad \Delta_\parallel \;\; = \;\; \frac{(N^{\downarrow\Uparrow} - N^{\uparrow\Uparrow})}{(N^{\downarrow\Uparrow} + N^{\uparrow\Uparrow})} \tag{19}$$

where $N^{\uparrow\Downarrow}$ ($N^{\uparrow\Uparrow}$) and $N^{\uparrow\Rightarrow}$ ($N^{\uparrow\Rightarrow}$) represent the rate of scattered electrons for each bin in x and Q^2 when the electron beam helicity and target spin are parallel or perpendicular. ϕ is the angle between the scattering plane and the plane formed by the incoming beam and the perpendicular target polarization. $P_b = 0.80$ and $P_t = 0.40$ are the beam and target polarization respectively. The target length (40 cm) is chosen such that no extra dilution of the asymmetry occurs from unpolarized scattering off the glass windows. However, empty target measurements will be performed to insure that no spurious unpolarized background originating in the target area reduces the measured physics asymmetries. The kinematics and electron rates are presented in Table 3. We used the Whitlow 1990 [50] parametrization of unpolarized structure functions from measurements of deep inelastic scattering on the proton and the deuteron. We added incoherently the appropriate structure functions to generate the ^{3}He cross sections. The rates were determined assuming a solid angle evaluated from the bins shown in Fig. 7 and a luminosity varying from 6.0×10^{35} cm^{-2}s^{-1} to 8.0×10^{35} cm^{-2}s^{-1}. The times for the transverse and longitudinal measurements were determined by optimizing the time sharing for the best precision on the integrand $\tilde{d}_2$. If we set

$$\alpha = \frac{MQ^2}{4\alpha^2}\frac{x^2y^2}{(1-y)(2-y)}\sigma_0\left(3\frac{1+(1-y)\cos\theta}{(1-y)\sin\theta} + \frac{4}{y}\tan\frac{\theta}{2}\right) \tag{20}$$

$$\beta = \frac{MQ^2}{4\alpha^2}\frac{x^2y^2}{(1-y)(2-y)}\sigma_0\left(\frac{4}{y} - 3\right) \tag{21}$$

The optimum ratio between the parallel and perpendicular counts is

$$N_\parallel = \frac{\beta}{\alpha}N_\perp \tag{22}$$

The total number of counts $N_\perp$ is given by

$$N_\perp = \frac{\alpha(\alpha+\beta)}{P_b^2 P_t^2 f^2 (\Delta\tilde{d}_2)^2} \tag{23}$$

$f = W_1^n/W_1^{3He}$ is the fraction of scattering originating from the neutron compared to ^{3}He. We required an absolute statistical uncertainty on the integrand $\Delta\tilde{d}_2^n$ between 7.5×10^{-3} and 5×10^{-3} at different x bins. This in turn leads to an absolute statistical precision on d_2^n of $\Delta d_2^n \approx 1.18\times10^{-3}$. This value is to be compared with $\Delta d_2^n \approx 5 \times 10^{-3}$ of SLAC E155X.
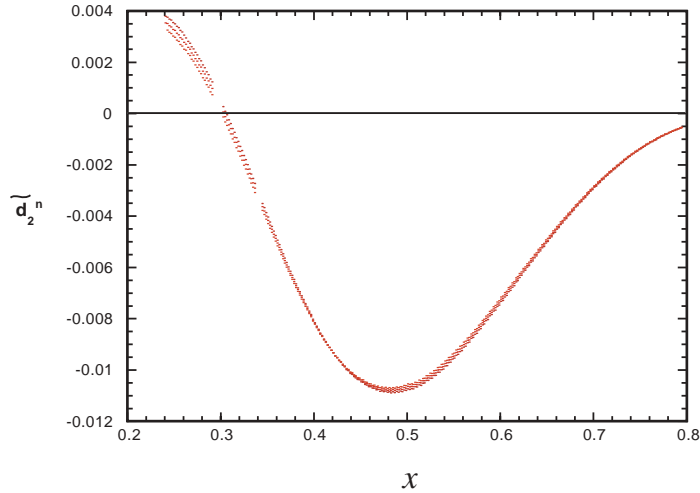
The pion background was estimated using the EPC program [51] which was normalized against measurements carried at JLab in a similar kinematic range. The results of the estimate are listed in Table 1 were the π/e^- ratio ranges from a negligible value in the highest x bin to a value of about twenty in the lowest x bin. Given the pion rejection performance of the combination Čerenkov and lead glass calorimeter, we should be able to keep this correction at a negligible level. Furthermore, we shall also measure the pion asymmetry using the hadron spectrometer in the lowest three x bins.

The radiative corrections (RC) will be performed in two stages. First the internal corrections will be evaluated following the procedure developed by Bardin and Shumeiko[52] for the unpolarized case and extended to the spin dependent lepto-production cross sections by Akushevish and Shumeiko[53, 54]. Second, using these internally corrected cross sections, the external corrections (for thick targets) are applied by extending the procedure developed for the unpolarized cross sections by Tsai[55, 56] with modifications appropriate for this experiment.

To evaluate the experimental systematic uncertainty of d_2^n we used relative uncertainties in the cross sections and asymmetries achieved in E94-010. Table 4 summarizes these uncertainties. One item of concern was the effect of the target relative spin misalignment between the transverse and

Table 1: π^-/e^- each x bin planned in this measurement

E_i (GeV)	θ_e °	E' (GeV)	x	W (GeV)	$d\sigma^{\pi^-}$ (nb/GeV/sr)	π^- rate (Hz)	π^-/e^-
5.70	16.40	4.310	0.766	1.22	0.51	0.03	0.006
5.70	16.63	4.197	0.710	1.30	0.94	0.09	0.013
5.70	16.90	4.064	0.652	1.40	1.68	0.20	0.024
5.70	17.24	3.903	0.593	1.50	2.98	0.48	0.030
5.70	17.70	3.705	0.534	1.62	5.40	1.31	0.062
5.70	18.33	3.458	0.475	1.76	10.4	2.67	0.118
5.70	19.14	3.173	0.422	1.90	20.8	5.01	0.264
5.70	20.27	2.833	0.372	2.06	44.7	28.54	0.673
5.70	22.16	2.375	0.321	2.26	120.3	92.13	2.41
6.00	22.70	2.152	0.277	2.47	253.3	141.25	6.04
6.00	25.14	1.760	0.251	2.62	574.9	245.44	18.7

Figure 10: Effect of target relative spin misalignment by 0.5° between the transverse and longitudinal measurements

longitudinal direction measurements. Fig. 10 shows this effect at each value of x on the integrand of d_2. A relative error of 0.5° in the relative direction of the transverse versus perpendicular results in a relative error $\Delta d_2/d_2 = 0.15\%$. Using the Weigel *et al.* [33] model of g_2 and g_1 we estimated $\Delta d_2/d_2$ to be of the order of 10 % and thus an absolute systematic uncertainty of about 10^{-3}. We believe we can achieve a relative error of 0.2° in the target spin alignment.

Even with our improved projected statistical precision the total uncertainty in d_2^n is still dominated by the statistical accuracy of the measurement not its systematic.

An elastic scattering asymmetry measurement is planned at low energy ($E_i = 1.0$ GeV $\theta = 17.5°$) in order to calibrate our spin dependent absolute cross sections. This quantity can be evaluated

Table 2: List of the systematic error contributions to d_2^n

Item description	Subitem description	Relative uncertainty
Target polarization		4 %
Beam polarization		3 %
Asymmetry (raw)		
	• Target spin direction $(0.5°)$	$\approx 1.5 \times 10^{-3}$
	• Beam charge asymmetry	200 ppm
Cross section (raw)		
	• PID efficiency	≈ 1 %
	• Background Rejection efficiency	≈ 1 %
	• Beam charge	< 1 %
	• Beam position	< 1 %
	• Acceptance cut	2-3 %
	• Target density	2-3 %
	• Nitrogen dilution	2-3 %
	• Dead time	<1 %
	• Finite Acceptance cut	<1%
Radiative corrections		≤ 10 %
From ^{3}He to Neutron correction		5 %
Total effect		≤ 10 %
Estimate of contributions	$\int_{0.003}^{0.241} \tilde{d}_2^n \; dx$	4.8×10^{-4}
from unmeasured regions	$\int_{0.767}^{0.999} \tilde{d}_2^n \; dx$	3.9×10^{-5}
Projected absolute statistical uncertainty		$\Delta d_2 \approx 1.18 \times 10^{-3}$
Projected absolute systematic uncertainty assuming $d_2 = 5 \times 10^{-3}$		$\Delta d_2 \approx 5 \times 10^{-4}$

Table 3: Parameters per bin in (Q^2,x) plane for the proposed experiment

E_i (GeV)	bin central p (GeV)	x	Δx	Q^2 (GeV^2)	W (GeV)	Rate (Hz)	Time$_\perp$ hours	Time$_\parallel$ hours
5.700	4.31	.766	.580E-01	2.00	1.22	5.03	157.	79.1
5.700	4.20	.710	.580E-01	2.00	1.30	6.85		
5.700	4.06	.652	.570E-01	2.00	1.40	8.23		
5.700	3.90	.593	.590E-01	2.00	1.50	16.0	122.	43.9
5.700	3.71	.534	.590E-01	2.00	1.62	21.1		
5.700	3.46	.475	.590E-01	2.00	1.76	22.6	88.0	23.9
5.700	3.17	.422	.480E-01	2.00	1.90	19.0	151.	34.2
5.700	2.83	.372	.520E-01	2.00	2.06	42.4	99.3	18.2
5.700	2.38	.321	.340E-01	2.00	2.26	38.1	83.2	11.5
6.000	2.15	.277	.270E-01	2.00	2.47	23.4	70.8	7.61
6.000	1.76	.251	.180E-01	2.00	2.61	13.1	121.	10.2

using the measured electric and magnetic form factors of ^{3}He. This measurement would actually determine the polarization of the ^{3}He nuclei along the electron beam path. False asymmetries will be checked to be consistent with zero by comparing data with target spins in opposite directions.

Also contributing to the dilution of the asymmetry is the pair-electron contamination. This correction is x dependent, and is relevant only in the lowest x region. This contamination was estimated to be no more than 6% in the worst case and will be measured in this experiment by reversing the spectrometer polarity on the right arm spectrometer.

The spectrometers cannot be used in a symmetric configuration when taking data since they don't access the same maximum range of momentum. For this reason the low x data will be taken mainly using the HRS-r spectrometer and most of the large x data will be acquired using the HRS-l spectrometer. Tables 4 and 5 show the kinematics and time for each spectrometer acquiring data. The right spectrometer will also be used to measure the positron contamination at the lowest x bins, while the HRS-l completes its measurements at large x. We will use the HRS-l for 619 hours with beam on target to complete this measurement.

Table 4: Sequence of measurements carried by the HRS-l spectrometer

E_i GeV	θ deg	HRS-l Central p GeV		Time$_\perp$ hours	Time$_\parallel$ hours
6.0	22.5	2.167		35.4	3.8
6.0	25.0	1.756		60.5	5.1
5.7	17.5	4.069		157	79.1
5.7	17.5	3.794		122	43.9
5.7	17.5	3.538		88	23.9
			Total	462.9	155.8

Table 5: Sequence of measurements carried by the HRS-r spectrometer

E_i GeV	θ deg	HRS-r Central p GeV		Time$_\perp$ hours	Time$_\parallel$ hours
6.0	22.5	2.167		35.4	3.8
6.0	25.0	1.756		60.5	5.1
5.7	20.0	3.075		151.	34.2
5.7	20.0	2.867		99.3	18.2
5.7	22.5	2.324		83.2	11.5
			Total	429.4	72.8

5 Spin Structure Functions: From ^{3}He to the Neutron

For spin-dependent structure, because the deuteron polarization is shared roughly equally between the proton and neutron, extraction of neutron spin structure functions requires a precise knowledge of the proton spin structure, in addition to the nuclear effects [57]. This problem is compounded by the fact that the spin-dependent structure functions of the proton are typically much larger than those of the neutron, making extraction of the latter especially sensitive to small uncertainties in the proton structure functions. On the other hand, since the neutron in ^{3}He carries almost 90% of the nuclear spin, polarized ^{3}He is an ideal source of polarized neutrons.

The three-nucleon system has been studied for many years, and modern three-body wave functions have been tested against a large array of observables which put rather strong constraints on the nuclear models [58]. In particular, over the past decade considerable experience has been acquired in the application of three-body wave functions to deep-inelastic scattering [59, 60, 61].

The conventional approach employed in calculating nuclear structure functions in the region $0.3 < x < 0.8$ is the impulse approximation, in which the virtual photon scatters incoherently from individual nucleons in the nucleus [62]. Corrections due to multiple scattering, NN correlations or multi-quark effects are usually confined to either the small-x ($x < 0.2$), or very large-x ($x > 0.9$) regions. In the impulse approximation the g_1 structure function of ^{3}He, in the Bjorken limit ($Q^2, \nu \to \infty$), is obtained by folding the nucleon structure function with the nucleon momentum distribution Δf_N ($N = p, n$) in ^{3}He:

$$g_1^{^3\text{He}}(x) = \int_x^3 \frac{dy}{y} \left\{ 2\Delta f_p(y)\, g_1^p(x/y) + \Delta f_n(y)\, g_1^n(x/y) \right\}, \tag{24}$$

where y is the fraction of the ^{3}He momentum carried by the nucleon, and the dependence on the scale, Q^2, has been suppressed. The nucleon momentum distributions $\Delta f_N(y)$ are calculated from the three-body nuclear wave function, which are obtained by either solving the Faddeev equation [63] or using variational methods [60], and are normalized such that:

$$\int_0^3 dy\, \Delta f_N(y) = \rho_N, \tag{25}$$

where ρ_N is the polarization of the nucleon in ^{3}He. While the full three-body wave function involves summing over many channels, in practice the three lowest states, namely the S, S' and D, account for over 99% of the normalization. Typically, one finds $\rho_n \approx 87\%$ and $\rho_p \approx -2\%$ [58, 59, 60, 61, 63].

The smearing in Eq.(24) incorporates the effects of Fermi motion and nuclear binding. Correctly accounting for these effects is important when attempting to extract information on nucleon structure functions from nuclear data at $x > 0.6$, as well as for determining higher moments of structure functions, in which the large-x region is more strongly weighted.

The nuclear corrections to the g_2^n structure function can be evaluated analogously to those for g_1^n. One can estimate the order of magnitude of the effects by considering firstly the twist-2 part of g_2^n, which is determined from g_1^n through the Wandzura-Wilczek relation [30, 66]:

$$g_2^{^3\text{He}}(x)\Big|_{\text{tw}-2} = -g_1^{^3\text{He}}(x) + \int_x^3 \frac{dy}{y}\, g_1^{^3\text{He}}(x/y), \tag{26}$$

where $g_1^{^3\text{He}}$ is given by Eq.(24). The main effect numerically at moderate to large x is due to the difference between the neutron and ^{3}He polarizations, as the effects due to smearing peak at the level of a few percent at $x \sim 0.6$. Similarly, the difference in the second moments of $g_2^{^3\text{He}}$ between the convolution results using different ^{3}He wave functions is a few percent [68,69]. Moreover,

since the main objective of the experiment is to extract the second moment of $3g_2^n + 2g_1^n$, namely $\int dx \, x^2(3g_2^n(x) + 2g_1^n(x))$, the sensitivity of the correction to x variations of the integrand is reduced compared to a direct extraction of the g_2 or g_1 structure functions themselves.

While the nuclear model dependence of the nuclear correction appears to be relatively weak for the twist-2 approximation in the Bjorken limit, an important question for the kinematics relevant to this experiment is how are these effects likely to be modified at finite Q^2? To address this question one needs to obtain generalizations of Eqs. (24) and (26) which are valid at any Q^2, and which can incorporate the twist-3 component of g_2. In fact, at finite Q^2 one finds contributions from g_1^N to $g_2^{^3\mathrm{He}}$, and from g_2^N to $g_1^{^3\mathrm{He}}$. The latter vanish in the Bjorken limit, but the former are finite, although they depend on the Fermi momentum of the bound nucleons. These corrections can be calculated by working directly in terms of the (unintegrated) spectral function $S(\vec{p}, E)$, where p is the bound nucleon momentum and E is the separation energy, rather than in terms of the momentum distribution functions $\Delta f_N(y)$. Following Schulze & Sauer [61], it is convenient to parameterize the ^{3}He spectral function according to:

$$S(\vec{p}, E) \;=\; \frac{1}{2}\left(f_0 + f_1 \vec{\sigma}_N \cdot \vec{\sigma}_A + f_2\left[\vec{\sigma}_N \cdot \hat{p}\,\vec{\sigma}_A \cdot \hat{p} \;-\; \frac{1}{3}\vec{\sigma}_N \cdot \vec{\sigma}_A\right]\right) , \tag{27}$$

where $\vec{\sigma}_N$ and $\vec{\sigma}_A$ are the spin operators of the nucleon and ^{3}He, respectively, and the functions $f_{0,1,2}$ are scalar functions of $|\vec{p}|$ and E. The function f_0 contributes to unpolarized scattering only, while f_1 and f_2 determine the spin-dependent structure functions. In terms of these functions, at finite Q^2 one has a set of coupled equations for $g_1^{^3\mathrm{He}}$ and $g_2^{^3\mathrm{He}}$ [68]:

$$xg_1^{^3\mathrm{He}}(x, Q^2) + (1 - \gamma^2)xg_2^{^3\mathrm{He}}(x, Q^2)$$
$$= \sum_{N=p,n}\int d^3p \, dE \, (1 - \frac{\epsilon}{M})\left\{\left[\left(1 + \frac{\gamma p_z}{M} + \frac{p_z^2}{M^2}\right)f_1 + \left(-\frac{1}{3} + \hat{p}_z^2 + \frac{2\gamma p_z}{3M} + \frac{2p_z^2}{3M^2}\right)f_2\right] zg_1^N(z, Q^2)\right.$$
$$\left. + (1 - \gamma^2)(1 + \frac{\epsilon}{M}\left[f_1 + \left(\frac{p_z^2}{\vec{p}^2} - \frac{1}{3}\right)f_2\right]\frac{z^2}{x}g_2^N(z, Q^2)\right\} , \tag{28}$$

$$xg_1^{^3\mathrm{He}}(x, Q^2) + xg_2^{^3\mathrm{He}}(x, Q^2)$$
$$= \sum_{N=p,n}\int d^3p \, dE \, (1 - \frac{\epsilon}{M})\left\{\left[\left(1 + \frac{p_x^2}{M^2}\right)f_1 + \left(\vec{p}_x^2 - \frac{1}{3} + \frac{2p_x^2}{3M^2}\right)f_2\right] zg_1^N(z, Q^2)\right.$$
$$\left. + \left[\left(1 + \frac{p_x^2}{M^2}(1 - z/x)\right)f_1 + \left(\vec{p}_x^2 - \frac{1}{3} + \frac{2p_x^2}{3M^2}(1 - z/x) - \frac{\gamma p_z \hat{p}_x^2}{M}\frac{z}{x}\right)f_2\right] zg_2^N(z, Q^2)\right\} , \tag{29}$$

with $\gamma = \sqrt{1 + 4M^2x^2/Q^2}$ a kinematical factor parameterizing the finite Q^2 correction, $\epsilon \equiv \vec{p}^2/4M - E$, and $z = x/(1 + (\epsilon + \gamma p_z)/M)$. Equations (28) and (29) can then be solved to obtain $g_1^{^3\mathrm{He}}$ and $g_2^{^3\mathrm{He}}$ explicitly. For $Q^2 \to \infty$ Eqs. (28) and (29) reduce to simple one-dimensional convolution expressions, as in Eq. (24). At finite Q^2, however, the smearing function effectively becomes x and Q^2 dependent, so that the amount of smearing in general will depent on the shape of the nucleon structure functions.

The nuclear correction of most interest for this experiment is that to the g_2 structure function. One can test the sensitivity to the kinematical Q^2 dependence, as distinct from the Q^2 dependence in the nucleon structure function itself, by taking the same input neutron structure function for all values of Q^2 at which $xg_2^{^3\mathrm{He}}$ is evaluated. One finds [68] that the effect of the kinematical Q^2 dependence turns out to be rather small at $Q^2 \sim 1$–2 GeV^2, and only becomes noticable for low $Q^2 \sim 0.2$ GeV^2. Furthermore, at these values of Q^2 the g_1^n contribution to $g_2^{^3\mathrm{He}}$ is negligible

compared with the lowest order neutron polarization correction. This confirms earlier analyses of the nuclear corrections by the Rome-Perugia group [69].

There was also an investigation in Ref. [67] into the role of the $\Delta(1232)$ in deep-inelastic scattering on polarized ^{3}He and its effects on the g_1 neutron spin structure function extraction. The authors estimated that when taking the effect of the Δ into account the values of the first moment of g_1^n increases by $6 \div 8$ %.

In summary, all of the nuclear structure function analyses that have been performed suggest that both the neutron g_1^n and g_2^n structure functions can be extracted from ^{3}He data with minimal uncertainties associated with nuclear corrections. Estimating all the corrections and their uncertainties we come to the conclusion that in this experiment the statistical error on the final result is still the dominant error.
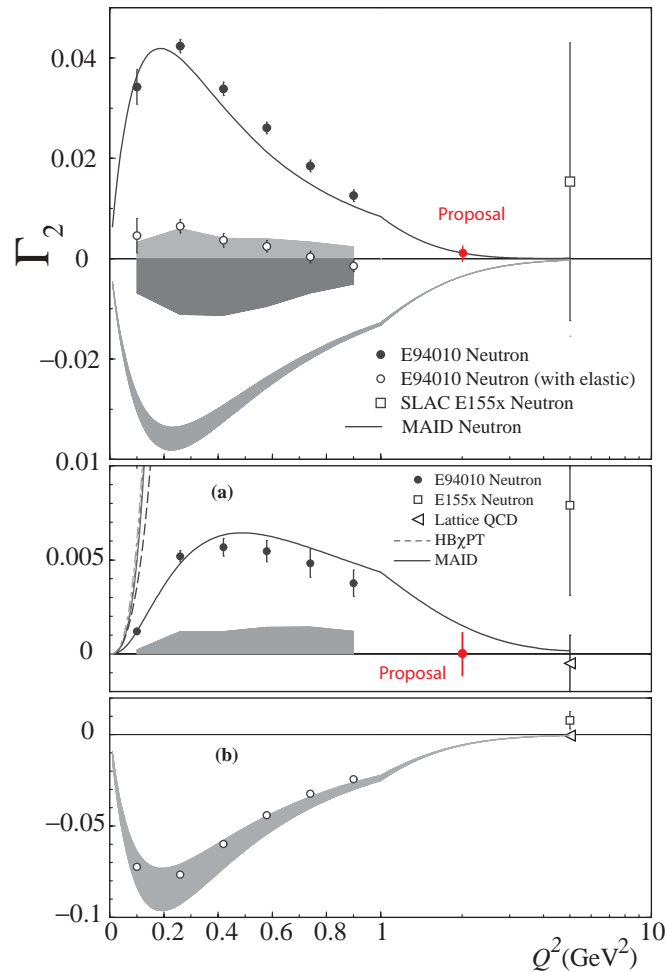
6   Summary and Beam Request

Figure 11: d_2^n and Γ_2^n projected results at $Q^2 = 2$ GeV^2 from this proposal compared to JLab E94-010 and SLAC E155X. Description is similar to that of Fig. 4 and Fig 5.

In summary, we propose to carry out a precision determination of d_2^n. We will determine asymmetries in the region $(0.24 \leq x \leq 0.8)$ (see Fig 11) from a measurement using a high pressure polarized ^{3}He target (P_t= 40%) and the highest available energies (5.7 and 6.0 GeV) of the polarized beam (P_b=80%). This measurement requires 462.2 hours of beam on target for the measurement of the transverse asymmetry and 155.8 hours for the measurement of the longitudinal asymmetry, along with 60 hours for the beam energy change, spectrometer momentum changes, elastic scattering calibration and beam and target polarization measurements. We therefore request a total of 679 hours (28 days) of beam time to achieve a statistical uncertainty on d_2^n of $\Delta d_2^n \approx 1.18 \times 10^{-3}$ at $Q^2 = 2.0$ GeV^2 in the measured x range.

References

[1] E. Shuryak and A. Vainshtein, Nuc. Phys. B **201** (1982) 141.

[2] R. L. Jaffe and X. Ji, Phys. Rev. D **43** (1991) 724.

[3] B. W. Filippone and X. Ji, Adv. in Nucl. Phys. **26**, 1 (2001).

[4] D. Adams *et al.*, Phys. Lett. **B336** (1994) 125.

[5] P. L. Anthony *et al.*, Phys. Rev. Lett. **71** (1993) 959.

[6] P. L. Anthony *et al.*, Phys. Rev. D **54** (1996) 6620.

[7] K. Abe *et al.*, Phys. Rev. Lett. **76** (1996) 587.

[8] K. Abe *et al.*, Phys. Lett. B **404** (1997) 377.

[9] P. L. Anthony *et al.*, Phys. Lett. B**458** (1999) 529.

[10] X. Ji Nucl. Phys. **B402** (1993) 217.

[11] X. Ji and P. Unrau, Phys. Lett. B **333** (1994) 228.

[12] S. A. Larin and J. A. M. Vermaseren, Phys. Lett. B **259**, 345 (1991) and references therein; S. A. Larin, Phys. Lett. B **334**, 192 (1994).

[13] S. Wandzura and F. Wilczek, Phys. Lett. B **72**, 195 (1977).

[14] F. E. Close and R. G. Roberts, Phys. Lett. B **336**, 257 (1994).

[15] Göckeler *et al.*, Phys. Rev. D **63** 074506 (2001).

[16] X. Ji, in Proceeding of the Workshop on Deep Inelastic scattering and QCD, Editors: JF. Laporte et Y. Sirois Paris, France, 24-28 April, 1995 (ISBN 2-7302-0341-4).

[17] X. Ji and W. Melnitchouk, Phys. Rev. D **56**, 1 (1997).

[18] J. Edelmann, G. Piller, W. Weise, N. Kaiser, Nucl. Phys. A **665** (2000) 125.

[19] S. Simula, M. Osipenko, G. Ricco and M. Tauiti, hep/0205118 and references therein.

[20] SLAC E155: P. L. Anthony *et al.*, Phys. Lett. B **553**, 18 (2003).

[21] H. Burkhardt and W. N. Cottingham, Ann. Phys. **56** (1970) 453.

[22] R. Jaffe, Comments Nucl. Part. Phys. 19 (1990) 239.

[23] I. P. Ivanov *et al.*, Phys. Rep. **320**, 175 (1999).

[24] M. Anselmino, A. Efremov and E. Leader, Phys. Rep. **261**, 1 (1995).

[25] M. Amarian *et al.*, Phys. Rev. Lett. **89**, 242301 (2002).

[26] G. Altarelli, B. Lampe, P. Nason and G. Ridolfi, Phys. Lett. B **334**, 187 (1994).

[27] X. Ji and W. Melnitchouk (private communication)

[28] JLab E97-103 experiment, Spokespeople T. Averett and W. Korsh. see http://hallaweb.jlab.org/physics/experiments/he3/g2/temp/

[29] K. Abe *et al.*, Phys. Rev. D **58** (1998) 112003-1.

[30] S. Wandzura and F. Wilczek, Phys. Lett. B **72** (1977) 195.

[31] JLab E01-012 experiment, Spokespeople N. Liyanage, J. P. Chen and S. Choi.

[32] JLab E01-006 experiment, Spokesperson O. Rondon,

[33] H. Weigel, L. Gamberg, H. Reinhart, Phys. Rev. D**55** (1997) 6910.

[34] M. Wakamatsu, Phys. Lett B **487** (2000) 118.

[35] M. Stratmann, Z. Phys. C **60** (1993) 763.

[36] X. Song, Phys. Rev. D **54** (1996) 1955.

[37] E. Stein, Phys. Lett. B **343** (1995) 369.

[38] B. Ehrnsperger, A Schäfer, Phys. Rev. D **52** (1995) 2709.

[39] I. Balitsky, V. Barun, A. Kolesnichenko, Phys. Lett. B **242** (1990) 245; B **318** (1995) 648 (E).

[40] D. Drechsel, S. Kamalov and L. Tiator, Phys. Rev. D **63**, 114010 (2001).

[41] C. W. Kao, T. Spitzenberg and M. Vanderhaeghen, Phys. Rev. D **67**, 016001 (2003).

[42] M.A. Bouchiat, T.R. Carver and C.M. Varnum, Phys. Rev. Lett. **5** (1960) 373.

[43] N.D. Bhaskar, W. Happer, and T. McClelland, Phys. Rev. Lett. **49** (1982) 25.

[44] W. Happer, E. Miron, S. Schaefer, D. Schreiber, W.A. van Wijngaarden, and X. Zeng, Phys. Rev. A **29** (1984) 3092.

[45] T.E. Chupp, M.E. Wagshul, K.P. Coulter, A.B. McDonald, and W. Happer, Phys. Rev. C **36** (1987) 2244.

[46] K.P. Coulter, A.B. McDonald, W. Happer, T. E. Chupp, and M.E. Wagshul, Nuc. Inst. Meth. in Phys. Res. **A 270** (1988) 90.

[47] N.R. Newbury, A.S. Barton, P. Bogorad, G. D. Cates, M. Gatzke, H. Mabuchi, and B. Saam, Phys. Rev. A **48** (1993) 558.

[48] K.P. Coulter, A.B. McDonald, G.D. Cates, W. Happer, T.E. Chupp, Nuc. Inst. Meth. in Phys. Res. A**276** (1989) 29 .

[49] A. Abragam, Principles of Nuclear Magnetism (Oxford University Press, New York, 1961).

[50] L. Whitlow, SLAC-report-357 (1990).

[51] J. W. Lightbody Jr. and J.S. O'Connell, Computers in Physics **2** (1988) 57.

[52] D. Yu. Bardin and N. M. Shumeiko, Nucl. Phys. B **127** (1977) 1251.

[53] T.V. Kuchto and N. M. Shumeiko, Nucl. Phys. B **219** (1983) 412.

[54] I. V. Akushevich and N. M. Shumeiko, J. Phys. **G**: Nucl. Part. Phys. **20** (1994) 513.

[55] L. W. Mo and Y. S. Tsai, Rev. Mod. Phys. **41** (1969) 205.

[56] Y. S. Tsai, SLAC-PUB-848 (1971).

[57] W. Melnitchouk, G. Piller and A.W. Thomas, Phys. Lett. B **346** (1995) 165; S. A Kulagin, W. Melnitchouk, G. Piller and W. Weise Phys. Rev. C **52** (1995) 932.

[58] J.L. Friar et al., Phys. Rev. C **42** (1990) 2310.

[59] R.M. Woloshyn, Nucl. Phys. A **496** (1989) 749.

[60] C. Ciofi degli Atti, E. Pace and G. Salme, Phys. Rev. C **46** (1992) R1591; C. Ciofi degli Atti, S. Scopetta, E. Pace, G. Salme, Phys. Rev. C **48** (1993) 968;

[61] R.W. Schulze and P.U. Sauer, Phys. Rev. C **48** (1993) 38.

[62] D.F. Geesaman, K. Saito and A.W. Thomas, Ann. Rev. Nucl. Part. Sci. **45** (1995) 337.

[63] I.R. Afnan, F. Bissey and A.W. Thomas, Phys. Rev. C**64** (2001) 024004.

[64] E. Leader, A.V. Sidorov and D.B. Stamenov, Int. J. Mod. Phys. A **13** (1998) 5573; Phys. Rev. D **58** (1998) 114028.

[65] I.R. Afnan, F. Bissey, J. Gomez, A.T. Katramatou, W. Melnitchouk, G.G. Petratos and A.W. Thomas, Phys. Lett. B **493** (2000) 36.

[66] F. Bissey, W. Melnitchouk, A. W. Thomas, in preparation.

[67] C. Boros, V. Guzey, M. Strikman, A.W. Thomas, hep-ph/0008064

[68] S.A. Kulagin and W. Melnitchouk, in preparation.

[69] S. Scopetta, private communication.

Jefferson Lab PAC20
Proposal Cover Sheet

Experimental Hall: _____A_____

Days Requested for Approval: ___35___

❐ Proposal Title:

Measurement of the Neutron d_2^n Matrix Element: A linear Combination of the Electric χ_E and Magnetic χ_B Color Polarizabilities

Proposal Physics Goals
Indicate any experiments that have physics goals similar to those in your proposal.

Approved, Conditionally Approved, and/or Deferred Experiment(s) or proposals:

E94-010, E97-103, E99-117, E01-012 and E01-006

Contact Person

Name: Zein-Eddine Meziani
Institution: Temple University
Address: Department of Physics, Barton Hall A323
Address: 1900 North 13th Street
City, State, ZIP/Country: Philadelphia, PA, 19122/USA
Phone: (215) 204-5971   Fax: (215) 204-2569
E-Mail: meziani@unix.temple.edu

Jefferson Lab Use Only

Receipt Date:_____

By:_____

BEAM REQUIREMENTS LIST

JLab Proposal No.: _____   Date: _____

Hall: ___A___   Anticipated Run Date: _____   PAC Approved Days: _____

Spokesperson: __X. Jiang, Z.-E. Meziani__   Hall Liaison: _____J. P. Chen_____
Phone: _____(215) 204 5971, (757) 269 7011_____
E-mail: ____meziani@unix.temple.edu____

List all combinations of anticipated targets and beam conditions required to execute the experiment.
(This list will form the primary basis for the Radiation Safety Assesment Document (RSAD) calculations that
must be performed for each experiment.)

Condition No.	Beam Energy (MeV)	Mean Beam Current (µA)	Polarization and Other Special Requirements (e.g., time structure)	Target Material (use multiple rows for complex targets — e.g., w/windows)	Material Thickness (mg/cm²)	Est. Beam-On Time for Cond. No. (hours)
1	6000.	15.	Polarization 80%	^{3}He	50	145
	6000.	15.		Glass window	44	
2	5700.	15.	Polarization 80%	^{3}He	50	641
	5700.	15.		Glass window	44	

The beam energies, E_{Beam}, available are: $E_{Beam} = N \times E_{Linac}$ where N = 1, 2, 3, 4, or 5. E_{Linac} = 800 MeV, i.e.,
available E_{Beam} are 800, 1600, 2400, 3200, and 4000 MeV. Other energies should be arranged with the
Hall Leader before listing.

HAZARD IDENTIFICATION CHECKLIST

JLab Proposal No.: _____ E-01-111 _____   Date: _____ 5/31/2001 _____

Check all items for which there is an anticipated need.

Cryogenics	Electrical Equipment	Radioactive/Hazardous Materials
_____ beamline magnets	_____ cryo/electrical devices	List any radioactive or hazadorous/ toxic materials planned for use:
_____ analysis magnets	_____ capacitor banks	_____
_____ target	_____ high voltage	_____
type: _____	_____ exposed equipment	_____
flow rate: _____		_____
capacity: _____		

Pressure Vessels	Flammable Gas or Liquids	Other Target Materials
19 mm inside diameter	type: _____	___ Beryllium (Be)
13 atm operating pressure	flow rate: _____	___ Lithium (Li)
Glass window material	capacity: _____	___ Mercury (Hg)
~100 μm window thickness		___ Lead (Pb)
	Drift Chambers	___ Tungsten (W)
	type: _____	___ Uranium (U)
	flow rate: _____	_X_ Other (list below)
	capacity: _____	^{3}He, N$_2$ and Rb
		_____

Vacuum Vessels	Radioactive Sources	Large Mech. Structure/System
_____ inside diameter	_____ permanent installation	_____ lifting devices
_____ operating pressure	_____ temporary use	_____ motion controllers
_____ window material	type: _____	_____ scaffolding or
_____ window thickness	strength: _____	_____ elevated platforms

Lasers	Hazardous Materials	General:
type: Laser diode system	____ cyanide plating materials	
wattage: 7x30 W	____ scintillation oil (from)	Experiment Class:
class: IV	____ PCBs	
	____ methane	_X_ Base Equipment
Installation:	____ TMAE	_____ Temp. Mod. to Base Equip.
_X_ permanent *	____ TEA	_____ Permanent Mod. to
_____ temporary	____ photographic developers	Base Equipment
* for this experiment	____ other (list below)	_____ Major New Apparatus
Use:	_____	
_____ calibration	_____	Other: Polarized ^{3}He target
_____ alignment		with Laser Hut

Measurement of the Neutron d_2^n Matrix Element: A Linear Combination of the Electric χ_E and Magnetic χ_B Color Polarizabilities

P. Bertin

Université Blaise Pascal De Clermont-Ferrand, Aubiere 63177, France

J.-P. Chen, E. Chudakov, C. W. de Jager, J. Gomez, O. Hansen, J. LeRose,
N. Liyanage, R. Michaels, S. Nanda, A. Saha, B. Reitz, B. Wojtsekhowski

Jefferson Lab, Newport News, VA 23606, USA

A.T. Katramatou, K. McCormick, G.G. Petratos

Kent State University, Kent, OH 44242

W. Korsch, P. Zolnierczuk

University of Kentucky, Lexington, KY 40506, USA

W. Bertozzi, Z. Chai, S. Gilad, D.W. Higinbotham, M. Rvachev, S. Sirca,
Y. Xiao, X. Zheng, J. Zhou and Z. Zhou

Massachusetts Institute of Technology, Cambridge, MA 02139, USA

F. Benmokhtar, S. Dieterich, R. Gilman, C. Glashausser,
X. Jiang (Spokesperson), G. Kumbartzki, R. Ransome, S. Strauch

Rutgers University, Piscataway, NJ 08855, USA

Seonho Choi, A. Lukhanin, Z.-E. Meziani (Spokesperson),
K. Slifer, P. Solvignon

Temple University, Philadelphia, PA 19122, USA

S. Binet, G. Cates, A. Deur, J. Singh, A. Tobias

University of Virginia, Charlottesville, VA 22901, USA

T. Averett, J. M. Finn, D. Armstrong, K. Griffioen, K. Kramer
V. Sulkosky, X. Zhu, J. Roche

College of William and Mary, Williamsburg, VA 23185, USA

and the

Hall A Collaboration

June 2, 2001

Contact: Z.-E. Meziani (meziani@unix.temple.edu)

Abstract

We propose to make a measurement of the spin-dependent scattering cross section for a longitudinally polarized electron beam off a transversely and longitudinally polarized ^{3}He target. The measurement will cover excitation energies across the resonance and deep inelastic regions at constant 4-momentum transfer $Q^2 = 2$ (GeV/c)^2. We will extract the linear combination $2g_1 + 3g_2$ of spin structure functions and evaluate the neutron d_2^n matrix element. This measurement will significantly improve the precision of the neutron d_2^n world data and test the predictions of several models including the updated lattice QCD calculation of this quantity. The matrix element d_2^n reflects the response of the color electric and magnetic fields to the polarization of the nucleon. Because d_2^n is a higher moment of a special linear combination of g_1^n and g_2^n it is dominated by the contributions from the large x region. CEBAF at Jefferson Lab is ideal to perform such a measurement. Since the quantity of interest is an integral we expect that the uncertainty on the nuclear corrections applied in the extraction of the neutron quantity from ^{3}He will not spoil the result at the present stage of statistical precision.

1   <u>Introduction and Motivation</u>

In inclusive polarized lepton-nucleon deep-inelastic scattering, one can access two spin-dependent structure functions of the nucleon, g_1 and g_2. While g_1 can be understood in terms of the Feynman parton model which describes the scattering in terms of *incoherent* parton scattering, g_2 cannot. Rather, one has to consider parton correlations initially present in the participating nucleon, and the associated process is a *coherent* parton scattering in the sense that more than one parton takes part in the scattering. Indeed, using the operator product expansion (OPE) [1, 2], it is possible to interpret the g_2 spin structure function beyond the simple quark-parton model, in terms of the technical jargon in QCD, g_2 is a higher-twist structure function. As such, it is exceedingly interesting because it provides a unique opportunity to study the quark-gluon correlations in the nucleon which cannot otherwise be accessed.

In a recent review Ji [3] explained that higher-twist processes cannot be cleanly separated from the leading twist because of the so-called infrared renormalon problem first recognized by t' Hooft. This ambiguity arises from separating quarks and gluons pre-existing in the hadron wave function from those produced in radiative processes. Such a separation turns out to be always scheme dependent. Nevertheless, the g_2 structure function is an **exception** because it contributes at the leading order to the spin asymmetry of longitudinally-polarized lepton scattering on transversely-polarized nucleons. Thus, g_2 is among the *cleanest* higher-twist observables.

Why does the g_2 structure function contain information about the quark and gluon correlations in the nucleon? According to the optical theorem, g_2 is the imaginary part of the spin-dependent Compton amplitude for the process $\gamma^*(+1) + N(1/2) \rightarrow \gamma^*(0) + N(-1/2)$,
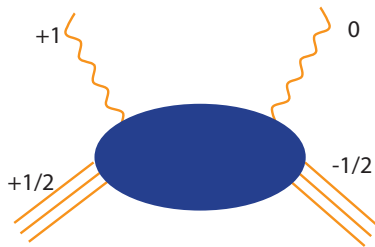

Figure 1: Compton amplitude of $\gamma^*(+1) + N(1/2) \rightarrow \gamma^*(0) + N(-1/2)$.

where γ^* and N denote the virtual photon and the nucleon, respectively, and the numbers in the brackets are the helicities. Thus this Compton scattering involves the t-channel helicity exchange $+1$. When it is factorized in terms of parton sub-processes, the intermediate partons must carry

this helicity exchange. Because of the chirality conservation in vector coupling, massless quarks in perturbative processes cannot produce a helicity flip. Nevertheless, in QCD this helicity exchange may occur in the following two ways (see Fig. 2): first, single quark scattering in which the quark carries one unit of orbital angular momentum through its transverse momentum wave function; second, quark scattering with an additional transversely-polarized gluon from the nucleon target. The two mechanisms are combined in such a way to yield a gauge-invariant result. Consequently, g_2 provides a direct probe of the quark-gluon correlations in the nucleon wave function.
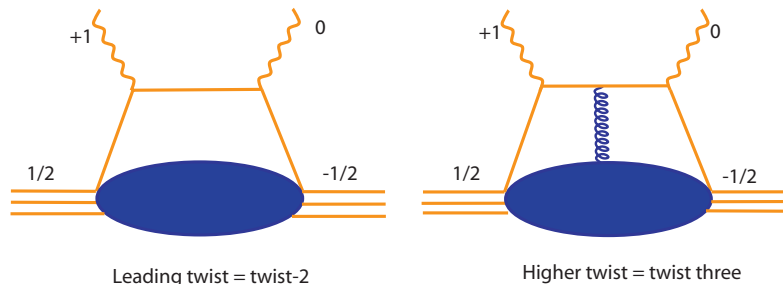

Figure 2: Twist-two and twist-three contributions to Compton scattering

The piece of interesting physics we want to focus on in this proposal contains the second moment in x of a linear combination of g_1 and g_2,

$$d_2(Q^2) \quad = \quad a_2(Q^2) + 3\int_0^1 x^2 g_2(x, Q^2)dx \tag{1}$$

$$= \quad 2\int_0^1 x^2 g_1(x, Q^2)dx + 3\int_0^1 x^2 g_2(x, Q^2)dx \tag{2}$$

where $a_2(Q^2)$ is a twist-two matrix element related to the second moment of the $g_1(x)$ structure function. The $d_2(Q^2)$ matrix element is a twist-three matrix element which is related to a certain quark gluon correlation,

$$\langle PS|\frac{1}{4}\bar{\psi}g\tilde{F}^{\sigma(\mu}\gamma^{\nu)}\psi|PS\rangle = 2d_2 S^{[\sigma}P^{(\mu]}P^{\nu)} \; , \tag{3}$$

where $\tilde{F}^{\mu\nu} = (1/2)\epsilon^{\mu\nu\alpha\beta}F_{\alpha\beta}$, and $(\cdots)$ and $[\cdots]$ denote symmetrization and antisymmetrization of indices, respectively. The structure of the above operator suggests that it measures a quark *and* a gluon amplitude in the initial nucleon wavefunction [1, 2].

The significance of $d_2(Q^2)$ has been articulated by Ji and we quote, "*we ask when a nucleon is polarized in its rest frame, how does the gluon field inside of the nucleon respond? Intuitively, because of the parity conservation, the color magnetic field $\vec{B}$ can be induced along the nucleon polarization and the color electric field $\vec{E}$ in the plane perpendicular to the polarization*". After introducing the color-singlet operators $O_B = \psi^\dagger g\vec{B}\psi$ and $O_E = \psi^\dagger \vec{\alpha} \times g\vec{E}\psi$, we can define the gluon-field polarizabilities χ_B and χ_E in the rest frame of the nucleon,

$$\langle PS|O_{B,E}|PS\rangle = \chi_{B,E} 2M^2\vec{S} \; . \tag{4}$$

Then d_2 can be written as

$$d_2 = (2\chi_B + \chi_E)/3 \; . \tag{5}$$

Thus d_2 is a measure of the response of the color electric and magnetic fields to the polarization of the nucleon.

2   Experimental Situation for $d_2^{n,p}$ Matrix Elements

The early measurements of the g_2 spin structure function performed by the SMC [4] and E142 [5, 6] collaborations in the 90's were meant to reduce the systematic errors when extracting g_1 due to g_2's contribution in the measured parallel asymmetries. As the statistical precision of g_1 improved a better measurement of g_2 was required to minimize the error on g_1. E143 [7], E154 [8] and E155 [9] collaborations evaluated d_2 and published their results. It is only recently that a dedicated experiment, known as the SLAC E155X [10] was performed to measure g_2 with much improved statistical precision on the proton and the deuteron [11]. Presently the precision of the world data on g_2 is dominated by E155X (see Fig. 3) which has improved the statistical precision over previous experiments by a factor of three.
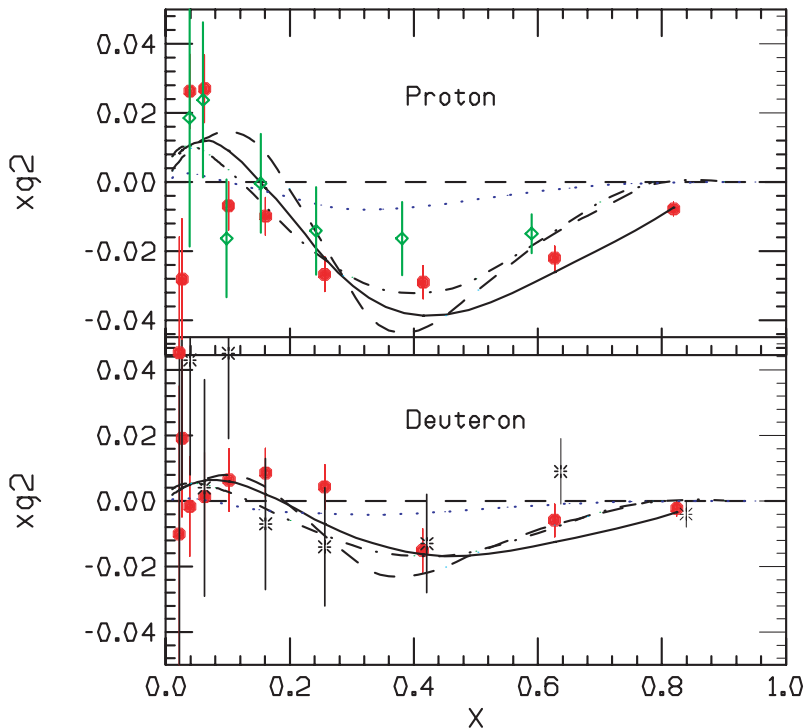

Figure 3: Preliminary E155X results (filled circles) for xg_2^p (top panel) and xg_2^d (bottom panel) compared to xg_2^{WW} (solid line), and several nucleon models; a bag model of Stratmann (dot-dashed line), a chiral soliton model of Weigel *et. al.* (dashed line) and a relativistic bag model of Song (dotted line) (see text for references). SLAC E143 (proton) at 29 GeV and SLAC E155 at 38 GeV (deuteron) results are represented by the diamonds and stars respectively

The precision of the proton measurement of g_2 spin structure function is consistent with g_2^{WW} [15] (the leading twist contribution evaluated using the world fit to the g_1 structure function data) , the bag model calculation of Stratmann [19] and the chiral soliton model of Weigel *et al.* [18]. However, it clearly disagrees with the center-of-mass bag model of Song [21]. From those experimental results we can safely say that higher twist effects are small for the proton. While a comparison of the x dependence of g_2 with a calculation based on fundamental principles like that of Lattice QCD is not possible, the d_2 matrix element offers a unique opportunity for such comparison at this stage of statistical precision. Our ultimate interest lies on a direct comparison of the second moment of $(3g_2 + 2g_1)$ with the lattice QCD calculations.
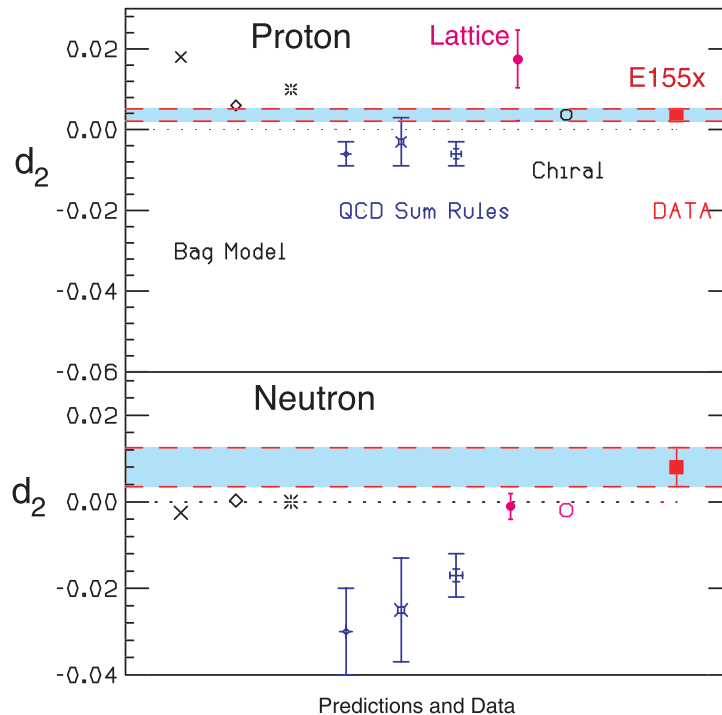
Figure 4: Preliminary E155X results of the nucleon d_2 matrix element compared to several theoretical calculations (see text). Upper panel is for the proton and lower panel for the neutron.

Fig. 4 shows preliminary results of the SLAC E155X d_2 matrix element compared to several calculations. For the proton the results are generally consistent with the chiral quark model [18]and some bag models [19, 20, 22] while one to two standard deviations away from the QCD sum rule calculations [23, 24, 25]. The comparison with the lattice QCD calculation [27] is promising but the error bar on this calculation is still large. The situation for the proton clearly poses a challenge to the theoretical approaches based on fundamental principles of QCD. The Lattice Hadron Collaboration based at Jefferson Lab has plans to calculate this matrix element for the proton and the neutron [12].

For the neutron the situation is less clear since most models predict values consistent with a negative value or zero while the experimental result is positive and 2σ away from zero. Since g_2^n in these models is negative at large x it is conceivable that the poor precision (Fig. 5) of the data in this region is affecting the overall sign of the result. It is important to note that from the point of view of a simple quark model, the d_2 matrix element of the neutron should be much smaller than that of the proton because of SU(6) spin-flavor symmetry. Therefore with the present precision of E155x neutron data it is difficult to draw any conclusions on the sign and size of the neutron higher twist (twist-tree) contribution. Because the d_2 matrix element is a second moment in x of the linear combination $(2g_1 + 3g_2)$ the situation for the neutron can be improved significantly at Jefferson Lab. Fortunately, because of the x^2 weighting, we do not need very precise data at very small x and can use the world existing and future data in the region $x < 0.24$.

As an important first step JLab experiment E97-103 [13], scheduled to run this summer, will provide a precision measurement of g_2^n in the deep inelastic region at low x ($0.17 < x < 0.21$) and will investigate its Q^2 evolution in the range $0.56 < Q^2 < 1.4$ (GeV^2) for a fixed value of $x \approx 0.2$. The unprecedented statistical accuracy expected in E97-103 should allow us to probe the size of higher twists contributions by comparing directly the measured g_2^n to the leading twist

contribution (twist-two contribution known as $g_2^{n(WW)}$ [15]). Two other approved experiments, JLab experiment E01-012 [16] which uses a polarized ^{3}He target and JLab experiment E01-006 [17] which uses polarized NH_3 and ND_3 targets, will add to the wealth of neutron spin structure functions data (g_1^n and g_2^n) but with an emphasis on the g_1 spin structure function.

The neutron result of g_2 extracted from the proton and deuteron measurements of E155X is shown in Fig. 5 along with what is expected from this proposed experiment. While in the case of the proton the bag model of Stratmann [19] and the chiral soliton model of Weigel et al. [18] seem to peak at the same value of x (see Fig. 3), it is not the case for the neutron; however in both models the Burkhardt-Cottingham sum rule is fulfilled and the d_2 matrix element values are similar. Our statistical precision at each x value is not good enough for discriminating between these two models but will provide an improvement of a factor of four on the statistical uncertainty of d_2
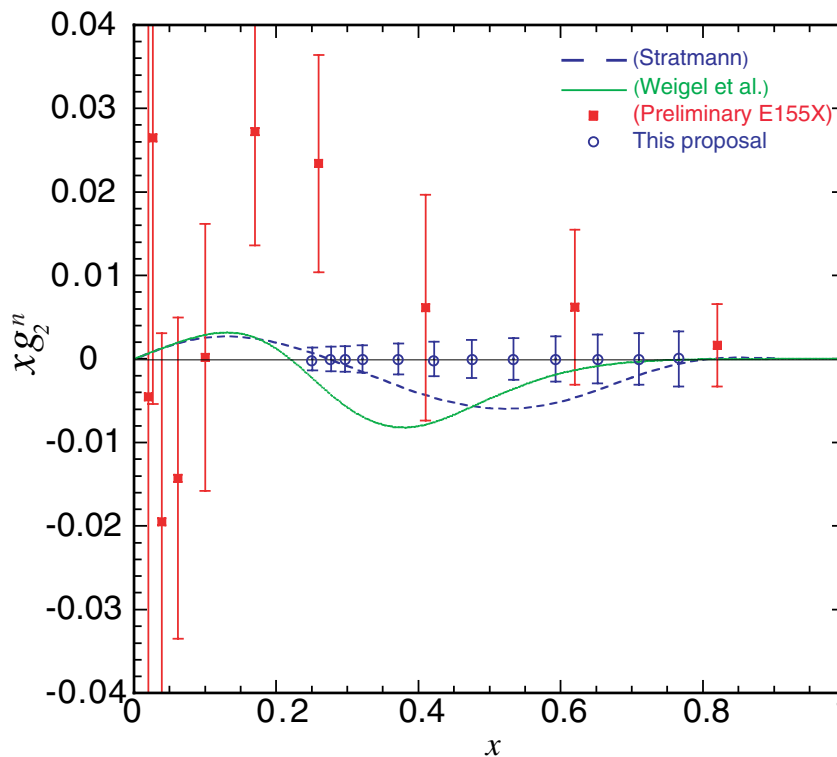

Figure 5: Preliminary E155X results of the xg_2^n extracted by subtracting the proton from the deuteron following the prescription described in Ref.[14]. We also show the resulting statistical error achievable in this proposal on xg_2 with a measurement optimized for d_2. The calculations are those of Stratmann's bag model [19] (dashed line) and Weigel et. al.'s chiral soliton model [18] (solid line)

On the experimental side this situation can be improved using a target complementary to polarized deuterium (namely polarized ^{3}He) in order to extract the neutron information. JLab is in a unique position to provide high luminosity to measure the large x region with good statistical precision. Unlike in previous experiments, world data fits of $R = \sigma_L/\sigma_T$, F_2 and g_1 will not be used to evaluate g_2, rather we shall measure absolute polarized cross sections for both directions of the target spin, parallel and perpendicular and extract g_2. Furthermore, in order to evaluate d_2 in those experiments, it is common practice to evolve the measured g_2 data from the measured Q^2

to a common Q^2 value, however, this evolution is not well understood for the twist-tree part of g_2. In contrast, our data will be measured at a constant Q^2.

At large x, the $1/Q^2$ corrections to the twist-three might be important. However, because of the parton-hadron duality, the $1/Q^2$ contribution to the moment is negligible for $Q^2 \geq 2 \text{ GeV}^2$.

We shall describe in this proposal how CEBAF is in a unique position to improve the neutron measurement of d_2^n by a factor of four.

3   Proposed Experiment

We propose to measure the unpolarized cross section σ_0^{3He}, the parallel asymmetry $A_\parallel^{3He}$ and perpendicular asymmetry $A_\perp^{3He}$ at a constant Q^2. We will use the longitudinally polarized ($P_b = 0.8$) CEBAF electron beam and a 40-cm-long high pressure polarized ^{3}He target. The measurement will be performed at two incident electron beam energies E_i = 5.7 GeV and 6.0 GeV using both HRS spectrometers at four scattering angles θ = 17.5°, 20.0°, 22.5° and 25.0°. Five momentum settings for each spectrometer will cover the range $0.24 \leq x \leq 0.8$ at Q^2= 2.0 (GeV)^2. The target polarization orientation will be set longitudinal or transverse to the beam with a value of $P_t = 0.40$ while the beam helicity will be reversed at a rate of 30 Hz. A beam current of 15 μA combined with a target density of 2.5×10^{20} atoms/cm^3 provides a luminosity ranging between 5.9×10^{35} cm^{-2}s^{-1} and 8.3×10^{35} cm^{-2}s^{-1} depending on the effective target length at various angles.

3.1   Kinematics

The kinematic settings were chosen to allow a measurement at constant Q^2 over as wide an excitation energy range as possible. Fig. 6 shows in the (Q^2, x) plane the experimental excitation range we plan to cover from the pion threshold to the deep inelastic region including the nucleon resonance region. In order to keep Q^2 constant for each measured x bin, the scattering angle must range from 17.5° to 25°. Then by taking into account the angular acceptance of the HRS spectrometers ($\Delta\theta \approx \pm 25$ mrad) we find a continuous coverage of the x range at constant Q^2 (diamonds of different sizes shown on Fig. 6)

The main contribution to d_2 arises from the large x region because of the weighting of g_1 and g_2 by x^2 in the integration over x. The measurement of this region with high precision is important. In tables 3, 4 and 5 we have listed the kinematical conditions for each spectrometer needed to cover the proposed x region.

3.2   The Polarized Beam

In this proposal we shall assume, that the achievable beam polarization at CEBAF is 80% with a current of 15μA. While about 70% electron beam polarization has been delivered on a regular basis to E94-010 and E95-001 we are optimistic that by the time this experiment runs and with the experience gained using the strained GaAs cathodes, 80% beam polarization will be achieved. The polarization of the beam will be measured with the Hall A Moller and Compton polarimeters.

3.3   The Polarized ^{3}He Target

The polarized target will be based on the principle of spin exchange between optically pumped alkali-metal vapor and noble-gas nuclei [28, 29, 30]. It is the same as that used in JLab experiments E94-010, E95-001 and E97-103 in Hall A.

A central feature of the target will be sealed glass target cells, which under operating conditions, will contain a ^{3}He pressure of about 10 atmospheres. As indicated in Fig. 7, the cells will have
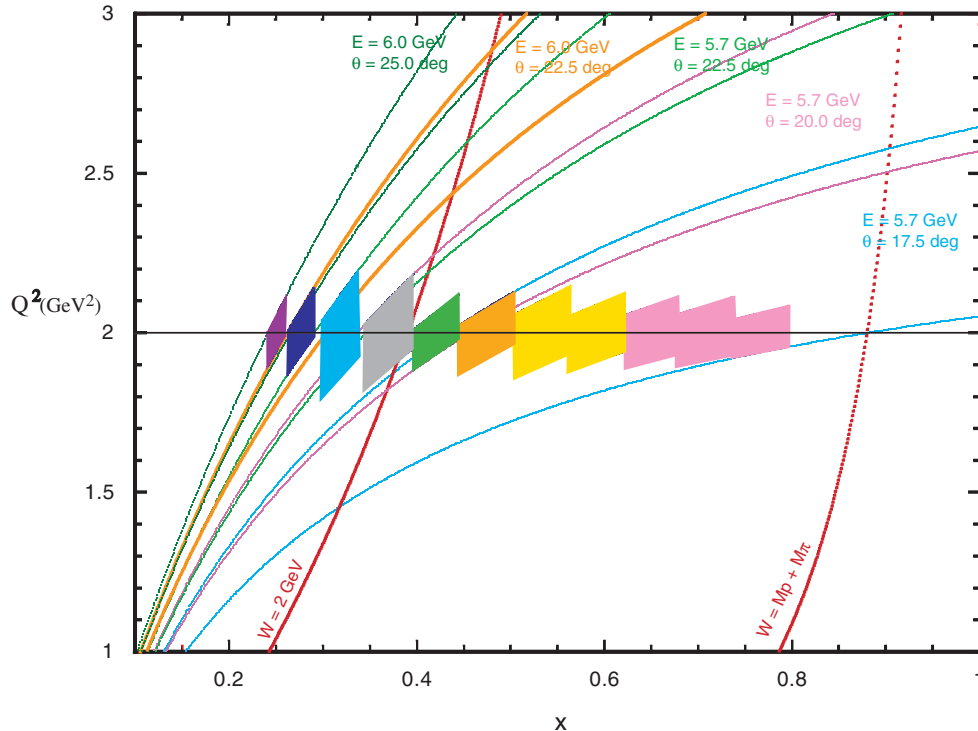
Figure 6: Proposed kinematic range for the measurement at a constant average Q^2 of 2 GeV^2. Each diamond represents the size of an (x, Q^2) bin chosen for this measurement. Each pair of common colored lines is plotted to indicate the possible range of (x, Q^2) due to the angular acceptance of the spectrometer for a fixed incident energy and scattering angle. The electron beam incident energy and the scattering angle and momentum of each spectrometer is chosen to keep the measured data at constant Q^2.

two chambers, an upper chamber in which the spin exchange takes place, and a lower chamber, through which the electron beam will pass. In order to maintain the appropriate number density of the alkali-metal Rubidium the upper chamber will be kept at a temperature of 170–200° using an oven constructed of high temperature plastic Torlon. The density of the target will be about 2.5×10^{20} atoms/cm^3. The lower cell length will be 40 cm such that the end glass windows are not seen by the spectrometer acceptance when it is set at a scattering angle of 17.5° and larger. The effective target thickness will range from 6.0×10^{21} atoms/cm^2 to 8.3×10^{21} atoms/cm^2, since the spectrometer acceptance sees a length of 7 cm/$\sin \theta_e$

The main components of the target are shown in Fig. 7. The main "coils" shown are large Helmholtz coils used to apply a static magnetic field of about 25 Gauss. Also shown are the components for the NMR and EPR polarimetry. The NMR components of the target include a set of RF drive coils, and a separate set of pickup coils. Not shown in the figure are the NMR electronics, which include an RF amplifier, a lock-in amplifier, some bridge circuitry, and the capability to sweep the static magnetic field. The EPR components include an EPR excitation coil and a photodiode for detection of the EPR line. The oven shown in Fig. 7 is heated with forced hot air. The optics system include a system of 4 diode lasers for longitudinal pumping and 4 for transverse pumping. A polarizing beam splitter, lens system and a quarter wave plate are required to condition each laser beam line and provide circular polarization.

3.3.1   Operating Principles

The time evolution of the ^{3}He polarization can be calculated from a simple analysis of spin-exchange and ^{3}He nuclear relaxation rates[31]. Assuming the ^{3}He polarization $P_{^3He} = 0$ at $t = 0$,

$$P_{^3He}(t) = P_{Rb} \left(\frac{\gamma_{SE}}{\gamma_{SE} + \Gamma_R} \right) \left(1 - e^{-(\gamma_{SE} + \Gamma_R)\, t} \right) \tag{6}$$

where γ_{SE} is the spin-exchange rate per ^{3}He atom between the Rb and ^{3}He, Γ_R is the relaxation rate of the ^{3}He nuclear polarization through all channels other than spin exchange with Rb, and P_{Rb} is the average polarization of the Rb atoms. Likewise, if the optical pumping is turned off at $t = 0$ with $P_{^3He} = P_0$, the ^{3}He nuclear polarization will decay according to

$$P_{^3He}(t) = P_0\, e^{-(\gamma_{SE} + \Gamma_R)\, t}. \tag{7}$$

The spin exchange rate γ_{SE} is defined by

$$\gamma_{SE} \equiv \langle \sigma_{SE}\, v \rangle\, [Rb]_A \tag{8}$$

where, $\langle \sigma_{SE}\, v \rangle = 1.2 \times 10^{-19}$ cm^3/sec is the velocity-averaged spin-exchange cross section for Rb–^{3}He collisions[31, 32, 33] and $[Rb]_A$ is the average Rb number density seen by a ^{3}He atom. The target operates with $1/\gamma_{SE} = 8$ hours. From equation (6) it is clear that the best possible ^{3}He polarization is obtained by maximizing γ_{SE} and minimizing Γ_R. But from equation (8) we can see that maximizing γ_{SE} means increasing the alkali-metal number density, which in turn means more
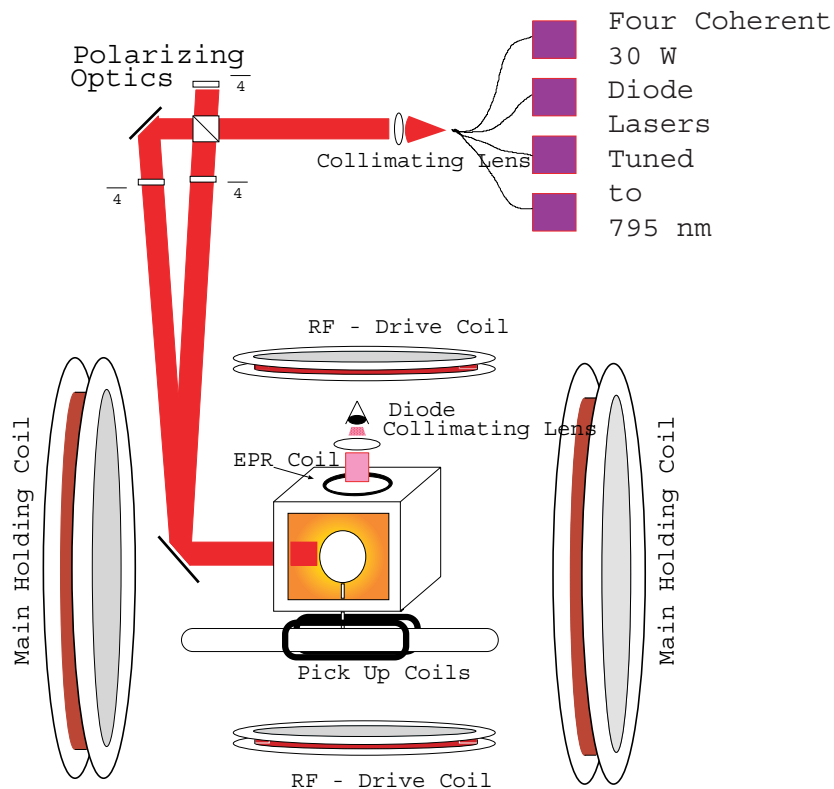

Figure 7: JLab Hall A polarized ^{3}He target setup.

laser power. The number of photons needed per second must compensate for the spin relaxation of Rb spins. In order to achieve $1/\gamma_{\mathrm{SE}} = 8$ hours, about 50 Watts of usable laser light at a wavelength of 795 nm will be required.

The rate at which polarization is lost is characterized by Γ and has four principle contributions. An average electron beam current of about 15 μA will result in a depolarization rate of $\Gamma_{beam} = 1/30$ hours [34]. The cells produced in previous experiments typically have an intrinsic rate of $\Gamma_{cell} = 1/50$ hours. This has two contributions, relaxation that occurs during collisions of ^{3}He atoms due to dipole-dipole interactions, and relaxation that is largely due to the interaction of the ^{3}He atoms with the walls. Finally, relaxation due to magnetic field inhomogeneities was held to about $\Gamma_{\nabla B} = 1/100$ hours. Collectively, under operating conditions, we would thus expect

$$\Gamma_R = \Gamma_{beam} + \Gamma_{cell} + \Gamma_{\nabla B} = 1/30 \, \text{hours} + 1/50 \, \text{hours} + 1/100 \, \text{hours} = 1/16 \, \text{hours}.$$

Thus, according to equation (6), the target polarization cannot be expected to exceed

$$P_{max} = \frac{\gamma_{\mathrm{SE}}}{\gamma_{\mathrm{SE}} + \Gamma_{\mathrm{R}}} = 0.66$$

Realistically, a Rb polarization of 100% in the pumping chamber will not be achieved, which will reduce the polarization to about 40%.

During E94-010 and E95-001 we achieved a polarization of about 30-35% when a beam current of 15μA was used. The beam depolarization was slightly larger than expected and this was the first time that such a large beam current was used for an extended period time. An R&D effort is underway by JLab and the polarized ^{3}He target collaboration to improve the achievable polarization under the beam conditions proposed in this experiment.

3.3.2   Target Cells

The length of the cell has been chosen to be 40 cm so that the end windows are not within the acceptance of the Hall A spectrometers at angles equal to 17.5° and larger. The end windows themselves will be about 100 μm thick.

3.3.3   The Optics System

As mentioned above, approximately 50 W of "usable" light at 795 nm will be required. By "usable", we mean circularly polarized light that can be readily absorbed by the Rb. It should be noted that the absorption line of Rb has a full width of several hundred GHz at the high pressures of ^{3}He at which we will operate. Furthermore, since we will operate with very high Rb number densities that are optically quite thick, even light that is not well within their absorption line width can still be absorbed.

The laser system is similar to that used in E94-010. It consists of commercially available 30 Watt fiber-coupled diode laser systems (from COHERENT INC.). Four such lasers are used to pump along the transverse direction and three along the longitudinal direction. The efficiency of these lasers has been tested during experiment E94-010 and E95-001 and found to be totally adequate for this experiment's needs.

3.3.4   Polarimetry

Polarimetry is accomplished by two means. During the experiment, polarization is monitored using the NMR technique of adiabatic fast passage (AFP)[35]. The signals are calibrated by comparing the ^{3}He NMR signals with those of water. The calibration is then independently verified by studying the frequency shifts that the polarized ^{3}He nuclei cause on the electron paramagnetic resonance

(EPR) lines of Rb atoms [34]. Both methods were used in E94-010 and we found as expected that the NMR measurements with water calibration are consistent with the EPR results.

3.4 The Spectrometers Setup

We plan to use both HRS spectrometers in Hall A. We will use the right spectrometer with its standard detector package for electrons and the left spectrometer with an added double layer lead glass calorimeter which was first used in E94-010. Each spectrometer will then consist of;

- Two vertical Drift Chambers (VDCs) for the measurement of momentum and production angle.

- Gas Čerenkov counter for pion rejection.

- A set of scintillators for triggering on charged particles.

- A double layer lead glass calorimeter for additional pion rejection.

As the E94-010 analysis shows, the pion rejection factor with the Čerenkov counter and the lead glass calorimeter are better than 2×10^{-4} which is sufficient for our worst case.

Because the maximum momentum attainable by each spectrometer is different (4.30 GeV for the HRS-l and 3.17 GeV for the HRS-r) we have assigned HRS-l to perform the measurements for electron momenta greater than 3 GeV and HRS-r for those measurements with momenta equal or less than 3 GeV. We optimized the time sharing between the two spectrometers (see Table 4 and 5). Although we need to make few spectrometer angle changes to keep our measurement at constant Q^2. Specific advantages make these spectrometers a well matched tool for the proposed measurement.

- Good electron events in the spectrometer are in principle due only to electron scattering off ^{3}He nuclei since the target cell glass windows are outside the spectrometer acceptance. However, excellent target reconstruction by the HRS spectrometers allows for better background rejection.

- An excellent resolution of the spectrometers permits the measurement of elastic scattering off ^{3}He needed for an absolute calibration of the detector in order to measure absolute cross sections.

4 Evaluation of d_2^n Matrix Element

The goal of this experiment is to obtain the d_2 matrix element from the direct measurement of the unpolarized cross section σ_0 and the parallel $A_\parallel$ and perpendicular $A_\perp$ asymmetries on ^{3}He. Equivalently the d_2 matrix element is obtained from the measurement of the linear combination of the spin structure functions $g_1(x, Q^2)$ and $g_2(x, Q^2)$ and forming the second moment of this combination namely,

$$d_2(Q^2) = \int_0^1 x^2 [2g_1(x, Q^2) + 3g_2(x, Q^2)] \ dx = \int_0^1 \tilde{d}_2(x, Q^2) \ dx \tag{9}$$

The spin structure functions can be expressed in terms of asymmetries and unpolarized cross sections as follow;

$$g_1 = \frac{MQ^2}{4\alpha^2} \frac{y}{(1-y)(2-y)} 2\sigma_0 \left[A_\parallel + \tan\frac{\theta}{2} A_\perp \right] \tag{10}$$

$$g_2 = \frac{MQ^2}{4\alpha^2} \frac{y^2}{2(1-y)(2-y)} 2\sigma_0 \left[-A_\parallel + \frac{1 + (1-y)\cos\theta}{(1-y)\sin\theta} A_\perp \right] \tag{11}$$

where σ_0 is the unpolarized cross section, Q^2 is the four momentum transfer, α the electromagnetic coupling constant, θ the scattering angle and $y = (E - E')/E$ the fraction of energy transferred to the target. $A_\parallel$ and $A_\perp$ are the parallel and perpendicular asymmetries,

$$A_\parallel = \frac{\sigma^{\downarrow\Uparrow} - \sigma^{\uparrow\Uparrow}}{2\sigma_0}, \qquad A_\perp = \frac{\sigma^{\downarrow\Rightarrow} - \sigma^{\uparrow\Rightarrow}}{2\sigma_0} \tag{12}$$

From (10), (11) and (12) we can express the integrand of the d_2 matrix element directly in terms of measured asymmetries and unpolarized cross section as follows:

$$\begin{aligned}
\tilde{d}_2(x, Q^2) &= x^2[2g_1(x, Q^2) + 3g_2(x, Q^2)] \tag{13} \\
&= \frac{MQ^2}{4\alpha^2} \frac{x^2y^2}{(1-y)(2-y)}\sigma_0\left[\left(3\frac{1+(1-y)\cos\theta}{(1-y)\sin\theta} + \frac{4}{y}\tan\frac{\theta}{2}\right)A_\perp + \left(\frac{4}{y} - 3\right)A_\parallel\right] \tag{14}
\end{aligned}$$

The above expression of the integrand is used for the following purposes:

- Determination of the time sharing between the transverse and the longitudinal measurement to minimize the statistical error on d_2 not on g_2 as in previous experiments.

- Determination of the effect of the target polarization orientation misalignment on the systematic error of d_2

- Determination of the systematic error on d_2 due to the systematic errors of the cross section and asymmetries measurements.
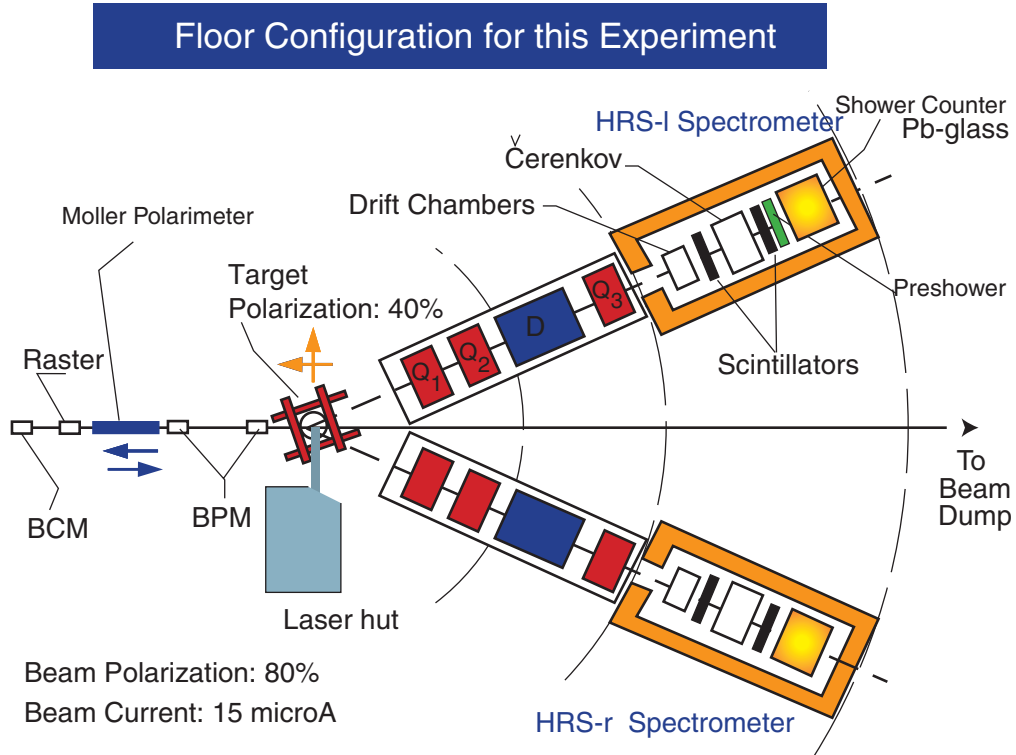

Figure 8: JLab Hall A floor setup using the HRS spectrometers and the polarized 3He target.

The measurement consists of collecting data at two incident energies ($E_i = 5.7$ GeV and 6.0 GeV) and four scattering scattering angles ($\theta = 17.5°, 20.0°, 22.5°$ and $25.0°$) and for eight spectrometer momentum settings to cover the range $0.25 \leq x \leq 0.8$. The measured raw ^{3}He counting parallel asymmetry $\Delta_\parallel$ and perpendicular asymmetry $\Delta_\perp$ are converted to the experimental asymmetries $A_\parallel^{3He}$, and $A_\perp^{3He}$ respectively, using the relation

$$A_\perp^{3He} = \frac{\Delta_\perp}{P_b P_t \cos\phi} \qquad\qquad A_\parallel^{3He} = \frac{\Delta_\parallel}{P_b P_t} \tag{15}$$

$$\Delta_\perp = \frac{(N^{\uparrow\Rightarrow} - N^{\uparrow\Rightarrow})}{(N^{\uparrow\Rightarrow} + N^{\uparrow\Rightarrow})} \qquad\qquad \Delta_\parallel = \frac{(N^{\downarrow\Uparrow} - N^{\uparrow\Uparrow})}{(N^{\downarrow\Uparrow} + N^{\uparrow\Uparrow})} \tag{16}$$

where $N^{\uparrow\Downarrow}$ ($N^{\uparrow\Uparrow}$) and $N^{\uparrow\Rightarrow}$ ($N^{\uparrow\Rightarrow}$) represent the rate of scattered electrons for each bin in x and Q^2 when the electron beam helicity and target spin are parallel or perpendicular. ϕ is the angle between the scattering plane and the plane formed by the incoming beam and the perpendicular target polarization. $P_b = 0.80$ and $P_t = 0.40$ are the beam and target polarization respectively. The target length (40 cm) is chosen such that no extra dilution of the asymmetry occurs from unpolarized scattering off the glass windows. However, empty target measurements will be performed to insure that no spurious unpolarized background originating in the target area reduces the measured physics asymmetries. The kinematics and electron rates are presented in Table 3. We used the Whitlow 1990 [36] parametrization of unpolarized structure functions from measurements of deep inelastic scattering on the proton and the deuteron. We added incoherently the appropriate structure functions to generate the ^{3}He cross sections. The rates were determined assuming a solid angle evaluated from the bins shown in Fig. 6 and a luminosity varying from 6.0×10^{35} cm^{-2}s^{-1} to 8.0×10^{35} cm^{-2}s^{-1}. The times for the transverse and longitudinal measurements were determined by optimizing the time sharing for the best precision on the integrand $\tilde{d}_2$. If we set

$$\alpha = \frac{MQ^2}{4\alpha^2} \frac{x^2 y^2}{(1-y)(2-y)} \sigma_0 \left(3 \frac{1 + (1-y)\cos\theta}{(1-y)\sin\theta} + \frac{4}{y} \tan\frac{\theta}{2} \right) \tag{17}$$

$$\beta = \frac{MQ^2}{4\alpha^2} \frac{x^2 y^2}{(1-y)(2-y)} \sigma_0 \left(\frac{4}{y} - 3 \right) \tag{18}$$

The optimum ratio between the parallel and perpendicular counts is

$$N_\parallel = \frac{\beta}{\alpha} N_\perp \tag{19}$$

The total number of counts $N_\perp$ is given by

$$N_\perp = \frac{\alpha(\alpha + \beta)}{P_b^2 P_t^2 f^2 (\Delta\tilde{d}_2)^2} \tag{20}$$

$f = W_1^n / W_1^{3He}$ is the fraction of scattering originating from the neutron compared to ^{3}He We required an absolute statistical uncertainty on the integrand $\Delta\tilde{d}_2^n = 7.5\times 10^{-3}$ at each x bin. This in turn leads to an absolute statistical precision on d_2^n of $\Delta d_2^n \approx 1.25 \times 10^{-3}$. This value is to be compared with $\Delta d_2^n = 5\times10^{-3}$ from SLAC E155X.

The pion background was estimated using the EPC program [37] which was tested against measurements carried at JLab in a similar kinematic range. The results of the estimate are listed in Table 1 were the π/e^- ratio ranges from a negligible value in the highest x bin to a value of about twenty in the lowest x bin. Given the pion rejection performance of the Čerenkov and Lead glass calorimeter combination, we should be able to keep this correction at a negligible level. Furthermore, we shall measure the pion asymmetry using the hadron spectrometer in the lowest three x bins.

Table 1: π^-/e^- each x bin planned in this measurement

E_i (GeV)	θ_e °	E' (GeV)	x	W (GeV)	$d\sigma^{\pi^-}$ (nb/GeV/sr)	π^- rate (Hz)	π^-/e^-
5.70	16.40	4.310	0.766	1.22	0.51	0.03	0.006
5.70	16.63	4.197	0.710	1.30	0.94	0.09	0.013
5.70	16.90	4.064	0.652	1.40	1.68	0.20	0.024
5.70	17.24	3.903	0.593	1.50	2.98	0.48	0.030
5.70	17.70	3.705	0.534	1.62	5.40	1.31	0.062
5.70	18.33	3.458	0.475	1.76	10.4	2.67	0.118
5.70	19.14	3.173	0.422	1.90	20.8	5.01	0.264
5.70	20.27	2.833	0.372	2.06	44.7	28.54	0.673
5.70	22.16	2.375	0.321	2.26	120.3	92.13	2.41
6.00	22.70	2.152	0.277	2.47	253.3	141.25	6.04
6.00	25.14	1.760	0.251	2.62	574.9	245.44	18.7

The radiative corrections (RC) will be performed in two stages. First the internal corrections will be evaluated following the procedure developed by Bardin and Shumeiko[38] for the unpolarized case and extended to the spin dependent lepto-production cross sections by Akushevish and Shumeiko[39, 40]. Second, using these internally corrected cross sections, the external corrections (for thick targets) are applied by extending the procedure developed for the unpolarized cross sections by Tsai[41, 42] with modifications appropriate for this experiment.

To evaluate the experimental systematic uncertainty of d_2^n we used relative uncertainties in the cross sections and asymmetries achieved in E94-010. Table 4 summarizes these uncertainties. One item of concern was the effect of the target relative spin misalignment between the transverse and longitudinal direction measurements. Fig. 9 shows this effect at each value of x on the integrand of d_2. A relative error of $0.5°$ in the relative direction of the transverse versus perpendicular results in a relative error $\Delta d_2/d_2 = 0.15\%$. Using the Weigel et $al.$ [18] model of g_2 and g_1 we estimated $\Delta d_2/d_2$ to be of the order of 10 % and thus an absolute systematic uncertainty of about 10^{-3}. We believe we can achieve a relative error of $0.2°$ in the target spin alignment.

Even with our improved projected statistical precision the total uncertainty in d_2^n is still dominated by the statistical.

An elastic scattering asymmetry measurement is planned at low energy ($E_i = 1.0$ GeV $\theta = 17.5°$) in order to calibrate our spin dependent absolute cross sections. This quantity can be evaluated using the measured electric and magnetic form factors of ^{3}He. This measurement would actually determine the polarization of the ^{3}He nuclei along the electron beam path. False asymmetries will be checked to be consistent with zero by comparing data with target spins in opposite directions.

Also contributing to the dilution of the asymmetry is the pair-electron contamination. This correction is x dependent, and is relevant only in the lowest x region. This contamination was estimated to be no more than 6% in the worst case and will be measured in this experiment by reversing the spectrometer polarity on the right arm spectrometer.

The spectrometers cannot be used in a symmetric configuration when taking data since they don't access the same maximum range of momentum. For this reason we can only save about 456 hours using the HRS-r spectrometer and most of the large x data will be acquired using the HRS-l spectrometer. Tables 4 and 5 show the kinematics and time for each spectrometer acquiring data.

Table 2: List of the systematic error contributions to d_2^n

Item description	Subitem description	Relative uncertainty
Target polarization		4 %
Beam polarization		3 %
Asymmetry (raw)		
	• Target spin direction (0.5°)	$\approx 1.5 \times 10^{-3}$
	• Beam charge asymmetry	200 ppm
Cross section (raw)		
	• PID efficiency	≈ 1 %
	• Background Rejection efficiency	≈ 1 %
	• Beam charge	< 1 %
	• Beam position	< 1 %
	• Acceptance cut	2-3 %
	• Target density	2-3 %
	• Nitrogen dilution	2-3 %
	• Dead time	<1 %
	• Finite Acceptance cut	<1%
Radiative corrections		≤ 5 %
Total effect		$\Delta d_2 \approx 5 \times 10^{-4}$
Estimate of contributions	$\int_{0.003}^{0.241} \tilde{d}_2^n \; dx$	4.8×10^{-4}
from unmeasured regions	$\int_{0.767}^{0.999} \tilde{d}_2^n \; dx$	3.9×10^{-5}
From ^{3}He to Neutron correction		5%

Table 3: Parameters per bin in (Q^2,x) plane for the proposed experiment

| E_i (GeV)	bin central p (GeV)	x	Δx	Q^2 (GeV^2)	W (GeV)	Rate (Hz)	Time$_\perp$ hours	Time$_\parallel$ hours
5.70	4.31	.766	.58E-01	2.00	1.22	5.03	166.	82.2
5.70	4.20	.710	.58E-01	2.00	1.30	6.85	166.	82.2
5.70	4.06	.652	.57E-01	2.00	1.40	8.23	144.	63.7
5.70	3.90	.593	.59E-01	2.00	1.50	16.0	167.	65.5
5.70	3.71	.534	.59E-01	2.00	1.62	21.1	110.	37.4
5.70	3.46	.475	.59E-01	2.00	1.76	22.6	125	35.8
5.70	3.17	.422	.48E-01	2.00	1.90	19.0	148	35.1
5.70	2.83	.372	.52E-01	2.00	2.06	42.4	63.6	12.2
5.70	2.38	.321	.34E-01	2.00	2.26	38.1	64.9	9.4
6.00	2.15	.277	.27E-01	2.00	2.47	23.4	104	11.5
6.00	1.76	.251	.18E-01	2.00	2.61	13.1	179.	15.4
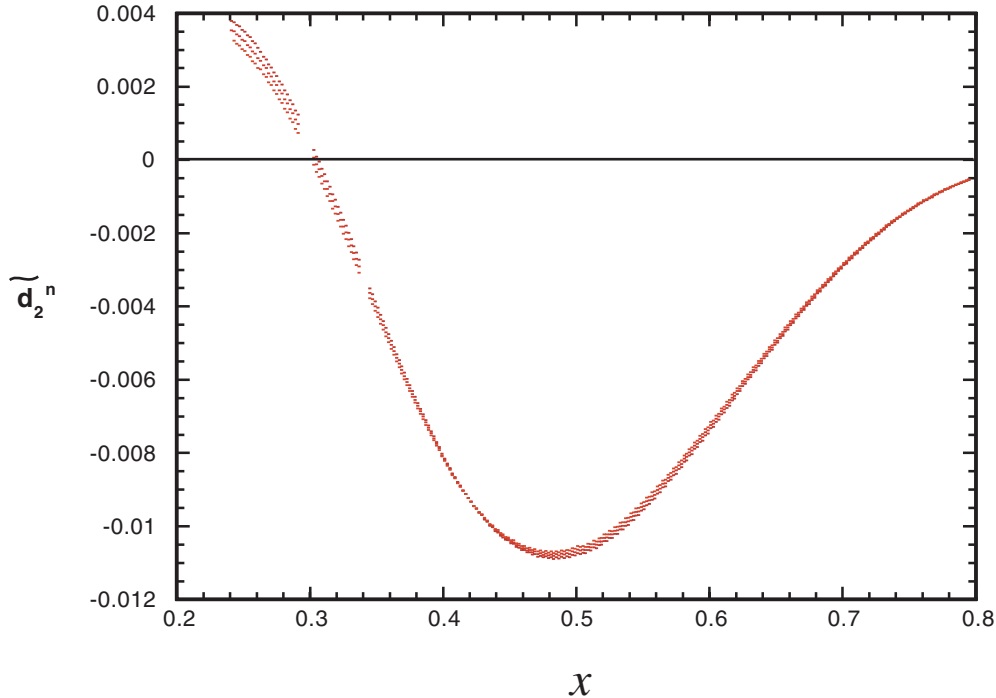
Figure 9: Effect of target relative spin misalignment by $0.5°$ between the transverse and longitudinal measurements

The right spectrometer will measure mainly the low x data points and will also be used to measure the positron contamination at the lowest x bins, while the HRS-l completes its measurements at large x. We will use the HRS-l for 787 hours with beam on target to complete this measurement.

5 Spin Structure Functions: From ^{3}He to the Neutron

Most of the current information on the spin-independent structure functions of the neutron comes from experiments on the deuteron. For spin-dependent structure, because the deuteron polarization is shared roughly equally between the proton and neutron, extraction of neutron spin structure functions requires a precise knowledge of the proton spin structure, in addition to the nuclear effects [43]. This problem is compounded by the fact that the spin-dependent structure functions of the proton are typically much larger than those of the neutron, making extraction of the latter especially sensitive to small uncertainties in the proton structure functions. On the other hand, since the neutron in ^{3}He carries almost 90% of the nuclear spin, polarized ^{3}He is an ideal source of polarized neutrons.

The three-nucleon system has been studied for many years, and modern three-body wave functions have been tested against a large array of observables which put rather strong constraints on the nuclear models [44]. In particular, over the past decade considerable experience has been acquired in the application of three-body wave functions to deep-inelastic scattering [45, 46, 47].

The conventional approach employed in calculating nuclear structure functions in the region $0.3 < x < 0.8$ is the impulse approximation, in which the virtual photon scatters incoherently from individual nucleons in the nucleus [48]. Corrections due to multiple scattering, NN correlations or multi-quark effects are usually confined to either the small-x ($x < 0.2$), or very large-x ($x > 0.9$)

Table 4: Sequence of measurements carried by the HRS-l spectrometer

E_i GeV	θ deg	HRS-l Central p GeV		Time$_\perp$ hours	Time$_\parallel$ hours
6.0	22.5	2.167		42.	5.7
6.0	25.0	1.756		89.5	7.7
5.7	17.5	4.069		166	82.2
5.7	17.5	3.794		167	65.5
5.7	17.5	3.538		125	35.8
			Total	589.5	196.9

Table 5: Sequence of measurements carried by the HRS-r spectrometer

E_i GeV	θ deg	HRS-r Central p GeV		Time$_\perp$ hours	Time$_\parallel$ hours
6.0	22.5	2.167		42.	5.7
6.0	25.0	1.756		89.5	7.7
5.7	20.0	3.075		148.	35.1
5.7	20.0	2.867		63.6	12.2
5.7	22.5	2.324		64.9	9.4
			Total	408	56.7

regions. In the impulse approximation the g_1 structure function of ^{3}He is obtained by folding the nucleon structure function with the nucleon momentum distribution in ^{3}He, Δf_N:

$$g_1^{^3\mathrm{He}}(x) \;=\; \int_x^3 \frac{dy}{y}\; \left\{ 2\Delta f_p(y)\, g_1^p(x/y) \;+ \Delta f_n(y)\, g_1^n(x/y) \right\}, \tag{21}$$

where y is the fraction of the ^{3}He momentum carried by the nucleon, and the dependence on scale, Q^2, has been suppressed. The nucleon momentum distributions $\Delta f_N(y)$ are calculated from the three-body nuclear wave function, which are obtained by either solving the Faddeev equation [49] or using variational methods [46], and are normalized such that:

$$\int_0^3 dy\; \Delta f_N(y) \;=\; \rho_N \;, \tag{22}$$

where ρ_N is the polarization of the nucleon in ^{3}He. While the full three-body wave function involves summing over many channels, in practice the three lowest states, namely the S, S' and D, account for over 99% of the normalization. Typically, one finds $\rho_n \approx 87\%$ and $\rho_p \approx -2\%$ [44, 45, 46, 47, 49].

The smearing in Eq.(21) incorporates the effects of Fermi motion and nuclear binding, which can become sizable at large x. Correctly accounting for these effects is important when attempting to extract information on nucleon structure functions from nuclear data at $x > 0.6$, as well as for determining higher moments of structure functions, in which the large-x region is more strongly weighted.

The nuclear corrections to the g_2^n structure function can be evaluated analogously to those for g_1^n. However, because the magnitude of g_2 is expected to be small, one could anticipate nuclear effects to play a bigger role here than in g_1^n. A difficulty in determining the size of the nuclear corrections to g_2^n is the fact that very little is known about the shape of g_2^n as a functions of x. One can estimate the order of magnitude of the possible effects by considering the twist-2 part of g_2^n, which is determined from g_1^n through the Wandzura-Wilczek relation [15] [52]:

$$g_2^{^3\mathrm{He}}(x)\Big|_{\mathrm{tw}-2} \;=\; -g_1^{^3\mathrm{He}}(x) \;+ \int_x^3 \frac{dy}{y}\; g_1^{^3\mathrm{He}}(x/y) \;, \tag{23}$$

where $g_1^{^3\mathrm{He}}$ is given by Eq.(21).

Since the main objective of the experiment is to extract the second moment of $3g_2^n + 2g_1^n$, namely $\int dx\, x^2(3g_2^n(x) + 2g_1^n(x))$, the effects of Fermi motion at large x may be somewhat magnified.

In Fig. 10 we compare $x^2 g_2^{^3\mathrm{He}}(x)$ calculated by including the effects of Fermi smearing (dashed) and without smearing (dot-dashed) [52]. The two dashed curves correspond to the full, smeared calculation with different ^{3}He model wave functions [49, 51]. For reference the twist-2 part of the neutron g_2^n is also shown (solid). The difference in the second moments of $g_2^{^3\mathrm{He}}$ between the smearing and no-smearing cases, is again at the level of a few percent, as is the difference between the convolution results using different ^{3}He wave functions.

Although the quantitative results for g_2 cannot be viewed as definitive without also considering the twist-3 contribution, there is no reason to expect the twist-3 component to have a dramatic x-dependence so as to significantly alter the scale of the nuclear effects seen in Fig. 10.

All of the nuclear structure function analyses that have been performed instead suggest that both the neutron g_1^n and g_2^n deep-inelastic structure functions can be extracted from ^{3}He data with minimal uncertainties associated with nuclear corrections. Recently there was an investigation into the role of the $\Delta(1232)$ in deep inelastic scattering on polarized ^{3}He and how it affects the g_1 neutron spin structure function extraction [53]. The authors estimated that when taking the effect of the Δ into account the values of the first moment of g_1^n increases by $6 \div 8$ %.

Estimating all the corrections and their uncertainties we come to the conclusion that in this experiment the statistical error on the final result is still the dominant error.
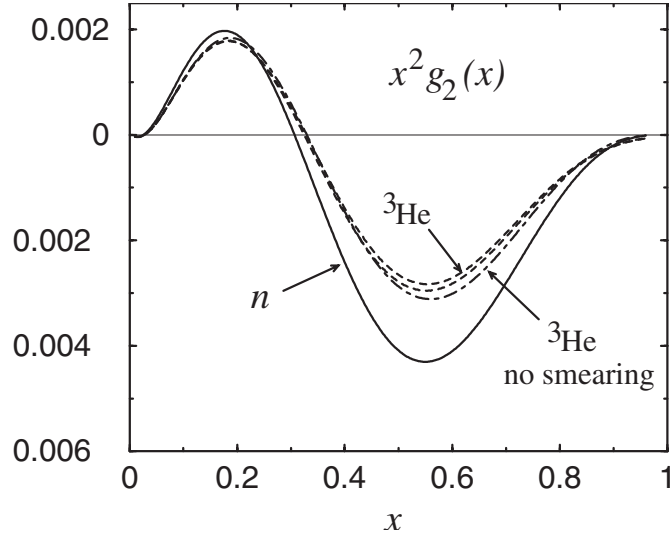
Figure 10: Structure function $x^2 g_2(x)$ for ^{3}He, calculated taking into account effects of smearing due to Fermi motion and binding, with two different model ^{3}He wave functions (dashed), and without smearing (dot-dashed) [52]. For reference the neutron structure function is also shown (solid).

6 Summary and Beam Request

In summary, we propose to carry out a precision determination of the neutron twist-three matrix element d_2^n. We will determine asymmetries in a large x region ($0.24 \leq x \leq 0.8$) (see Fig 11) from
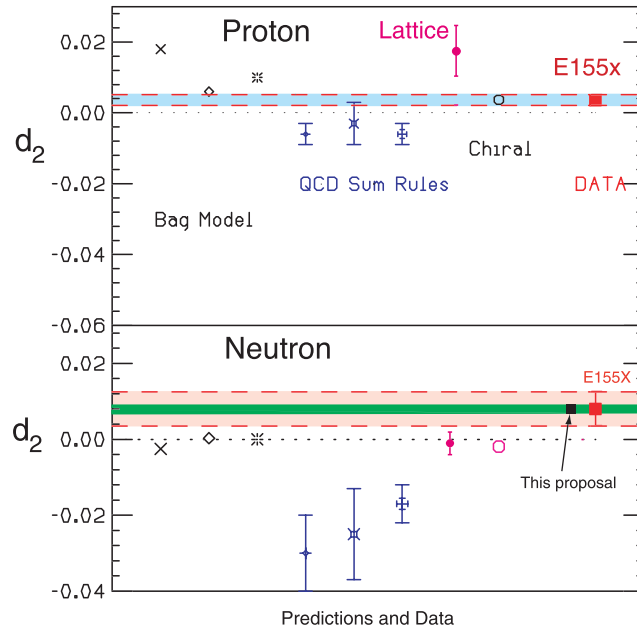

Figure 11: Same figure as Fig. 4 but with the d_2^n projected result from this proposal compared to E155X.

a measurement using a high pressure polarized ^{3}He target (P_t= 40%) and the highest available energies (5.7 and 6.0 GeV) of the polarized beam (P_b=80%). This measurement requires 589.5 hours of beam on target for the measurement of the transverse asymmetry and 197 hours for the measurement of the longitudinal asymmetry, along with 60 hours for the beam energy change, spectrometer momentum changes, elastic scattering calibration and beam and target polarization measurements. We therefore request a total of 846.5 hours (35 days) of beam time to achieve a statistical uncertainty on d_2^n of $\Delta d_2^n \approx 1.2 \times 10^{-3}$ at $Q^2 = 2.0$ GeV^2 in the measured x range.

References

[1] E. Shuryak and A. Vainshtein, Nuc. Phys. B **201** (1982) 141.

[2] R. L. Jaffe and Xiangdong Ji, Phys. Rev. D **43** (1991) 724.

[3] B. Filippone and X. Ji, hep-ph/0101224.

[4] D. Adams *et al.*, Phys. Lett. **B336** (1994) 125.

[5] P. L. Anthony *et al.*, Phys. Rev. Lett. **71** (1993) 959.

[6] P. L. Anthony *et al.*, Phys. Rev. D **54** (1996) 6620.

[7] K. Abe *et al.*, Phys. Rev. Lett. **76** (1996) 587.

[8] K. Abe *et al.*, Phys. Lett. B **404** (1997) 377.

[9] P. L. Anthony *et al.*, Phys. Lett. B**458** (1999) 529.

[10] SLAC Experiment E155X, Spokespeople: R. Arnold and J. McCarthy, (1996).

[11] (E155X) P. Bosted (for the E155X collaboration), "Very preliminary results for the spin structure function g2 from SLAC E155x", Nuc. Phys. A **666** (2000) 300c-303c

[12] X. Ji, (private communication)

[13] JLab E97-103 experiment, Spokespeople T. Averett and W. Korsh. see (http://hallaweb.jlab.org/physics/experiments/he3/g2/temp/

[14] K. Abe *et al.*, Phys. Rev. D **58** (1998) 112003-1.

[15] S. Wandzura and F. Wilczek, Phys. Lett. B **72** (1977) 195.

[16] JLab E01-012 experiment, Spokespeople N. Liyanage, J. P. Chen and S. Choi.

[17] JLab E01-006 experiment, Spokesperson O. Rondon,

[18] H. Weigel, L. Gamberg, H. Reinhart, Phys. Rev. D**55** (1997) 6910.

[19] M. Stratmann, Z. Phys. C **60** (1993) 763.

[20] X. Ji and P. Unrau, Phys. Lett. B **333** (1994) 228.

[21] X. Song, Phys. Rev. D **54** (1996) 1955.

[22] X. Ji and W. Melnitchouk, Phys. Rev. D **56** (1997) 5511.

[23] E. Stein, Phys. Lett. B **343** (1995) 369.

[24] B. Ehrnsperger, A Schäfer, Phys. Rev. D **52** (1995) 2709.

[25] I. Balitsky, V. Barun, A. Kolesnichenko, Phys. Lett. B **242** (1990) 245; B **318** (1995) 648 (E).

[26] M. Gockeler, Phys. Rev. D **53** (1996) 2317.

[27] M. Gockeler *et al.*, hep-lat/0011091.

[28] M.A. Bouchiat, T.R. Carver and C.M. Varnum, Phys. Rev. Lett. **5** (1960) 373.

[29] N.D. Bhaskar, W. Happer, and T. McClelland, Phys. Rev. Lett. **49** (1982) 25.

[30] W. Happer, E. Miron, S. Schaefer, D. Schreiber, W.A. van Wijngaarden, and X. Zeng, Phys. Rev. A **29** (1984) 3092.

[31] T.E. Chupp, M.E. Wagshul, K.P. Coulter, A.B. McDonald, and W. Happer, Phys. Rev. C **36** (1987) 2244.

[32] K.P. Coulter, A.B. McDonald, W. Happer, T. E. Chupp, and M.E. Wagshul, Nuc. Inst. Meth. in Phys. Res. **A 270** (1988) 90.

[33] N.R. Newbury, A.S. Barton, P. Bogorad, G. D. Cates, M. Gatzke, H. Mabuchi, and B. Saam, Phys. Rev. A **48** (1993) 558.

[34] K.P. Coulter, A.B. McDonald, G.D. Cates, W. Happer, T.E. Chupp, Nuc. Inst. Meth. in Phys. Res. A**276** (1989) 29 .

[35] A. Abragam, Principles of Nuclear Magnetism (Oxford University Press, New York, 1961).

[36] L. Whitlow, SLAC-report-357 (1990).

[37] J. W. Lightbody Jr. and J.S. O'Connell, Computers in Physics **2** (1988) 57.

[38] D. Yu. Bardin and N. M. Shumeiko, Nucl. Phys. B **127** (1977) 1251.

[39] T.V. Kuchto and N. M. Shumeiko, Nucl. Phys. B **219** (1983) 412.

[40] I. V. Akushevich and N. M. Shumeiko, J. Phys. **G**: Nucl. Part. Phys. **20** (1994) 513.

[41] L. W. Mo and Y. S. Tsai, Rev. Mod. Phys. **41** (1969) 205.

[42] Y. S. Tsai, SLAC-PUB-848 (1971).

[43] W. Melnitchouk, G. Piller and A.W. Thomas, Phys. Lett. B **346** (1995) 165; S. A Kulagin, W. Melnitchouk, G. Piller and W. Weise Phys. Rev. C **52** (1995) 932.

[44] J.L. Friar et al., Phys. Rev. C **42** (1990) 2310.

[45] R.M. Woloshyn, Nucl. Phys. A **496** (1989) 749.

[46] C. Ciofi degli Atti, E. Pace and G. Salme, Phys. Rev. C **46** (1992) R1591; C. Ciofi degli Atti, S. Scopetta, E. Pace, G. Salme, Phys. Rev. C **48** (1993) 968;

[47] R.W. Schulze and P.U. Sauer, Phys. Rev. C **48** (1993) 38.

[48] D.F. Geesaman, K. Saito and A.W. Thomas, Ann. Rev. Nucl. Part. Sci. **45** (1995) 337.

[49] I.R. Afnan, F. Bissey and A.W. Thomas, nucl-th/0012081..

[50] E. Leader, A.V. Sidorov and D.B. Stamenov, Int. J. Mod. Phys. A **13** (1998) 5573; Phys. Rev. D **58** (1998) 114028.

[51] I.R. Afnan, F. Bissey, J. Gomez, A.T. Katramatou, W. Melnitchouk, G.G. Petratos and A.W. Thomas, Phys. Lett. B **493** (2000) 36.

[52] F. Bissey, W. Melnitchouk, A. W. Thomas, in preparation; W. Melnitchouk, private communication.

[53] C. Boros, V. Guzey, M. Strikman, A.W. Thomas, hep-ph/0008064